University of Alberta

Regional Climate Modeling over the Glaciated Regions of the Canadian High Arctic

by

Benjamin P. Gready

A thesis submitted to the Faculty of Graduate Studies and Research
in partial fulfillment of the requirements for the degree of

Doctor of Philosophy

Department of Earth and Atmospheric Sciences

Fall 2012
Edmonton, Alberta

Abstract

The Canadian Arctic Islands (CAI) contain the largest concentration of terrestrial ice outside of the continental ice sheets. Mass loss from this region has recently increased sharply due to above average summer temperatures. Thus, increasing the understanding of the mechanisms responsible for mass loss from this region is critical. Previously, Regional Climate Models (RCMs) have been utilized to estimate climatic balance over Greenland and Antarctica. This method offers the opportunity to study a full suite of climatic variables over extensive spatially distributed grids. However, there are doubts of the applicability of such models to the CAI, given the relatively complex topography of the CAI. To test RCMs in the CAI, the polar version of the regional climate model MM5 was run at high resolution over Devon Ice Cap. At low altitudes, residuals (computed through comparisons with in situ measurements) in the net radiation budget were driven primarily by residuals in net shortwave (NSW) radiation. Residuals in NSW are largely due to inaccuracies in modeled cloud cover and modeled albedo. Albedo on glaciers and ice sheets is oversimplified in Polar MM5 and its successor, the Polar version of the Weather Research and Forecast model (Polar WRF), and is an obvious place for model improvement. Subsequently, an inline parameterization

of albedo for Polar WRF was developed as a function of the depth, temperature and age of snow. The parameterization was able to reproduce elevation gradients of seasonal mean albedo derived from satellite albedo measurements (MODIS MOD10A1 daily albedo), on the western slope of the Greenland Ice Sheet for three years. Feedbacks between modelled albedo and modelled surface energy budget components were identified. The shortwave radiation flux feeds back positively with changes to albedo, whereas the longwave, turbulent and ground energy fluxes all feed back negatively, with a maximum combined magnitude of two thirds of the shortwave feedback magnitude. These strong feedbacks demonstrate that an accurate albedo parameterization must be run inline within an RCM, to accurately quantify the net surface energy budget of an ice sheet. Finally, Polar WRF, with the improved albedo parameterization, was used to simulate climatic balance over the Queen Elizabeth Islands for the summers of 2001 to 2008. Climatic balance was derived from the output using energy balance and temperature index melt models. Regional mass balance was calculated by combining climatic balance with estimates of iceberg discharge. Mass balance estimates from the model agreed, within the bounds of uncertainty, with estimates from previous studies, thus supporting the assertion that mass loss from the QEI accelerated during the first decade of the 21st century. Melt rates on the seven major icecaps of the QEI became more correlated to one another during the period 2001-2008. However, precipitation became less correlated from 2003-2008. These observations are coincident with dramatic increases in melt on all of the ice caps, and it is speculated that both are caused by decreases in the scale of disturbances delivering precipitation to the region over time.

Acknowledgements

First and foremost I thank my PhD supervisors Dr. Martin Sharp and Dr. Andrew Bush. Both have provided tremendous support throughout the last five and a half years. I am particularly grateful to Dr. Sharp for the numerous rounds of comprehensive edits provided in the final few months of writing. I am grateful for them allowing me absolute freedom in my research objectives, but offering support and guidance where necessary. I am very thankful for their flexibility and understanding in allowing me to pursue non academic interests, and at times work remotely. I thank my examination committee for the many useful comments that have greatly improved the thesis.

I owe a large debt of gratitude to Dr. Jason Box and his research group at the Byrd Polar Research Centre, Ohio State University, who hosted me in November 2009. It was with the guidance of Dr. Box that I was able to program the albedo parameterization inline into Polar WRF, which was presented in chapter three.

I thank all of my family for their love and support throughout this lengthy process, even at the times when finishing seemed impossible. I thank Maya for putting up with me, even when I was terribly short fused during the long nights of writing. Without her support, I could not have finished. I also thank her for reading through so many drafts of my work, and offering much help with my writing.

I thank Jamie Davis and Alex Gardner who have both offered tremendous technical and moral support with my research, and great friendship throughout. I also thank Angus Duncan, Faye Wyatt, Emily Moss, Inka Koch, Linsey Nicholson and Gabrielle Gascon for being fantastic office mates and friends over the last 5 years. I also thank the numerous members of the glaciology group with whom it has been a pleasure to work.

I thank John England, Jeff Kavanagh, Peter Kershaw, Alex Wolf, Tom Chacko and Duane Froese for their mentorship and guidance while I was at the University of Alberta. I also thank the numerous friends from the department and further a field who have supported me and made my life interesting in Edmonton. Particularly, I thank John Postma, Geir Moholdt, Steven Mamet, Collin Quarrie, Scott Williamson, Jess Vaughan, Mei Mei Chong and Josh Davies for extra curricular activities.

Table of Contents

Appendices

List of Tables

List of Figures

CHAPTER 1

Introduction

1.1 Motivation

The world's Glaciers and Ice Caps (GICs) and Ice Sheets, have been responding dramatically to recent climate warming (Church (2001); Jacob et al. (2012)). Multiple methods (hydrography, laser altimetry and satellite gravimetry) have shown global sea level to be rising at a (steric-corrected) rate of 1.3±0.6 mm yr^{-1} between 2005-2010 (Willis et al. (2010)). GICs cover roughly 5% of the area of the ice sheets (Radic and Hock (2010)), yet they account for 30% of the observed non-steric sea level rise (Jacob et al. (2012)). The disproportionate rate of mass wastage from GICs, relative to their area, makes them essential for study in terms of their contribution to sea level change, but also as indicators of processes that could take place on the continental ice sheets under future climate warming scenarios. The Canadian Arctic Islands (CAI) (containing Baffin, Bylot, Devon, Ellesmere and Axel Heiberg islands) contain the highest concentration of glacier ice outside the ice sheets of Greenland and Antarctica. With an ice covered area of approximately 160,000 km^2 (Dyurgerov et al. (2005, 2002); Radic and Hock (2010)), the CAI GICs were the largest contributor to sea level rise after the ice sheets between 2003 and 2010 (Jacob et al. (2012)). The mass contribution of CAI GICs to the ocean is determined by their mass balance. This has been estimated for the period 1995-2000 from repeat airborne laser surveys (Abdalati et al. (2004)), and for the period 2004-2009 by a variety of methods, including: repeat satellite gravimetry (GRACE) measurements, repeat satellite later altimetry (ICESat), and a temperature index mass budget model (Gardner et al. (2011)). During that period, the CAI ice caps lost mass at an accelerating rate, with mass loss being almost three times larger in the period 2007-2009 than during the period 2004-2006.

The CAI GICs have some of the longest continuous climatic balance records in the world, with four continuous records dating back to 1963 or earlier (Koerner (2005)) - a remarkable feat for an area so isolated. Using these data, Sharp et al. (2011) were able to put the recent mass loss from the region into a longer term perspective, demonstrating that 30-48% of the mass loss from the four monitored glaciers (Devon, Meighen and Melville South Ice Caps, and White Glacier) since 1963, has occurred since 2005.

A key quantity in mass balance studies is the climatic balance (Cogley et al. (2011)), which is the difference between accumulation (including internal accumulation through the refreezing of meltwater within snow or firn) and ablation at the surface or in the interior of an ice mass. The climatic balance provides the direct link between a glacier and the atmosphere. Recent estimates of climatic balance in the CAI have been based on field or satellite measurements, or on results from statistically based temperature index melt models (Burgess and Sharp (2008); Cogley and Adams (1998); Colgan et al. (2008); Gardner et al. (2011); Koerner (2005); Mair et al. (2005); Sharp et al. (2011); Shepherd et al. (2007)) Temperature index models rely on air temperature as their primary input (Reeh (1991)), which is attractive given the relatively high abundance of air temperature measurements, in comparison to other meteorological measurements, on glaciers. Large areas can be covered by interpolating input temperature fields to locations where measurements are required using constant or variable temperature-elevation lapse rates (Gardner et al. (2009)). However, in order to obtain climatic balance, precipitation must also be estimated. Gridded precipitation fields for the CAI have been obtained by a number of techniques including: Interpolation of the in-situ accumulation measurements of Koerner (2005), drilling short cores into the firn to detect the "bomb" layer depth (this method is explained in more detail later, but allows estimation of the mean annual accumulation between 1963 and the core date) and interpolating onto a regular grid, and through bilinear interpolation of NCEP/NCAR R1 Reanalysis (Kalnay et al. (1996)) precipitation fields, and bias correcting using in-situ measurements (Gardner et al. (2011)). These methods will be explained in more detail later.

Physically based climatic balance models, which take into account the surface energy budget of a glacier, have been applied over individual catchments in the CAI, for individual melt seasons (Arendt (1999); Arendt and Sharp (1999); Duncan (2011)). However, energy balance studies are limited by their need for spatially distributed data on multiple variables, which are expensive and logistically difficult to obtain, and therefore limited in spatial and temporal extent. Unlike the primary input to a temperature index model, (air temperature),there is no simple method of effectively interpolating the inputs for an energy balance model over large distances. Therefore, there have been no regional scale climatic balance studies in the CAI using an energy balance approach to date.

One method for estimating the fields necessary to run an energy budget mass balance model, is to use a Regional Climate Model (RCM). RCMs offer a method for dynamically downscaling low resolution input datasets to high resolution grids, using the physically based dynamics of a climate model. In recent years, RCMs have been tested over the ice sheets and improved as a result (Manning and Davis (1997); Hines et al. (1997,?); Van Lipzig et al. (1999); Guo et al. (2003); Monaghan et al. (2003); Van De Berg et al. (2006); Hines and Bromwich (2008); Hines et al. (2011)). Results of RCMs have been used to estimate the climatic balance of the Greenland ice sheet (Box et al. (2004, 2006); Ettema et al. (2009); Fettweis et al. (2005)). These studies have provided physically based estimates of the climatic balance on the Greenland ice sheet at high resolution (11km) from 1958-2007.

So far, there have been no RCM studies over the GICs of the CAI. Although previous studies have estimated regional climatic balance in the CAI on high resolution grids without using RCMs (e.g. Abdalati et al. (2004); Gardner et al. (2011)), the gains from running an RCM in the region would be significant. An RCM would provide the first regional, high resolution estimates of a number of key energy and mass balance related fields including: the radiation and turbulent energy fluxes, surface water vapor flux, blowing snow sublimation and redistribution. Studying the spatial and temporal patterns of these individual components, could provide new insights into the processes driving the climatic balance of the CAI. Since the RCM approach is physically based, if the method can be proved to work in the CAI, it could have applicability for forecasting future climatic balance, using global circulation model forecasts as boundary conditions. The overall objectives of this thesis are to (i) assess the performance of an RCM over the complex topography of the CAI, (ii) make adjustments to the RCM to achieve better performance, and (iii) simulate climatic balance in the CAI using the improved RCM, and study the high resolution (6km) output over individual ice caps in the region to better understand spatial and temporal variations in the climatic balance components.

1.2 Terminology

Understanding of glaciological mass balance has advanced dramatically in the last 50 years. Advances have outpaced the ability of the accepted nomenclature, which until 2011 were based on Anonymous (1969), to consistently describe the science. In recent years, many studies, although individually self consistent, have used contradictory definitions. A new comprehensive set of standard definitions for use by the glaciological community has been suggested by Cogley et al. (2011). I will use those standards throughout this thesis, and summarize the most important definitions below.

Throughout the thesis, unless otherwise stated, the term “glacier” will refer to glaciers, ice caps, icefields and ice sheets. I will often need to distinguish the ice caps, icefields and mountain glaciers from the ice sheets, and will do so using the abbreviation for Glaciers and Ice Caps (GICs) as mentioned above.

1.3 Mass Balance

The total mass of a glacier is assigned the symbol M. The change in mass of a glacier, ΔM, is known as the mass balance, and is a key quantity in glaciological studies as it characterizes net mass exchanges between a glacier and the wider hydrological system. Mass balance is defined simply as the difference between all accumulation and ablation on a glacier. Accumulation includes all processes that add mass, whereas ablation includes all processes that cause reductions in mass of a glacier. In the context of mass balance and its components, capital letters will denote quantities computed for an entire glacier, for a period of time Δt. Δt may be any length of time, but generally it is one calendar year, reflecting the seasonality of mass exchanges of a glacier. In this study, Δt will be taken to be 1 calendar year, between October 1 and September 30 of consecutive years, unless an alternative time period is stated. An equation for glacier-wide mass balance is:

$$\Delta M = C + A \tag{1.1}$$

Where C and A are accumulation and ablation respectively. The "positive inward" convention is used, which states that mass additions (accumulation) to the ice mass are positive, while mass losses (ablation) are negative, hence we are implicitly taking the difference in (1.1). The units of mass balance are those of mass (kg). However, due to the large scale of of the GICs studied in this thesis, mass balance will usually be given in Gigatons ($1Gt = 1 \times 10^{12} kg$).

Specific mass balance is the mass balance in a particular location. Specific balance takes the units of mass per unit area (kg m^{-2}), and is denoted by lower case "m". This applies to all quantities, thus the specific mass balance equation is:

$$\Delta m = c + a \tag{1.2}$$

Specific quantities are also computed over time Δt, which will be 1 calendar year unless otherwise stated. Mass balance and specific balance *rates* refer to partial derivatives with respect to time.

$$\dot{M} = \frac{\partial M}{\partial t} = \frac{\partial A}{\partial t} + \frac{\partial C}{\partial t} = \dot{A} + \dot{C} \tag{1.3}$$

$$\dot{m} = \frac{\partial m}{\partial t} = \frac{\partial a}{\partial t} + \frac{\partial c}{\partial t} = \dot{a} + \dot{c} \tag{1.4}$$

The official SI unit of time is the second, and therefore balance rates should be quoted "per second", or "per kilo-second" etc. However, mass balance is fundamentally tied to seasonality, and, at least for glaciers not located in the tropics, has a clear annual cycle. One year is not an official SI unit. The length of a year is not constant, but varies depending upon whether it is a leap year or not. Despite these concerns, mass balance rates will nonetheless be quoted "per year" unless otherwise stated. There is redundancy in the mass balance definitions, given that mass balance will usually be calculated over the period of a year, and balance rates are calculated "per year". I may use the two interchangeably, but deviations from the definitions will be specifically explained.

1.3.1 Mass balance of an ice column

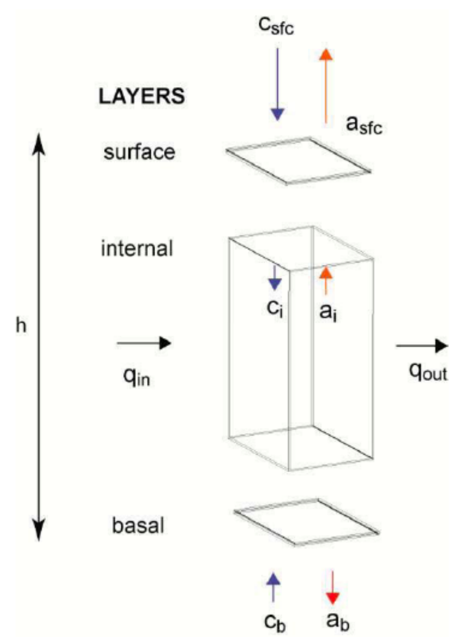

Figure 1.1: Systematic diagram of mass balance components in an ice column, (reproduced directly from Cogley et al. (2011)). a and c, with the subscripts "sfc", "i" and "b", refer to the specific accumulation and ablation, at the surface, internally in the ice column, and at the ice-bed interface respectively. q_{in} and q_{out} are the ice fluxes into and out of the column respectively, due to glacier motion. h is the depth of the column.

Figure 1.1 illustrates the components of mass balance within an ice column.

The specific balance rate of that column may be written:

$$\dot{m} = \dot{c}_{sfc} + \dot{a}_{sfc} + \dot{c}_i + \dot{a}_i + \dot{c}_b + \dot{a}_b + \frac{(q_{in} - q_{out})}{ds} \tag{1.5}$$

subscripts sfc, i and b refer to surface, internal and basal respectively. q_{out} and q_{in} refer to depth averaged ice fluxes in and out of the ice column due to dynamic flow, and $ds = dx\ dy$ refers to the fixed horizontal dimensions of the column. This can be written more succinctly as,

$$\dot{m} = \dot{b} - \vec{\nabla} \cdot \vec{q} \tag{1.6}$$

which is equivalent to the continuity equation for a glacier, if ice density is assumed constant. In this definition, $\dot{b} = \dot{c}_{sfc} + \dot{a}_{sfc} + \dot{c}_i + \dot{a}_i + \dot{c}_b + \dot{a}_b = \dot{b}_{sfc} + \dot{b}_i + \dot{b}_b$, is the climatic-basal balance rate, and refers to all aspects of the mass balance, apart from changes in thickness due to spatial gradients in glacier motion. $\dot{b}_{sfc} = \dot{c}_{sfc} + \dot{a}_{sfc}$ is the surface balance rate, $\dot{b}_i = \dot{c}_i + \dot{a}_i$ is the internal balance rate, and $\dot{b}_b = \dot{c}_b + \dot{a}_b$ is the basal balance rate. The significance of $\dot{b}_i$ and $\dot{b}_b$ depend upon the type of glacier, climatic conditions, and geological properties of the area. $\dot{b}_i$ generally refers to the refreezing of percolating melt water within glacier firn. It is an important term in glaciers where the near surface firn is at sub-freezing temperatures and latent heat due to refreezing of meltwater is easily conducted into the cold firn. However, it is insignificant on temperate glaciers, where the entire glacier is at the pressure melting point. Thus, it will have a varying degree of importance in polythermal glaciers depending upon location. The term b_b is insignificant in most locations, however in geographical areas with high geothermal activity, (such as Vatnajokull Ice Cap in Iceland), this term is very important. Since this situation does not apply to the CAI, this term is not considered in this thesis.

By integrating (1.6) over the surface area (S) of a glacier, we obtain an alternative form of (1.3):

$$\dot{M} = \int_S (\dot{b} - \vec{\nabla} \cdot \vec{q}) dS \tag{1.7}$$

Using the divergence theorem, this becomes:

$$\dot{M} = \int_S \dot{b} dS - \int_P \vec{q} \cdot \vec{n} dP \tag{1.8}$$

The first term on the right is the total climatic-basal balance rate. The second term on the right is the loop integral of $\vec{q} \cdot \vec{n}$ around the perimeter, P of the glacier, and $\vec{n}$ is a unit vector perpendicular to the path P. This second term represents the rate of ice crossing the perimeter of the glacier. For land terminating glacier fronts, the ice crossing the glacier boundary is zero when a glacier is in equilibrium, positive if the glacier is advancing, and negative if the glacier is retreating. For ocean terminating glacier fronts, it represents ice discharge from the glacier into the ocean, known as frontal ablation (A_f). Using the positive inward sign convention, and integrating with respect to time, (1.8) may be re-written:

$$\Delta M = B + A_f \tag{1.9}$$

However, it should be noted that (1.9) ignores any change in mass due to the advance or retreat of land terminating glacier fronts. Thus the total climatic-basal balance is separated from the frontal ablation in the mass balance equation. If both B and A_f can be estimated, the total mass balance of the glacier may also be estimated.

1.3.2 Climatic Balance

Often glacial studies refer to the climatic balance, $B_{clim} = B_{sfc} + B_i$. In many previous studies, this has been referred to as the surface mass balance, but this often led to confusion as to what combination of B_{sfc}, B_i and B_b is referred to. I adopt the new definitions of Cogley et al. (2011):

$$B = B_{clim} + B_b \tag{1.10}$$

Here B_{clim} is the climatic balance, and B_b is the basal balance. As was mentioned earlier, B_b is assumed to be insignificant in the CAI, and we therefore use B_{clim} as a close approximation to B. Thus, the mass balance equation used in this thesis is:

$$\Delta M = B_{clim} + A_f \tag{1.11}$$

1.4 Estimating Climatic Balance

1.4.1 Measurement Techniques

Two generic methods (geodetic and hydrological) are used to estimate the mass balance of a glacier. In the geodetic method, the surface elevation of a glacier is measured repeatedly. Differences in surface elevation between two times are used to estimate mass changes during that time, by using an assumed vertical density profile to convert height changes into mass changes. Surface elevation changes of the glacier are estimated from the differences between repeated DEMs derived from stereophotogrammetry of aerial photographs, or altimetry. Examples of each approach are given later in this introduction.

A challenging aspect of geodetic modelling is estimating an accurate firn density profile. The process of densification causes the surface elevation to lower. Such lowering cannot be distinguished from height changes due to accumulation (or ablation) by geodetic techniques. Densification can occur through the process of particle rearrangement at low densities (Anderson and Benson (1963)). Densification also occurs through pressure sintering, a process in which density is increased through the elimination of pore space and reduction of surface area (Anderson and Benson (1963)). Pressure sintering was originally used to describe the transformation of powders to solids in the field of powder metallurgy. Several mechanisms may be responsible for pressure sintering depending upon the applied pressure to snow or firn. Wilkinson (1988) presented a pressure sintering mechanism map which showed that at low pressures lattice diffusion controls the sintering rate, and as pressure increases, dislocation creep becomes the dominant form of sintering. At high pressures, rapid plastic flow occurs if a yield stress is overcome. Dislocation is the dominant process for firn with density between 50% and 98% of the density of glacial ice. Another mechanism that increases the firn densification rate is the refreezing of melt water and formation of ice lenses within the firn layers and snow pack (e.g. Koerner (1970)).

Researchers have developed several models to estimate the densification rate of firn. In one example, Herron and Langway (1980) developed empirical relationships for the depth-density profile of firn at several locations in Greenland and Antarctica. The relationships rely on the mean annual accumulation rate, mean annual firn temperature, and the snow surface density. Models such as described by Herron and Langway (1980) have provided a tool to estimate density profiles, which can be used to convert height differences to changes in mass. However, models such Herron and Langway (1980) assume that the densification rate is in steady state. This is often not an accurate assumption. For example, if a glacier experiences higher than average melt rates, there is more potential for meltwater refreezing within the firn pack, which increases the densification rate at that location.

In light of such variations to the densification rate, use of steady state models such as Herron and Langway (1980) inevitably introduces errors when converting glacier elevation changes into mass changes in the Geodetic method of estimating mass balance. In an attempt to improve upon the limitations of models such as Herron and Langway (1980), Reeh et al. (2005) developed a simple densification model that specifically accounts for the content of ice lenses within the snow pack. In the model, each annual layer is composed of an ice fraction and a firn fraction. Using the model, it was shown that for a 1k warming over Greenland, only 75% of surface lowering was due to melting, whereas 25% was due to increases in the densification rate.

A technique known as the "coffee can" method for measuring the densification rate in the field, was developed by Hamilton and Whillans (2000). In this technique, a borehole is drilled several meters into the firn. An anchor (originally a coffee can) is lowered into the borehole, with a non-stretchable wire attached and running to the surface. Subsequent measurements of the length of the wire give an indication of the densification rate of the snow and firn in that location. Despite the success of the coffee can technique, it only provides the densification rate at a single location, and it remains challenging to measure densification over large spatial grids. Thus the models described above are usually relied upon to estimate the densification rate for large areas.

The hydrological method of estimating mass balance involves differencing the total accumulation on a glacier with the total output. Accumulation is primarily due to precipitation, but in some areas can also contain significant contributions from blowing snow and avalanches. Another major source of accumulation in arctic glaciers is the refreezing of meltwater within the snow pack or firn layer. Ablation is primarily due to melt, however, evaporation and sublimation at the surface can also be significant, or even dominant in some areas. On ocean terminating glaciers, frontal ablation, primarily through iceberg calving, will also be a major contributor to ablation. The hydrological method forms the basis of the methods that are used to estimate regional mass balance in the CAI in this thesis. The most common methods for measuring ablation and accumulation will now be described.

Surface ablation may be measured through the use of ablation stakes. In this method, a hole is drilled several meters into the glacier surface, and a stake placed in the hole at the beginning of the melt season. The height of the surface, relative to the stake, is measured at the beginning of the season. Assuming that the stake was long enough to not melt out completely, the position of the surface is re-measured at the end of the season to find the height change of the surface. By assuming, or measuring a vertical density profile of the snow/firn/ice that has ablated, the height change can be converted into a mass change.

The method used to estimate accumulation depends on the timescale in which the measurement is required, and the facies zone in which the measurement is being made. For short term accumulations of less than a season duration, an ultra-sonic depth sensor may be placed on an automatic weather station to measure the distance to the snow surface. A very quick method for measuring accumulation is to probe the surface until a resistive surface is encountered. This surface is assumed to be the crust formed on the previous end of year summer surface, so measurement of the depth of this layer on the probe, allows estimation of the seasonal accumulation. However, there are several difficulties with this method: (i) snow density must be assumed or measured and (ii) in the dry snow zone, the previous year summer surface may not be obvious. Both of these issues may be overcome by digging a snow pit in which density measurements may be taken, and the previous year summer surface may be accurately distinguished. A snow pit also allows multiple years of accumulation to be investigated by digging through several years of accumulation, and analyzing the stratigraphy of the layers to estimate the accumulation for each year. On longer timescales, ice cores can be used to estimate mass balance. The analysis of core stratigraphy allows mass balance and melt records dating back hundreds of years with multi-year resolution (Koerner (1977), explained in greater detail in the next section).

A technique for measuring mean accumulation at points in the dry snow zone is down borehole gamma-spectroscopy. In 1962 atmospheric H-bomb tests were carried out, and the fallout was deposited as a radioactive layer in the CAI in 1963. Since then, the radioactive layer has been buried by accumulations on the ice caps. Measuring ice depth and density above this layer, allows estimating the total mass deposited at a point location since 1963 (Koerner and Taniguchi (1976)).

In the next section, some studies from the CAI that have used the techniques explained above are summarized.

1.4.2 Previous Studies in the CAI

Field measurements of mass balance in the CAI were pioneered by Fritz Muller on White Glacier, Axel Heiberg Island in the late 1950s and slightly later by Roy Koerner in the 1960s, who made measurements of the Devon, Meighen and Melville South Ice Caps. In Koerner's work, accumulations between the end of summer of one year, and the spring of the next, were measured at 1km intervals along several traverses across the ice cap. Depths were obtained by probing the snowpack, and measuring the depth of the previous end of summer crust, which offers firm resistance to a probe. Density measurements were made at 3km intervals (and showed little variation) along the transects, and allowed the depth measurements to be converted to accumulation masses. These accumulation measurements were first made in 1962,1963 and 1965 (Koerner (1966)). This efficient technique allowed maps of accumulation to be made, and links to be made with regional climate. Koerner (1970) detailed mass balance measurements made from 1961-1966 along the same traverse lines as

Koerner (1966). Mass balance was estimated using the accumulation maps of Koerner (1966) with ablation estimated from stake measurements made at 1-2km intervals. These ablation measurements were augmented by the placement of dye to estimate the formation of superimposed ice, and the use of percolation trays to estimate the volume of melt percolating through the current year's snow accumulation and refreezing in the firn layers of previous years. The dye method was used in the superimposed ice zone to prevent stakes from channelling melt water and therefore causing an over-estimation of superimposed ice formation. Percolation trays were used in the wet-snow zone, as percolating water penetrates through more than one year's accumulation in this zone (Paterson (1994), page 10). Koerner (1970) dug a 10m pit in the percolation zone, and through examination of the stratigraphy of melt years weas able to place this five year, spatially resolved mass balance record, in the context of a longer climatic balance record, at a single point, dating back to 1934. Koerner (1977) was able to trace stratigraphy in an ice core drilled at 1800 m.a.s.l on Devon ice cap to a depth of 150m. A proxy for summer melt for each year was found in the number and thickness of ice layers. Using this proxy, he was able to derive a 5 year resolution record back to 1254, which showed that the ice cap had experienced very warm summers since 1925, following colder summers between 1600 and 1925 (Koerner (1977)). The mass balance records of Koerner have been continued until present, and provide nearly 50 years of continuous measurement on the Devon, Meighen and Melville South Ice Caps (Koerner (2005)).

Mair et al. (2005) used the “bomb layer” technique to estimate 37 years of climatic balance on Devon ice cap. Average accumulation since 1963 was estimated by drilling boreholes and performing down borehole 137Cs gamma spectrometry at eight locations on the ice cap. These accumulations were interpolated to generate accumulation rate fields over the entire ice cap. To calculate ablation, and thus the climatic balance, a simple temperature index melt model was used (also known as a degree day model - see below). Air temperatures, the only input variable needed to simulate melt with temperature index melt models, were estimated by regressing shorter duration in-situ measurements of air temperature from the ice cap against long term temperatures recorded at Resolute Bay, Cornwallis Island. The relationship was then used to infer air temperatures on Devon ice cap from the Resolute Bay measurements, for the time periods for which in-situ measurements were not available. Thus, Mair et al. (2005) obtained both accumulation and ablation fields over Devon ice cap, and therefore were able to estimate 37 years of climatic balance.

With advances in technology, it has become possible to spatially resolve mass balance on much larger scales. One such method, as explained earlier, is the geodetic method, taking advantage of remotely sensed measurements of a glacier surface's height. Abdalati et al. (2004) flew repeated laser altimetry surveys over all the major GICs in CA in 1995 and 2000. They used a simple densification model to convert height differences to estimates of mass balance for the period 1995-2000. More recently, Burgess and Sharp (2008) used the difference in elevation between two digital elevation models, to obtain a more uniformly distributed assessment of surface height change on Devon ice cap. Elevations derived from 1960s aerial photography were compared to those derived from the 2005 NASA Airborne Topographic Mapper surveys. In this study the "coffee can" technique (Hamilton and Whillans (2000)) was used to estimate densification rates.

Mair et al. (2009) used a combination of down borehole 137Cs gamma spectrometry, ablation stakes and snow pit analyses to generate climatic balance estimates for the Prince of Wales Icefield from 1963-2003. As in Mair et al. (2005), the borehole measurements provided long term accumulation measurements. The ablation stake and snow pit measurements were made along two transects across the North and South of the Icefield respectively, giving good spatial coverage, but short duration measurements (May 2002-May 2003). By comparing the long term accumulation at 6 boreholes with the 2002-2003 short term climatic balance at nearby stake/snow pit sites, Mair et al. (2009) derived a multiplication factor to convert stake mass balance measurements for 2002-2003 to values representative of the 1963-2003 mean, which was used for locations with elevations above 800m. Mair et al. (2009) used a combination of elevation dependence and proximity to the North Water Polynya to extrapolate point climatic balance measurements to the entire ice field. This is explained in greater detail below.

Most recently, Gardner et al. (2011) presented 500m resolution mass balance estimates for the entire CAI from 2003-2009. In this study, three separate techniques were used for estimating the mass balance of the region: (i) Repeat satellite gravimetry (GRACE) (ii) repeat satellite laser altimetry (ICESat) - which is another "height change technique" - and (iii) a temperature index model, driven by 700mb air temperatures from the NCEP/NCAR R1 dataset (Kalnay et al. (1996)), downscaled using the variable lapse rate method of Gardner et al. (2009). The three techniques all showed that the CAI ice caps have recently had a highly negative mass balance rate, which accelerated over the study period. This was consistent with the findings of Sharp et al. (2011), who showed, based on field measurements of climatic balance, that 30-48% of the mass loss from four glaciers in the CAI since 1963 occurred between 2005 and 2010.

1.5 Modelling Climatic Balance

In order to model climatic balance, it is necessary to model melt and accumulation. In this section, I will introduce two methods for modelling melt, thus, setting the stage to explain how these methods have been applied on distributed grids over glaciers.

1.5.1 Modelling melt: Energy Balance Method

Neither the temperature nor the phase of a glacier surface will change, unless there is a net gain or loss of energy at the surface (Paterson (1994), page 58). When the surface temperature is below the pressure melting point of ice, a net gain of energy at the surface will cause the surface to heat up, whereas a net loss will cause the surface to cool. Generally, 2110 J of energy are required to raise the temperature of 1kg of ice by 1K. This quantity is known as the heat capacity of ice (c_p = 2110J kg^{-1} K^{-1}), and is the proportionality constant linking the energy input to a glacier surface, to the corresponding change in temperature of the surface (Paterson (1994), page 67).

If the surface of a glacier is heated (through a net gain in energy) to the pressure melting point, any subsequent gain in energy at the surface will cause melting. The phase change from solid to liquid requires energy. For water, it requires exactly 3.34×10^5J to melt 1kg of ice at atmospheric pressure, and this quantity is known as the latent heat of fusion of water, ($L_f = 3.34 \times 10^5$J kg^{-1}). Under melting conditions, L_f is the constant of proportionality between the available melt energy, and melt volume.

The energy balance at the surface of a glacier is computed by considering all of the inputs and outputs of energy at the surface. First I will present the energy balance equation, and then explain each of the terms. Conservation of energy requires closure of the energy balance, and this is expressed mathematically as:

$$Q_{RAD} + Q_H + Q_L + Q_G + Q_R + Q_N = 0 \tag{1.12}$$

In this expression (Hock (2005)), the symbols have the following meaning:

- Q_{RAD}: Net radiation flux, obtained from incoming and outgoing longwave and shortwave radiation fluxes
- Q_H: Sensible heat flux
- Q_L: Latent heat flux
- Q_G: Heat flux to the ground
- Q_R: Heat flux due to refreezing of rain
- Q_N: Energy flux available for melting snow or ice when the surface temperature (T_{ground}) $= 0°C$. When $T_{ground} < 0°C$, Q_N is the energy flux

available for changing T_{ground}

I use the positive inward sign convention for all terms in (4.14), thus energy fluxes to the surface are positive, whereas fluxes from the surface are negative.

Net radiation flux

Black body objects emit radiation at a distinct range of energies and wavelengths. The intensity of radiation emitted from a black body of temperature T, at wavelength λ, is given by Planck's law:

$$I(\lambda, T) = \frac{2hc^2(\lambda^{-5})}{e^{\frac{hc}{\lambda K_B T}} - 1} \tag{1.13}$$

Here, I is spectral radiance, h is Planck's constant, c is the speed of light and K_B is the Boltzmann constant. Specifically, I is the energy, per unit time, per unit area, emitted at wavelength λ, from a black body. By integrating (1.13) over all possible wavelengths, and considering the radiation emitted from the surface through a half-sphere, the total energy flux from the black body (P) can be formulated. The equation is known as the Stefan-Boltzmann law:

$$P = \epsilon\sigma T^4 \tag{1.14}$$

$$\sigma = \frac{2\pi^5 K_B^4}{15c^2h^3} \tag{1.15}$$

Where $\sigma = 5.67 \times 10^{-8} Js^{-1}m^{-2}K^{-4}$, is the Stefan-Boltzmann constant, and ϵ is the emissivity of the surface, assumed to be 1 for a black body.

Radiation at the surface of a glacier may be derived from solar, terrestrial or atmospheric sources. Due to the disparity between the temperatures of the surface of the sun (∼5800 K) and the earth (∼290 K), there is little overlap in the frequency spectra of the radiation they emit. Solar radiation, commonly referred to as shortwave radiation (SW), is emitted predominantly in the visible, near-visible infrared and near-visible ultraviolet parts of the spectrum ($\lambda \approx 0.15 - 4\mu$m). Due to lower emission temperatures, terrestrially sourced radiation is emitted predominantly in the thermal infrared part of the spectrum ($\lambda \approx 4 - 120\mu$m). Terrestrial/atmospheric radiation, due to its long wavelength compared to solar radiation, is commonly referred to as longwave radiation (LW). Since solar and terrestrial sources of radiation have such little overlap, they are measured and modelled separately from each other.

At the surface of a glacier, incident SW radiation may come directly from the sun (D_I), or from diffuse solar radiation that has been scattered in the atmosphere (D_s) or reflected from another terrestrial surface (D_t). The global incident SW radiation ($SW^{\downarrow}$) is the sum of these three sources, integrated over a half sphere above the glacier surface: $SW^{\downarrow} = D_I + D_s + D_t$. Outgoing SW radiation $SW^{\uparrow}$ is due to the reflection of $SW^{\downarrow}$, and is calculated as $SW^{\uparrow} = \alpha SW^{\downarrow}$. α is the surface albedo, and is the proportion of shortwave radiation reflected by the glacier surface. Albedo is highly dependent upon the specific conditions of the snow or ice surface. For snow, albedo depends upon the age, density, water and impurity content and grain size of the snow. For ice, albedo depends upon the crystal structure, impurity content, presence of bubbles, and presence of liquid water, amongst other factors.

Incident longwave radiation at the surface may be from either the atmosphere ($LW_s^{\downarrow}$) or the surrounding terrain ($LW_t^{\downarrow}$). Global incident longwave radiation is calculated, similarly to $SW^{\downarrow}$, by integrating the two sources over a half sphere above the glacier surface: $LW^{\downarrow} = LW_s^{\downarrow} + LW_t^{\downarrow}$. Since snow acts like a black body in the thermal infrared part of the spectrum, outgoing LW radiation is calculated using the glacier surface temperature in the Stefan Boltzmann law (1.14). Thus, the net radiation, Q_N is calculated as follows:

$$Q_{RAD} = SW^{\downarrow}(1-\alpha) + LW^{\downarrow} - \epsilon\sigma T_{ground}^4 \tag{1.16}$$

It should be noted that there is an additional outgoing longwave radiation flux (given by $(1-\epsilon)LW_t^{\downarrow}$), caused by the partial reflection of the incoming longwave radiation flux. However, this term is very small compared to the other terms in equation 1.16, and is therefore not included.

Turbulent Fluxes

The turbulent fluxes are the fluxes of sensible (Q_H) and latent (Q_L) heat at the glacier surface. The sensible heat flux at the glacier surface results from the process by which parcels of air from the surface are exchanged with parcels of air above the surface. If air at the surface is cooler than the air above, there will be a net gain in heat at the surface. On the other hand, if the air at the surface is warmer than the air above, then there will be a net loss of heat at the surface. Turbulence is modeled as conduction, with eddies taking the place of molecules (Paterson (1994), page 60).

$$Q_H = K_h \rho c_p \frac{\partial T}{\partial z} \tag{1.17}$$

K_h is the eddy diffusivity for heat, c_p is the specific heat capacity of air at constant pressure, and ρ is air density.

Latent heat, the heat flux due to the vertical flux of water vapor, is again visualized as resulting from the exchange of parcels of air between the surface and the the air above. When the surface has lower vapor pressure than the air above, the process brings air with higher vapor pressure to the surface. This induces deposition at the surface, and the latent heat released upon deposition causes the surface to gain energy. Conversely, if the surface has higher vapor pressure than the air above, as is often the case during melt, the turbulent mixing process brings less-moist air to the surface. The presence of dry(er) air at the surface promotes evaporation/sublimation, for which there is a latent heat requirement. The latent heat used by the process causes a net loss of energy from the surface. $Q_L$is treated using similar methods to Q_H, with the mass of water vapor per unit volume, m, taking the place of the heat energy per unit volume ($\rho c_p T$) (Paterson (1994), page 60-61).

$$Q_L = -L_v E = L_v K_w \frac{\partial m}{\partial z} = L_v K_w \left(\frac{-0.622\rho}{P} \right) \frac{\partial e}{\partial z} \tag{1.18}$$

Here, L_v is the latent heat of vaporization, K_w is the eddy diffusivity of water vapor and P is atmospheric pressure.

The eddy diffusivities for heat and water vapor exchange, K_h and K_w respectively, depend on the wind speed, surface roughness, and atmospheric stability above the glacier (Hock (2005)). The turbulent fluxes are difficult to measure, because they require measurements of temperature, vapor pressure, and windspeeds at multiple (preferably more than two) levels, which is expensive and difficult to accomplish on a glacier. Instead, researchers have used the bulk aerodynamic method to estimate the turbulent fluxes from measurements made at a single height above the surface (e.g. Braithwaite et al. (1998); Oerlemans and Klok (2002); Duncan (2011)). In this method, the surface is assumed to be at its triple point, and therefore, the surface assumes T=0°C and e=6.11mb (Hock (2005)). These assumptions, along with the assumption that windspeeds are zero at the ice surface, allow estimates of the turbulent fluxes to be made, from measurements at just one height above the ice surface.

Heat Flux into the Ground

The heat flux to the ground, Q_G is modeled with:

$$Q_G = K_{th} \frac{\partial T_{sub}(z_g)}{\partial z_g} \tag{1.19}$$

Where K_{th} is the thermal conductivity of the snow or ice below the glacier surface, T_{sub} is the subsurface temperature, and z_g is the depth below the surface (increasing downwards). Thus, if the surface of the glacier is warm compared to the layers below, it will lose heat; if it is colder than the layers below, it will gain heat.

Latent heat of freezing rain

There are glaciated areas in the CAI that receive substantial rain during the summer (Barr et al. (1966)). If rain falls in the wet snow, percolation, or dry snow zones, it will freeze inside the snowpack or underlying firn. As a result of this process, there is a release of latent heat, which is gained by the snowpack or firn. The latent heat of freezing rain is $Q_R = L_f P_{liq}$, where L_f is the latent heat of fusion, and P_{liq} is the rainfall rate per unit area.

Melt Energy

The residual from the energy budget, Q_M can be used in two ways (changing snowpack temperature, or melting), and thus, its name is a little misleading. As explained earlier, when the surface temperature is below the melting point, the energy flux either heats, or cools the surface, depending on sign. When the surface temperature is at the melt point, Q_M is used to melt the surface.

1.5.2 Modelling melt: Temperature Index Method

While the energy balance method of melt modelling provides a physical approach, it is often difficult to obtain the required measurements. Even if the required in-situ measurements are available, such measurements are very sensitive to instrument error, and assumptions must be made about atmospheric stability and surface properties (e.g. the surface roughness length). A simpler method to predict melt has been developed, which relies only on near surface temperature as an input (Reeh (1991)). The Temperature Index (TI) method exploits the fact that mean melt energy for a day is highly correlated to the mean near surface air temperature of that day, if the mean air temperature at 2m is $> 0°$ C (Braithwaite (1981); Ohmura (2001)). Using this method, seasonal melt is calculated as:

$$\Delta M = \sum_{i=\text{melt days}} \bar{\mathrm{T}}_i.\mathrm{K}_i \tag{1.20}$$

Where, on day i, $\bar{\mathrm{T}}_i$ is the mean air temperature and K_i (mm d^{-1} K^{-1}) is the degree day factor. The sum is calculated over all days with positive $\bar{\mathrm{T}}_i$. The degree day factor is the "constant" of proportionality linking melt volume and temperature. However, it should be noted that K_i is not constant, but varies significantly between different locations, and facies zones. Typically, separate values are assigned for snow and ice in TI models, to account for the inherent differences in the albedo and energy balance in the two cases (Ambach (1988)).

1.5.3 Upscaling models to large areas

We have described two methods to model glacier melt, which rely on different meteorological measurements. Here I describe methods that have been used to upscale the model results to the scale of an entire glacier, or even an entire region containing many glaciers. First I discuss methods to upscale the TI method, then I discuss the methods used in these studies to estimate precipitation, and finally, I consider methods used to estimate (over a large area) all of the variables needed for the energy balance approach.

In order to use a temperature index model on a distributed grid, temperature records must be interpolated to every point on that grid. Previous studies over Devon ice cap have used constant temperature lapse rates to interpolate in-situ temperature measurements onto a grid (e.g. Shepherd et al. (2007); Dowdeswell et al. (1997)). Mair et al. (2005) used air temperature data from a weather station in Resolute Bay as an approximation for temperature on icecaps. This was done by comparing in-situ measurements to the station data for a relatively short timespan when both were available. Anomalies between the two timeseries were calculated, and these anomalies were resampled and added at random, to the daily station temperature records for years in which there were no in-situ measurements. These corrected temperatures were used as an approximation for on-glacier temperatures. Gardner et al. (2009) found that using a constant lapse rate for interpolating temperatures in the CAI is not accurate, but rather the near surface lapse rate depends upon the upper (750mb) air temperature. Using variable temperature lapse rates to downscale the 750 mbar air temperature to the ice cap surface topography (Gardner et al. (2009)), Gardner et al. (2011) were able to estimate melt (as part of their climatic balance estimates) over a 500m grid for the entire CAI, for the period 2004-2009.

The methods described above allow studies to upscale (downscale in the case of Gardner et al. (2011)) temperature in order to compute melt estimates over entire glaciers. If the end goal is to model climatic balance, then the remaining challenge is to estimate precipitation on the same grid as melt. Here I describe some of the methods that have been used. On Devon ice cap, precipitation data from Koerner (1966) have been used to generate spatial maps of accumulation over the ice cap. Assuming the spatial distribution of precipitation to be constant through time, the longer term, but less spatially extensive precipitation records described by Koerner (2005) were used to find an offset for each year. Thus precipitation was estimated on a spatially extensive grid for a 40 year period (e.g. Shepherd et al. (2007)). These data were augmented by other precipitation data from beyond the perimeter of the icecap where in-situ measurements are logistically difficult, and therefore sparse. Precipitation data from 10 meteorological stations surrounding Devon ice cap were interpolated and combined with the precipitation grids, derived from Koerner (1966) and Koerner (2005), to form a combined precipitation grid. Mair et al. (2005) estimated the accumulation rate pattern by drilling 8 boreholes, and searching for the bomb layer, deposited in 1963 (see above). They interpolated these results to cover the entire ice cap. Gardner et al. (2011) used a bi-linear interpolation method to downscale NCEP/NCAR R1 $2.5° \times 2.5°$ reanalysis to the 500m grid used in their study. Thus, with the methods for upscaling precipitation, in combination with the methods for upscaling temperature, studies have been able to estimate climatic balance on regular grids, for Devon ice cap (Dowdeswell et al. (1997); Mair et al. (2005); Shepherd et al. (2007)), and for the entire QEI (Gardner et al. (2011)).

The examples above highlighted studies that have separately interpolated accumulation and ablation and combined the results to estimate climatic balance. Climatic balance has also been estimated at locations, and then upscaled to entire grids. Mair et al. (2009) calculated climatic balance for two transects on the Prince of Wales ice field in 2002-2003. By comparing with down borehole gamma spectroscopy measurements, they were able to estimate climatic balance from 1963-2003 along the transects (explained earlier). Mair et al.

(2009) used two methods to extrapolate climatic balance measurements over the entire icefield. In the first method, a second order polynomial was used to regress point climatic balance measurements with elevation. The process is done separately in four quadrants of the icecap, obtaining substantially different results for the 3 regression coefficients in each. The coefficient values are obtained at each point on a grid covering the icefield by using a kriging routine. Climatic balance at each point is estimated by applying the elevation from a DEM, with the extrapolated regression coefficients, to the regression relationship described above. In the second method used to extrapolate climatic balance to a regular grid covering the Prince of Wales icefield, a multiple regression is used. Climatic balance at each point was found to be linearly dependent upon the distance to the North Water Polynya, and quadratically dependent upon the elevation at that point. Thus, by using the DEM above, and calculating the distance to the North Water Polynya at each grid point, the multiple regression was used as a second method to determine climatic balance on a regular grid for the entire Prince of Wales icefield. Mair et al. (2009) simply take resultant climatic balance as the mean of the two methods. I now discuss methods for upscaling the energy balance melt model.

The challenges in interpolating just air temperature and precipitation, the minimum requirements for the simplest climatic balance models, are considerable. The challenges in interpolating the many meteorological variables required for energy balance melt modelling onto a spatially distributed, high resolution grid, covering a large region, are formidable. It has been done on a basin scale (e.g. Duncan (2011) on the Belcher glacier catchment of Devon ice cap), however, such studies are very expensive, logistically difficult, and the spatial and temporal coverages are limited.

For the ice sheets, researchers have used Regional Climate Models (RCMs) as physically based interpolators to downscale low resolution reanalysis datasets (e.g. the NCEP/NCAR R1 or final analysis datasets, or the North American Regional Reanalysis (NARR) dataset) to high resolution (Bromwich et al. (2001); Cassano et al. (2001); Guo et al. (2003); Hines and Bromwich (2008); Hines et al. (1997); Van Lipzig et al. (1999)). RCM output consists of a full suite of meteorological fields, suitable for running an energy balance model, or temperature index model. RCMs have been used for mass balance studies on Greenland (Box et al. (2004, 2006); Box and Rinke (2003); Ettema et al. (2009); Fettweis et al. (2005)) and Antarctica (Lenaerts et al. (2012)), and have provided high resolution (minimum of 11km for Greenland (Ettema et al. (2009)) and 27km for Antarctica (Lenaerts et al. (2012))) estimates of climatic balance, and its components over the entire ice sheets.

1.6 Regional Climate Models

In this thesis, I use two regional climate models. First, I use the Polar version of the Fifth-Generation Penn State/NCAR Mesoscale Model (Polar MM5). Later, I employ the Polar version of the Weather Research and Forecasting model (Polar WRF). In this section, I discuss the history of regional climate models, focussing on the models selected for use in this thesis, and the reasons they were chosen.

The history of MM5 has roots back as far as the late 1960's when R. Anthes developed a 3 layer hurricane model (Anthes and Johnson (1968)). In the

1970's Anthes and his students used the hurricane model as a basis for developing a mesoscale model (e.g. Anthes (1971); Diercks and Anthes (1976); Keyser and Anthes (1977)). In the ensuing years the model evolved from MM0 to MM3 (Anthes and Warner (1978); Warner et al. (1978); Warner (1989)). MM4 was developed jointly between Pennsylvania State University and NCAR in the 1980's as part of the Regional Acid Depositional Modelling Project. In the late 80's the Mesoscale and Microscale Meteorology (MMM) Division of the NCAR Earth System Laboratory (NESL) began to support MM4 as a community model through annual tutorials and workshops. The first successful demonstrations of an RCM were performed by Giorgi and Bates (1989) and Dickinson et al. (1989), in the Western United States. Since those studies, RCMs have been applied in all regions of the Earth, and have provided a means of downscaling low resolution reanalysis, or GCM datasets to high resolution grids (Wang et al. (2004)). In 1992 MM5 was released with improved physics and numerics, especially the new non-hydrostatic option. The final version of MM5, version 3.7.2, was released in May 2005 (Kuo (2004)). The successor to MM5, the Weather Research and Forecasting model (WRF) (Michalakes et al. (2004)), was released in 2006, and is currently in its third version.

1.6.1 Previous Work using Polar MM5 and Polar WRF

Several RCMs have been adapted for application to the polar regions (Cassano et al. (2001); Bromwich et al. (2001); Fettweis et al. (2005); Box and Rinke (2003); Hines and Bromwich (2008); Ettema et al. (2009)). In this section I explore some of the studies that have used Polar MM5 and Polar WRF.

Cassano et al. (2001) evaluated a series of Polar MM5 short term simulations over Greenland for a continuous one year period, between April 1997 and March 1998. This particular year was chosen to overlap with the Katabatic Wind and Boundary-Layer Front Experiment around Greenland during 1997 (KABEG'97) field experiment (Heinemann (1999)), and to coincide with the establishment of 14 GC-NET Automatic Weather Stations (AWS) collecting data simultaneously in the area. Model skill was primarily tested against near-surface data from the AWS for the entire annual cycle, but particular attention was given to the diurnal and synoptic time-scales. The European Centre for Medium Range Weather Forecasting (ECMWF) 2.5° Tropical Ocean-Global Atmosphere (TOGA) surface and upper air operational analysis provided the initial and boundary conditions for the simulations. ECMWF TOGA 1.125° global surface analysis were used to specify initial conditions for surface and sea surface temperature, deep soil temperature and snow cover. The presence/absence of sea ice was estimated from the sea surface temperature (SST), with sea ice considered to be present if SSTs were less than 271.7K. The model was run in a series of 48 hour runs. The first 24 hours of each run was treated as a spinup period and the output discarded. The second 24 hours of data from each run were used. The model was found to accurately forecast 48 hour atmospheric evolution in all seasons. It was found that the model predicts surface temperature and pressure with most skill, with slightly less skill in predicting water vapor mixing ratios and winds. The model used a fixed albedo over glaciated grid cells which creates errors in the net shortwave radiation budget in the melt season when, in reality, albedo is observed to decrease. During winter, when the radiation budget is dominated by longwave radiation and cloud interactions, the model showed a "surprising degree of skill" (Cassano et al. (2001)). However, the authors admit that thorough testing and validation with observations would be required to be confident of model performance, because the radiation budget could only be compared to data from one AWS. Cassano et al. (2001) conclude that as generally accurate model output is achieved through realistic physical processes, Polar MM5 may be used to provide a "self-consistent, high-resolution atmospheric forcing for other models". This study suggested that further analysis should include examination of cloud properties and their radiative effects, the surface energy balance and turbulent fluxes, and the boundary layer structure.

Bromwich et al. (2001) used two months (April and May 1997) of the Polar MM5 output used by Cassano et al. (2001) for comparison with the ECMWF operational analysis, AWS observations and aircraft observations (from the KABEG'97 experiment). Again Polar MM5 was shown to perform accurately in modelling both the large scale and low-level atmospheric features. The largest errors were found to occur in situations of low wind and high atmospheric stability, as it is difficult to parameterize turbulent eddy fluxes under these conditions (Bromwich et al. (2001)).

In April 2001, Monaghan et al. (2003) used 4 different models to aid the rescue of Dr. Ronald Shemenski from Antarctica. The models consisted of the ECMWF global forecast model, the National Centers for Environmental Prediction Aviation Model (AVN), NCAR global (regular) MM5 and Polar MM5. The most accurate models when compared to in situ observations were found to be those with the smallest grid spacing. Since the study was very close to the pole, the respective grid resolutions were important in determining grid spacing. The ECMWF and AVN models were run over grids with equal lat/lon spacings ($0.5^\circ \times 0.5^\circ$ and $1^\circ \times 1^\circ$ grid resolution respectively). Since physical distances between lines of longitude become small near the poles, the ECMWF had the highest overall grid resolution and performed with most skill, followed by Polar MM5, AVN, and the regular version MM5 with the lowest grid resolution and correspondingly lowest skill Although comparisons were only made for a short time period, Polar MM5 performed better than the regular MM5 for the Antarctic region. All of the models were shown to have more skill in the free atmosphere, which highlights the difficulty in successfully parameterizing the planetary boundary layer.

Guo et al. (2003) ran Polar MM5 over Antarctica and compared model output to in situ observations, upper-air data, and global atmospheric analyses, on diurnal to annual time-scales. The study showed that Polar MM5 captures both large and regional scale circulation features, with a generally small bias in most variables. Over all time-scales, Polar MM5 is most skillful in predicting surface pressure and temperature, wind direction and water vapor mixing ratio. The model was less skillful at predicting wind-speeds, as several of the strong wind events in the study were missed all together. Guo et al. (2003) concluded that although Polar MM5 simulations are impressive, additional model improvements are required. They specifically suggest that the vertical temperature profile would be better resolved by adding a higher altitude pressure level than the 100hpa level, which was the highest in their study.

Box et al. (2006), ran Polar MM5 over the Greenland ice sheet from 1988 to

2004 and used the output to study the variability of climatic mass balance over this time. The MM5 simulations were calibrated using various automatic weather station and glaciological datasets, detailed in the paper. Although errors both in the datasets forcing Polar MM5 and errors arising from the model itself made it impossible to achieve any "definitive" assessment of the temporal changes in surface mass balance, Box et al. (2006) showed a spatially coherent decrease in surface mass balance of the ice cap, and concluded that at least 100km^3 per year of melt was occurring over the period of the study.

As mentioned above, MM5 was replaced by a WRF in 2006. Since the release of WRF, researchers at Byrd Polar Research Center (BPRC) at the Ohio State University, have developed a Polar version of WRF called Polar WRF (Bromwich et al. (2009); Hines and Bromwich (2008); Hines et al. (2011)). Hines and Bromwich (2008) demonstrated that for June 2001, Polar WRF demonstrated slightly less skill in forecasting automatic weather station observed variables than Polar MM5. However, Polar WRF demonstrated increased skill in modelling the surface energy balance relative to Polar MM5, in all components except the sensible heat flux. Notably, the incoming longwave bias was reduced from -37 W m^{-2} in Polar MM5, to 3.5 W m^{-2} in Polar WRF.

1.7 Progression of chapters.

Regional Climate Model development has been progressing at a rapid pace, particularly over the last decade. This progress is driven by ever-improving computer resources, coupled with climate science rising to the forefront of political and scientific agendas in recent times. As such, the progression of papers in this thesis reflects the progress made in regional climate models between 2006 and 2012. In 2006, Polar MM5 represented the state of the art climate model for use in the Arctic, and hence the first chapter uses that model. However, when work began on the second and third chapters, Polar WRF had been developed and tested by researchers at the BPRC. In order to remain current, I began using Polar WRF which, along with RACMO2 is now the state of the art RCM for use in the polar regions.

1.7.1 Chapter 2: Assessing the performance of Polar MM5 over Devon Ice Cap, and Development of a Temperature Dependent Albedo Parameterization.

RCMs have been run over Greenland and areas of Antarctica, and estimates of climatic balance have been calculated from the output (Box et al. (2004, 2006); Box and Rinke (2003); Ettema et al. (2009); Fettweis et al. (2005)). The models generally performed with high accuracy over the relatively flat interiors of the large ice sheets. However, the models (run with a maximum resolution of 11km (Ettema et al. (2009))) were unable to sufficiently resolve the steep topographic gradients at the edge of the ice sheets (Van Den Broeke et al. (2008)). Given the relatively small scale of the CAI ice caps compared to the large ice sheets, a greater proportion of the ice area is located in the topographically complex marginal areas. Given the difficulties experienced at the steep edges of the ice sheets, the objective of Chapter 2 is to assess the ability of an RCM to operate in the complex topography of the CAA.

In Chapter 2, I assessed the performance of Polar MM5 over Devon Ice Cap.

The model was run for the summer of 2008, using four nested domains, with the innermost domain at 3km resolution, centred over Devon Ice Cap. The model was re-initiated every 48 hours, with a 24 hour spinup time. Re-initialization was required to prevent model drift, which is when, just as in weather forecasts, the model diverges from reality (personal communication with Aaron Wilson, BPRC). The method has been commonly used in other studies in Greenland (e.g. Cassano et al. (2001)) to prevent model drift. In Chapter 2, I was able to diagnose biases in the surface shortwave and longwave radiation budgets, identify patterns in the biases with respect to elevation, and identify deficiencies within Polar MM5 that could be causing such patterns. I also determined that model parameterizations of cloud cover and albedo, were likely causes of model bias in the radiation budget. Given that glacier albedo is simply set as a constant value of 0.8 in Polar MM5 (unless a satellite derived albedo is used e.g. Box et al. (2006)), albedo was determined to be an obvious area for model improvement.

Chapter 2 concludes by presenting an albedo parameterization for future implementation into the Polar MM5 framework. The parameterization takes into account a fundamental limitation of repeatedly restarting the model, which is that the model has no ”memory” beyond each 48 hour period. Given this limitation, the parameterization developed improves upon the current constant albedo value, by utilizing a sigmoidal relationship between the daily mean temperature and daily albedo. This relationship was deemed suitable for coding inline in Polar MM5, because it does not require any variables to be passed from one 48 hour run to the next, and despite its simplistic nature, represents a significant improvement over using a single, constant albedo value.

Following the work of Chapter 2, the objective for Chapter 3, was to implement the temperature dependent albedo parameterization into Polar MM5. However, given the subsequent development and validation of Polar WRF, Chapter 3 instead employed that RCM.

1.7.2 Chapter 3: Development of an ice sheet albedo parameterization for use in Polar WRF.

The Weather Research and Forecasting model (WRF) is the replacement for MM5 and is the model that will be maintained and used by researchers in the future. Thus, the original intent of Chapter 3, to improve the albedo parameterization in Polar MM5, was rendered obsolete with the development and widespread use of Polar WRF. Therefore, it was decided to change models for the remainder of the thesis, so that the work may be included in future releases of Polar WRF, and become a useful contribution to the Polar WRF community.

WRF is the successor to MM5, and shares much of the same code, but with an improved model framework. I therefore use the results found in Chapter 2 using Polar MM5, (namely the requirement for an improved albedo parameterization), as motivation for the work in Chapter 3. In Chapter 3, an ice sheet and glacier specific albedo parameterization is developed and fully integrated into the Polar WRF modelling system. By running the parameterization fully inline within the model, feedbacks are enabled between albedo and the model climate.

In Chapter 3, I was able to implement a far more ambitious albedo parameterization than that presented in Chapter 2. The key difference is that I was able to take variables from the output of one 48 hour run, and use them to initiate the next run. Thus, key surface properties used by the albedo parameterization were able to retain a “memory” of more than one 48 hour run. The parameterization accounts for the following physics:

- Snow aging, the rate of which is temperature dependent
- Increases in albedo due to fresh snow fall
- Shortwave radiation penetration into the snow pack.

The western margin of the Greenland ice sheet was chosen as the region of study for Chapter 3, since many previous studies have focussed on this region. Specifically, the existence of a cloud mask over this region (provided by Jason Box and David Decker, BPRC), allowed comparison with the MODIS MOD10A1 daily albedo product (Stroeve et al. (2006)).

The results of the chapter demonstrated the ability of the parameterization developed to reproduce elevation profiles of MOD10A1 albedo in both a cold year and a warm year. They also demonstrated that running the parameterization inline within Polar WRF altered the modelled climate significantly. The best calibration of the parameterization in Chapter 3, was chosen for use in Chapter 4.

1.7.3 Chapter 4: Modelling surface mass balance in the Northern Canadian Arctic Archipelago using output from Polar WRF.

The objective of Chapter 4 was to run Polar WRF, with the albedo parameterization developed in Chapter 3, over the Queen Elizabeth Islands (QEI) in the CAI. The QEI include all of the Canadian Arctic Islands north of the Parry Channel. Polar WRF was run at 6km resolution for 2001-2008, and is the first regional scale RCM study for the QEI. Using the output, I was able to use both the energy balance, and temperature index approaches, to estimate melt. Our results were consistent with previous geophysically and model-based regional mass balance estimates (Gardner et al. (2011)), and the acceleration of melt and negative mass balance after 2005 (Sharp et al. (2011)). Analysis of the seven major icecaps in the QEI allowed us to study regional trends in the climatic balance components. I was able to show that correlations of melt records between ice caps increased during the study period, whereas for precipitation, the correlations decreased from 2003-2008. I interpreted the findings as indicating that (i) the extreme melt taking place in the QEI is due to large high pressure systems being present over the entire region for extended periods in the summer, and (ii) as the climatic balance decreased during the study, precipitation, which also decreased, was delivered by smaller scale disturbances, which did not significantly interrupt melting over the entire QEI.

Bibliography

Abdalati, W., W. Krabill, E. Frederick, S. Manizade, C. Martin, J. Sonntag, R. Swift, R. Thomas, J. Yungel, and R. Koerner. "Elevation changes of ice caps in the Canadian Arctic Archipelago." *Journal of Geophysical Research* 109 (2004).

Ambach, W. "Interpretation of the positive-degree-days factor by heat balance characteristics – West Greenland." *Nordic Hydrology* 19 (1988).

Anderson, D. L. and C. S. Benson. "The Densification and Diagenesis of Snow." *Ice and Snow*. Ed. W.D. Kingery. MIT Press, 1963.

Anonymous. "Mass-balance terms.." *Journal of Glaciology* 8 (1969): 3–7.

Anthes, R. A. "A Numerical Model of the Slowly Varying Tropical Cyclone in Isentropic Coordinates." *Monthly Weather Review* 99 (1971).

Anthes, R. A. and D. R. Johnson. "Generation of Available Potential Energy in Hurricane Hilda (1964)." *Monthly Weather Review* 96 (1968).

Anthes, R. A. and T. T. Warner. "Development of hydrodynamic models suitable for air pollution and other mesometeorological studies." *Monthly Weather Review* 106 (1978).

Arendt, A. "Approaches to Modelling the Surace Albedo of a High Arctic Glacier." *Geografiska Annaler* 81 A (1999): 477–487.

Arendt, A. and M. Sharp. "Energy balance measurements on a Canadian High Arctic glacier and their implications for mass balance modelling." *Interactions Between the Cryosphere, Climate and Greenhouse Gases (Proceedings of IUGG 99 Symposium HS2, Birmingham, July 1999).* 1999.

Barr, W., R. C. Brooke, D. J. T. Hussel, R. H. King, and R M Koerner. "Devon Island programs 1966.." *Arctic* 20 (1966): 44–49.

Box, J. E., D. H. Bromwich, and L.S. Bai. "Greenland ice sheet surface mass balance 1991–2000: Application of Polar MM5 mesoscale model and in situ data." *Journal of Geophysical Research* 109 (2004).

Box, J. E., D. H. Bromwich, B. A. Veenhuis, L. S. Bai, J. C. Stroeve, J. C. Rogers, K. Steffen, T. Haran, and S. H. Wang. "Greenland ice sheet surface mass balance variability (1988-2004) from calibrated polar MM5 output." *Journal of Climate* 19 (Jun 2006): 2783–2800.

Box, J. E. and A. Rinke. "Evaluation of Greenland Ice Sheet Surface Climate in the HIRHAM Regional Climate Model Using Automatic Weather Station Data." *Journal of Climate* 16 (2003).

Braithwaite, R. J. "On glacier energy balance, ablation and air temperature.." *Journal of Glaciology* 27 (1981): 381–391.

Braithwaite, R.J., T. Konzelmann, C. Marty, and O.B. Olesen. "Reconnaisance study of glacier energy balance in north Greenland, 1993–94." *Journal of Glaciology* 44 (1998): 239–247.

Bromwich, D. H., J. J. Cassano, T. Klein, G. Heinemann, K. M. Hines, K. Steffen, and J. E. Box. "Mesoscale modeling of katabatic winds over Greenland with the Polar MM5." *Monthly Weather Review* 129 (2001): 2290–2309.

Bromwich, D.H., K. M. Hines, and L. S. Bai. "Development and testing of Polar Weather Research and Forecasting model: 2. Arctic Ocean." *Journal of Geophysical Research* 114 (2009).

Burgess, D and M Sharp. "Recent changes in thickness of the Devon Island ice cap, Canada." *Journal of Geophysical Research* 113 (2008).

Cassano, J. J., J. E. Box, D. H. Bromwich, L. Li, and K. Steffen. "Evaluation of polar MM5 simulations of Greenland's atmospheric circulation." *Journal of Geophysical Research* 106 (Dec 2001): 33867–33889.

Church, J. A. "Changes in Sea Level." *Climate Change* (2001).

Cogley, G J and W P Adams. "Mass balance of glaciers other than the ice sheets." *Journal of Glaciology* 44 (1998).

Cogley, J.G., R. Hock, L.A. Rasmussen, A.A. Arendt, A. Bauder, R.J. Braithwaite, P. Jansson, G. Kaser, M. Möller, L. Nicholson, and M. Zemp. "Glossary of Glacier Mass Balance and Related Terms." *IHP-VII Technical Documents in Hydrology.* 2011.

Colgan, W., J. Davis, and M. Sharp. "Is the high-elevation region of Devon Ice Cap thickening?." *Journal of Glaciology* 54 (2008): 428–436(9).

Dickinson, R. E., R.M. Errico, F Giorgi, and G. T. Bates. "A Regional Climate Model for the Western United States." *Climatic Change* (1989).

Dierks, J. W. and R. A. Anthes. “Diagnostic Studies of Spiral Rainbands in a Nonlinear Hurricane Model.” *Journal of Atmospheric Sciences* 33 (1976): 959–975.

Dowdeswell, J.A., J.O. Hagen, H. Bjornsson, A.F. Glazovsky, W.D. Harrison, P. Holmlund, J. Jania, R.M. Koerner, B. Lefauconnier, C.S.L. Ommanney, and R.H. Thomas. “The Mass Balance of Circum-Arctic Glaciers and Recent Climate Change.” *Quaternary Research* 48 (07 1997): 1–14(14).

Duncan, A. Spatial and Temporal Variations of the Surface Energy Balance and Ablation on the Belcher Glacier, Devon Island, Nunavut, Canada. Master’s thesis, University of Alberta, 2011.

Dyurgerov, M., M. Meier, and R. Armstrong. “Glacier Mass Balance and Regime: Data of Measurements and Analysis.” *University of Colorado Institute of Arctic and Alpine Research Occasional Paper 55* (2002).

Dyurgerov, M., M. Meier, and R. Armstrong. “Mass Balance of Mountain and Sub-Polar Glaciers Outside the Greenland and Antarctic ice sheets..” *Supplement to the M. Dyurgerov Occasional Paper 55, 2002.* (2005).

Ettema, J, M R. van den Broeke, E van Meijgaard, W Jan van de Berg, J L. Bamber, J E. Box, and R C. Bales. “Higher surface mass balance of the Greenland ice sheet revealed by high-resolution climate modeling.” *Geophys. Res. Lett.* 36 (06 2009).

Fettweis, X, H Gallée, L Lefebre, and J.P van Ypersele. “Greenland surface mass balance simulated by a regional climate model and comparison with satellite derived data in 1990-1991.” *Climate Dynamics* (2005): 623–640.

Gardner, A. S., G. Moholdt, B. Wouters, G. J. Wolken, D. O. Burgess, M. J. Sharp, G. Cogley, C. Braun, and C. Labine. “Sharply increased mass loss from glaciers and ice caps in the Canadian Arctic Archipelago.” *Nature* 473 (April 2011): 357–360.

Gardner, A. S., M. J. Sharp, R. M. Koerner, C. Labine, S. Boon, S. J. Marshall, D. O. Burgess, and D. Lewis. “Near-Surface Temperature Lapse Rates over Arctic Glaciers and Their Implications for Temperature Downscaling.” *Journal of Climate* 22 (2011/11/04 2009): 4281–4298.

Giorgi, G. and G. T. Bates. “The Climatological Skill of a Regional Climate Model Over Complex Topography.” *Monthly Weather Review* 117 (1989).

Guo, Z. C., D. H. Bromwich, and J. J. Cassano. “Evaluation of Polar MM5 simulations of Antarctic atmospheric circulation.” *Monthly Weather Review* 131 (Feb 2003): 384–411.

Hamilton, G. S. and I. M. Whillans. “Point measurements of mass balance of the Greenland Ice Sheet using precision vertical Global Positioning System (GPS) surveys.” *Journal of Geophysical Research* 105 (2000): 16295–16301.

Heinemann, G. “The KABEG’97 field experiment: An aircraft-based study of katabatic wind dynamics over the Greenland ice sheet.” *BOUNDARY-LAYER METEOROLOGY* 93 (Oct 1999): 75–116.

Herron, M. M. and C. C. Langway. “Firn Densification: An Empirical Model.” *Journal of Glaciology* 25 (1980).

Hines, K M. and D H. Bromwich. “Development and Testing of Polar Weather

Research and Forecasting (WRF) Model. Part I: Greenland Ice Sheet Meteorology..” *Monthly Weather Review* 136 (2008): 1971–1989.

Hines, K. M., D. H. Bromwich, L. S. Bai, M. Barlage, and A. G. Slater. “Development and Testing of Polar WRF. Part III: Arctic Land*.” *Journal of Climate* 24 (2011): 26–48.

Hines, K. M., D. H. Bromwich, and Z. Liu. “Combined global climate model and mesoscale model simulations of Antarctic climate.” *Journal of Geophysical Research* 102 (Jun 1997): 13747–13760.

Hines, K.M., D.H. Bromwich, and R.I. Cullather. “Evaluating moist physics for Antarctic mesoscale simulations.” *Annals of Glaciology* 25 (1997): 282–286.

Hock, R. “Glacier melt: a review of processes and their modelling.” *Progress in Physical Geography* 29 (2005): 362–391.

Jacob, T., J. Wahr, T. Pfeffer, and S. Swenson. “Recent Contributions of Glaciers and Ice Caps to Sea Level Rise.” *Nature* 10847 (2012).

Kalnay, E., M. Kanamitsu, R. Kistler, W. Collins, D. Deaven, L. Gandin, M. Iredell, S. Saha, G. White, J. Woollen, Y. Zhu, A. Leetmaa, R. Reynolds, M. Chelliah, W. Ebisuzaki, W.Higgins, J. Janowiak, K. C. Mo, C. Ropelewski, J. Wang, Roy Jenne, and Dennis Joseph. “The NCEP/NCAR 40-Year Reanalysis Project.” *Bulletin of the American Meteorological Society* (1996).

Keyser, D. K. and R. A. Anthes. “The Applicability of a Mixed Layer Model of the Planetary Boundary Layer to Real-Data Forecasting." *Monthly Weather Review* 105 (1977).

Koerner, R. M. "Accumulation on the Devon Island ice cap, Northwest Territories, Canada." *Journal of Glaciology* 6 (1966): 383–392.

Koerner, R M. "The Mass Balance of Devon Island Ice Cap, Northwest Territories, Canada 1961-66." *Journal of Glaciology* 9 (1970): 325–336.

Koerner, R. M. "Devon Island Ice Cap: Core Stratigraphy and Paleoclimate.." *Science* 196 (04 1977): 15–18.

Koerner, R. M. "Mass balance of glaciers in the Queen Elizabeth Islands, Nunavut, Canada." *Annals of Glaciology* 42 (2005).

Koerner, R. M. and H. Taniguchi. "Artificial radioactivity layers in the Devon Island ice cap, Northwest Territories, Canada." *Journal of Earth Sciences* 13 (1976).

Kuo, B. *The Penn State/NCARMesoscale Model: MM5.* 10 2004.

Lenaerts, J. T. M., M. R. van den Broeke, W. J. van de Berg, E. van Meijgaard, and P. K. Munneke. "A new, high-resolution surface mass balance map of Antarctica (1979–2010) based on regional atmospheric climate modeling." *Geophysical Research Letters* 39 (2012).

Mair, D., D. Burgess, and M. Sharp. "Thirty-seven year mass balance of Devon Ice Cap, Nunavut, Canada, determined by shallow ice coring and melt modelling." *Journal of geophysical research* 110 (2005).

Mair, D., D. Burgess, M. Sharp, J. A. Dowdeswell, T. Benham, S. Marshall, and F. Cawkwell. "Mass balance of the Prince of Wales Icefield, Ellesmere Island, Nunavut, Canada." *Journal of Geophysical Research* 114 (2009).

Manning, K.W. and C. A.A. Davis. "Verification and Sensitivity Experiments for the WISP94 MM5 Forecasts." *Weather and Forecasting* 12 (December 1997): 719–735.

Michalakes, J., J. Dudhia, D. Gill, T. Henderson, J. Klemp, W. Skamarock, and W. Wang. "The Weather Reseach and Forecast Model: Software Architecture and Performance." *proceedings of the 11th ECMWF Workshop on the Use of High Performance Computing In Meteorology, 25-29 October 2004, Reading, U.K.*. Ed. George Mozdzynski 2004.

Monaghan, A. J., D. H. Bromwich, H. L. Wei, A. M. Cayette, J. G. Powers, Y. H. Kuo, and M. A. Lazzara. "Performance of weather forecast models in the rescue of Dr. Ronald Shemenski from the South Pole in April 2001." *Weather and Forecasting* 18 (04 2003): 142–160.

Oerlemans, J. and E. J. Klok. "Energy Balance of a Glacier Surface: Analysis of Automatic Weather Station Data from the Morteratschgletscher, Switzerland." *Arctic, Antarctic and Alpine Research* 34 (2002): 477–485.

Ohmura, A. "Physical basis for the temperature-based melt-index method.." *American Meteorological Society* (04 2001): 753–761.

Paterson, W. S. B. *The Physics of Glaciers (3rd edn. ed.)*. Pergamon, Oxford, 1994.

Radic, V and R Hock. “Regional and global volumes of glaciers derived from statistical upscaling of glacier inventory data.” *Journal of Geophysical Research* 115 (2010).

Reeh, N. “Parameterization of melt rate and surface temperature on the Greenland ice sheet.” *Polarforschung* 59 (1991): 113–128.

Reeh, N., D. A. Fisher, R. M. Koerner, and H. B. Clausen. “An Empirical Firn-Densification Model Comprising of Ice Lenses.” *Annals of Glaciology* 42 (2005).

Sharp, M., D. O. Burgess, J. G. Cogley, M. Ecclestone, C. Labine, and G. J. Wolken. “Extreme melt on Canada’s Arctic ice caps in the 21st century.” *Geophysical Research Letters* 38 (2011).

Shepherd, A., D U Zhijun, T. J Benham, J. A Dowdeswell, and E. M. Morris. “Mass balance of Devon Ice Cap, Canadian Arctic.” *Annals of Glaciology* 46 (2007): 249–254(6).

Stroeve, J C., J E. Box, and T Haran. “Evaluation of the MODIS (MOD10A1) daily snow albedo product over the Greenland ice sheet.” *Remote Sensing of Environment* 105 (2006): 155 – 171.

Van De Berg, W. J., M. R. van den Broeke, C. H. Reijmer, and E. van Meijgaard. “Reassessment of the Antarctic surface mass balance using calibrated output of a regional atmospheric climate model.” *Journal of Geophysical Research* 111 (2006).

Van Den Broeke, M., P. Smeets, J. Ettema, and P. Kuipers Munneke. “Surface radiation balance in the ablation zone of the west Greenland ice sheet." *J. Geophys. Res.* 113 (2008).

Van Lipzig, N.P.M, E. Van Meijgaard, and Oerlemans. J. "Evaluation of a Regional Atmospheric Model Using Measurements of Surface Heat Exchange Processes from a Site in Antarctica." *Monthly Weather Review* 127 (1999): 1994–2011.

Wang, Y., L. R. Leung, J. L. McGregor, D. K. Lee, W. C. Wang, Y. Ding, and F Kimura. "Regional Climate Modelling: Progress, Challenges, and Prospects." *Journal of the Meteorological Society of Japan* 82 (2004): 1599–1628.

Warner, T. T. "Mesoscale atmospheric modeling." *Earth-Science Reviews* 26 (1989): 221–251.

Warner, T. T., R. A. Anthes, and A.L.McNab. "Numerical simulations with a three dimensional mesoscale model." *Monthly Weather Review* 106 (1978).

Wilkinson, D. S. "A Pressure-Sintering Model for the Densification of Polar Firn and Glacier Ice." *Journal of Glaciology* 34 (1988).

Willis, J.K., D.P. Chambers, C.-Y. Kuo, and C.K. Shum. "Global sea level rise: Recent progress and challenges for the decade to come.." *Oceanography* 23 (2010): 26–35.

CHAPTER 2

Analysis of Polar MM5 at 5 sites on Devon Island Ice Cap, and Development of a Temperature Based Albedo Parameterization

2.1 Introduction

Devon ice cap is one of the largest ice masses in the Canadian Arctic Archipelago (CAA), with an area of 12050 km^2, volume of 3980 km^3 and a maximum recorded ice thickness of 880m near the summit (Dowdeswell et al. (2004)). Previous studies have illustrated the important link between regional climate patterns and the climatic balance on this ice cap (Holmgren (1971); Alt (1978); Koerner (1977)). More recently flow and thinning rates have been estimated from field observations and remote sensing (Burgess et al. (2005); Burgess and Sharp (2008); Colgan et al. (2008); Mair et al. (2005)). Using these types of data in conjunction with statistically based methods, the mass balance over the past three decades has been quantified (Shepherd et al. (2007); Dowdeswell et al. (1997); Mair et al. (2005)). However, these studies suffer from either short duration, lack of temporal resolution or incomplete coverage of the ice cap. Most recently, Gardner et al. (2011) used 3 separate methods (mass budget model, repeat satellite laser altimetry (ICESat) and repeat satellite gravimetry (GRACE)) to estimate climatic balance on a high resolution grid over the entire CAA for 2004 to 2009. The study showed dramatic acceleration of mass loss from glaciers and ice caps in the CAA between the periods 2004-2006 and 2007-2009. In addition, it demonstrated that results from the statistically based temperature index model of Gardner et al. (2009) compared favourably to the results of two independent remotely sensed estimates of mass balance.

Researchers have adapted and tuned regional climate models (RCMs) to be run over the polar regions (Bromwich et al. (2001); Cassano et al. (2001); Guo et al. (2003); Hines et al. (1997); Monaghan et al. (2003); Fettweis et al. (2005); Gallée and Duynkerke (1997); Van Lipzig et al. (1999)). RCMs offer a physically based method to obtain values of distributed atmospheric variables on regularly spaced grids. This method, known as dynamic downscaling, allows meteorological fields to be simulated, at high resolution, over entire ice masses. Temporal resolution of output is high (typically ~3 hourly) using this method. Any time period, for which there are available input data, may be analysed, and there is potential for future forecasting by using General Circulation Model (GCM) output as the input data. RCM output has been used, with a full energy balance melt model, to calculate climatic balance over the Greenland Ice Sheet (Box et al. (2004, 2006)). Although these studies enabled researchers to study mass balance on a hitherto unachievable resolution, it was necessary to correct the model for significant bias before useful output was obtained.

The primary objective of this study is to assess the applicability of using an RCM to model the climate over the complex topography, characteristic of the Canadian Arctic Islands. To do so, we run a high resolution RCM over the Devon Island ice cap for the summer (June, July and August) of 2008. Model output is compared with measurements made at 5 automatic weather stations located on the Ice Cap. We assess model skill in predicting near surface temperature, incoming and outgoing shortwave and longwave radiation fluxes. The study aims to identify reasons for biases that we find in the comparisons. Albedo (α) prediction over glaciers has been previously approximated very crudely within regional climate models (e.g. a constant value used within the model, and satelite derived α used to correct the energy balance after the model has run (Box et al. (2004, 2006))). Thus, this study also explores the potential for improving the α parameterization within an RCM.

2.2 Methods

In this study we analyse Polar MM5 (introduced in the next section) simulations of surface energy balance by comparison with five Automatic Weather Stations (AWS) over Devon ice cap. The study focuses on the incoming and outgoing shortwave (SW$\downarrow$ and SW$\uparrow$) and longwave (LW$\downarrow$ and LW$\uparrow$), and net all-wave (NAW) radiation fluxes at the glacier surface. NSW and NLW refer to the net of the SW and LW fluxes:

$$\mathrm{NAW} = \mathrm{NSW} + \mathrm{NLW} \tag{2.1}$$

$$\mathrm{NSW} = \mathrm{SW}\downarrow - \mathrm{SW}\uparrow \tag{2.2}$$

$$\mathrm{NLW} = \mathrm{LW}\downarrow - \mathrm{LW}\uparrow \tag{2.3}$$

We also investigate the modelled near surface temperature (T). A relationship between modelled near T and measured α will be established. From this relationship, a possible α parameterization for use within a regional climate model will be suggested.

2.2.1 Polar MM5 Setup

The Fifth-Generation National Center for Atmospheric Research/Pennsylvania State Mesoscale Model (MM5), that has been modified for use in the Polar regions by the Polar Meteorology Group of the Byrd Polar Research Center at The Ohio State University (Bromwich et al. (2001); Cassano et al. (2001); Guo et al. (2003)) (known as Polar MM5) will be used for this study. It is one of the most highly tested RCMs, and has been specifically adapted for use in the polar regions.

Polar MM5 has been tested over both Antarctica and Greenland (Bromwich et al. (2001); Cassano et al. (2001); Guo et al. (2003)). Results of these analyses have been used to calculate climatic balance (Box et al. (2004, 2006)) over Greenland, using energy balance methods. A thorough description of the model may be found in Grell et al. (1994). Smaller ice masses, such as those found in the Canadian High Arctic, have a greater percentage of steep and complex terrain than the largely flat Greenland and Antarctic ice sheets. Thus, though the application of polar MM5 to the Canadian High Arctic is central to the goals of this study, it may be expected that the model will not perform with the same degree of accuracy over the Canadian High Arctic as it has over the polar ice sheets. Indeed, Cassano et al. (2001) illustrated that the model was less accurate at the edges of the ice sheets where the terrain becomes steep and more complex, and this is further supported by Van Den Broeke et al. (2008). To minimize this problem, Van Den Broeke et al. (2008) recommended running RCMs at sub-10 km grid resolution in areas of steep gradients.

Taking this recommendation, Polar MM5 was run at a 3 km resolution for the current study (explained in more detail below). Running Polar MM5 at such high resolution requires using the non-hydrostatic version of the model, which runs roughly 12% slower than the hydrostatic version. A thorough description of MM5 physics may be found in Grell et al. (1994).

In order to run MM5 at a computationally realizable grid size certain physical variables and processes must be parameterized at the sub-grid scale. The most important examples of these parameterizations in MM5 include: cumulus convection, cloud microphysics, turbulent fluxes in the planetary boundary layer (PBL), and radiation balance and thermal properties of the ground. These are the main processes that have been revised and tuned for Polar MM5 (Cassano et al. (2001)). The large scale precipitation and cloud processes in Polar MM5 are represented using a slightly modified version, to counteract a cloudy bias found in previous sensitivity studies (Hines et al. (1997); Manning and Davis (1997)), of the Reisner explicit microphysics parameterization (Reisner et al.

(1998)). Sub-grid cloud parameterization is performed by the Grell cumulus parameterization scheme, (Grell (1993); Grell et al. (1994)). In this scheme, clouds are modeled as two steady-state circulations, but there is no mixing between cloud and environmental air except at the bottom and top of the circulations. Turbulent fluxes in the planetary boundary layer are given by the 1.5-order turbulence scheme from the NCEP Eta model (Janjic (1994)). The longwave and shortwave radiative transfers through the atmosphere are calculated with a modified version of the NCAR Community Climate Model, version 2 (CCM2) radiation parameterization (Hack et al. (1993)). The modification to the scheme involves using predicted cloud water and ice mixing ratios from the above mentioned Reisner explicit microphysics parameterization scheme in place of the CCM2 values. Such modification combats a problem of overestimation of downwelling longwave radiation fluxes.

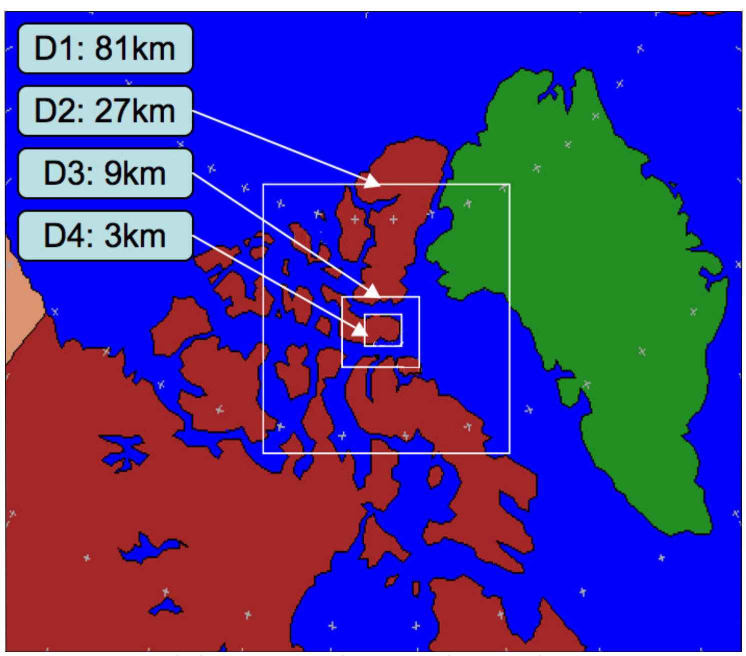

Figure 2.1: Four nested domains used to get 3km resolution over Devon ice cap.

As in Bromwich et al. (2001); Cassano et al. (2001); Guo et al. (2003) and Box et al. (2004, 2006), the simulations were run in “forecast” mode, which involves many 48-hour simulations to fill the desired time period. Each time period consists of a 24-hour spin up, to allow the model to equilibrate, followed by 48 hours of simulation. This method combats model drift over time. The simulations use 4 nested domains to “zoom in” on Devon Island at a 3km resolution (Figure 2.1). The model takes initial and boundary conditions from the 1 ° NCEP final analysis dataset, firstly in a large domain of 81km resolution, (61×49 grid points, time step 180s), and then it downscales to subsequent nested domains of 27km resolution (61×61 grid points, time step 180s), 9km resolution (58×49 grid points, time step 90s), and finally 3km resolution (82×64 grid points, time step 30s). Each domains had 24 terrain following vertical sigma coordinates. Model output is every 3 hours, so that diurnal cycles may be accurately resolved, which was a concern raised by Box et al. (2004) when model output was 6 hourly.

2.2.2 In-Situ Validation Data

Validation of Polar MM5 output is focused on the summer of 2008, the time-period with the most comprehensive AWS data over Devon ice cap. Figure 2.2 shows the location of the five AWS on the ice cap. Sites 1, 2 and 3 are located along a transect running from the ice cap summit to Croker Bay in the South West of the ice cap. Sites 4 and 5 are located on the Belcher Glacier in the North East of the ice cap. All of the stations have measured incoming and outgoing longwave and shortwave radiation. Sites 2,4 and 5 also have 2m air temperature measurements. The sites are numbered in order of

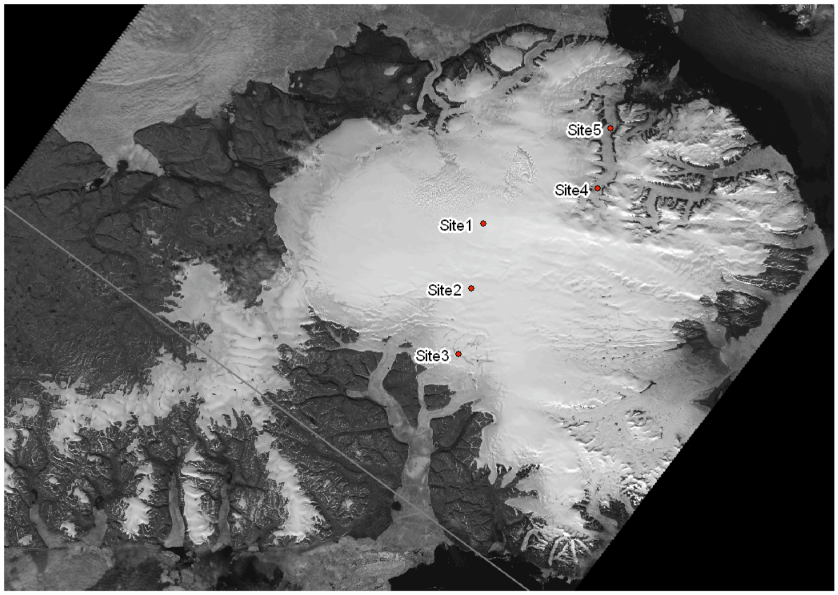

Figure 2.2: Location of AWS sites on Devon Island ice cap (image provided by Angus Duncan). Sites are numbered in order of decreasing elevation.

decreasing elevation and cover a range of altitudes from 1802 m.a.s.l, (site 1, upper accumulation zone), to 525 m.a.s.l (site 5, well into the ablation zone). Details of the measurements at each site are given in Table 2.1.

2.3 Results and Discussion

We investigate results of a Polar MM5 run for the summer of 2008 over Devon ice cap. A summary of model performance statistics is provided in Table 2.2. The SW↓ and SW↑ both exhibit Root Mean Square Errors (RMSE) in the range 46.9 - 69.2 W m^{-2}. This suggests that the model often exhibits large errors in predicted incoming solar radiation. We expect the SW↑ to exhibit similar behaviour to the SW↓, because it is reflected from a generally

Table 2.1: Information about the instruments used to measure the radiation components and temperature at the 5 AWS sites.

	Site 1	**Site 2**	**Site 3**	**Site 4**	**Site 5**
Latitude	75.34	75.18	75.01	75.43	75.58
Longitude	-82.68	-82.78	-82.88	-81.56	-81.44
Elevation (m.a.s.l)	1802	1415	994	925	525
Dates	Jun 1-Aug 31	Jun 1-Aug 31	Jun 1-Aug 31	Jun 13 - Jul 7	Jun 1 - Aug 1
Radiation comp's					
Instrument	CNR1	CNR1	CNR1	CM3/CG3	CM3/CG3
Manufacturer	Campbell Scientific	Campbell Scientific	Campbell Scientific	Kipp and Zonen	Kipp and Zonen
Accuracy	±5%	±5%	±5%	±10%	±10%
dates	Jun 1-Aug 31				
Temperature					
instrument	HMP45C212	HMP45C212	107B temperature probe	HMP45C212	HMP45C212
Manufacturer	Campbell Scientific	Campbell Scientific	Campbell Scientific	Campbell Scientific	Campbell Scientific
accuracy	$\pm 0.1°C$	$\pm 0.1°C$	$\pm 0.4°C$	$\pm 0.1°C$	$\pm 0.1°C$

Table 2.2: Summary of 5 AWS measurements and corresponding Polar MM5 estiimates at 5 AWS locations. All values have units W m $^{-2}$ apart from T2, which has units °C. Mean, standard deviations (stdv) and root mean square errors (RMSE) are computed from the daily averaged timeseries. Standard deviations are computed from three hourly timeseries with the daily means subtracted.

site 1 (1802m)	SW↓	SW↑	LW↓	LW↑	NET	
mean MM5	279.8	223.8	215.9	295.1	-23.2	
mean AWS	272.6	234.0	247.7	290.3	-4.0	
stdv mm5	108.9	87.1	9.6	3.1	16.0	
stdv AWS	111.9	90.9	3.7	2.2	25.7	
RMSE	58.2	46.9	44.9	10.7	30.3	
mean bias	5.7	-9.7	-31.6	4.9	-19.4	
site 2 (1415m)	SW↓	SW↑	LW↓	LW↑	NET	T2
mean MM5	248.9	199.1	237.4	302.3	-15.1	-2.6
mean AWS	278.4	218.4	257.5	298.0	19.4	-2.1
stdv MM5	96.0	76.8	11.0	3.2	16.7	0.3
stdv AWS	114.9	85.7	4.3	2.1	33.0	0.3
RMSE	69.2	57.7	35.7	10.0	42.0	1.6
mean bias	-30.8	-20.4	-20.0	4.4	-34.8	-0.5
site 3 (994m)	SW↓	SW↑	LW↓	LW↑	NET	
mean MM5	241.2	193.0	249.5	307.1	-9.3	
mean AWS	262.6	193.0	266.9	304.4	32.1	
stdv MM5	94.9	75.9	9.3	3.3	15.2	
stdv AWS	95.7	68.0	4.3	1.6	25.6	
RMSE	65.0	55.3	33.6	8.4	49.3	
mean bias	-22.6	-1.1	-17.3	2.8	-41.5	
site 4 (925m)	SW↓	SW↑	LW↓	LW↑	NET	T2
mean MM5	319.0	255.2	245.8	311.6	-2.0	0.2
mean AWS	307.7	225.5	271.3	310.6	44.6	0.9
stdv MM5	129.8	103.8	8.6	1.8	17.6	0.1
stdv AWS	84.1	79.9	3.1	2.0	14.5	-0.1
RMSE	58.7	67.1	35.2	6.3	60.5	2.2
mean bias	11.6	29.7	-25.9	1.4	-47.1	-0.8
site 5 (525m)	SW↓	SW↑	LW↓	LW↑	NET	T2
mean MM5	297.0	237.6	250.1	311.8	-2.3	-0.5
mean AWS	299.8	212.6	271.8	311.8	47.2	1.2
stdv MM5	112.6	90.0	9.0	2.6	18.5	0.2
stdv AWS	105.0	66.3	3.8	1.6	31.7	0.3
RMSE	59.3	61.8	31.4	4.3	66.3	2.3
mean bias	-2.1	25.4	-22.2	0.0	-49.7	-1.7

high α surface. Despite the relatively large RMSE, the mean bias is much lower (always less than half, and in the most extreme case, 20 times smaller). This suggests that the RMSE is caused by occurrences of over-prediction and under-prediction of SW↓ and SW↑. The most likely explanation for error in the SW↓ energy flux is that the model lacks skill in predicting cloud extent and/or type. Other possible factors contributing to SW↓ residuals include: i) errors in the model terrain gradient, ii) insufficiencies in the modelled atmospheric thickness, and iii) instrument error in the AWS measurements. Since SW↑ is reflected SW↓, any error in SW↓ will be directly translated into an error in SW↑. However, the fraction of SW↓ being reflected is prescribed by the albedo (α), and this is very crudely prescribed by Polar MM5 as a constant (0.8). This may be an accurate value for cold conditions with snow that has not undergone metamorphism, however, it is inaccurate for areas which experience melt and correspondingly snow metamorphism. This is evident, as the difference between the mean bias of SW↓ and SW↑ increases as the AWS elevation decreases (table 2.2).

Incoming longwave radiation (LW↓) had a RMSE ranging from 31.4 m^{-2} (525 m.a.s.l) to 44.9 W m^{-2} (1802m.a.s.l) with mean bias ranging from -17.3 m^{-2} (994 m.a.s.l) to -31.6 m^{-2} (1802 m.a.s.l). There was no evident elevation dependence in LW↓. Outgoing longwave radiation (LW↑) exhibited smaller RMSEs and mean biases than LW↓. This is attributed to the differences in the factors controlling LW↓ and LW↑: LW↑ is determined by the ground temperature through the Stefan-Boltzmann law, whereas LW↓ is dictated largely by the amount, type, and altitude of cloud cover.

2.3.1 Elevation Profile

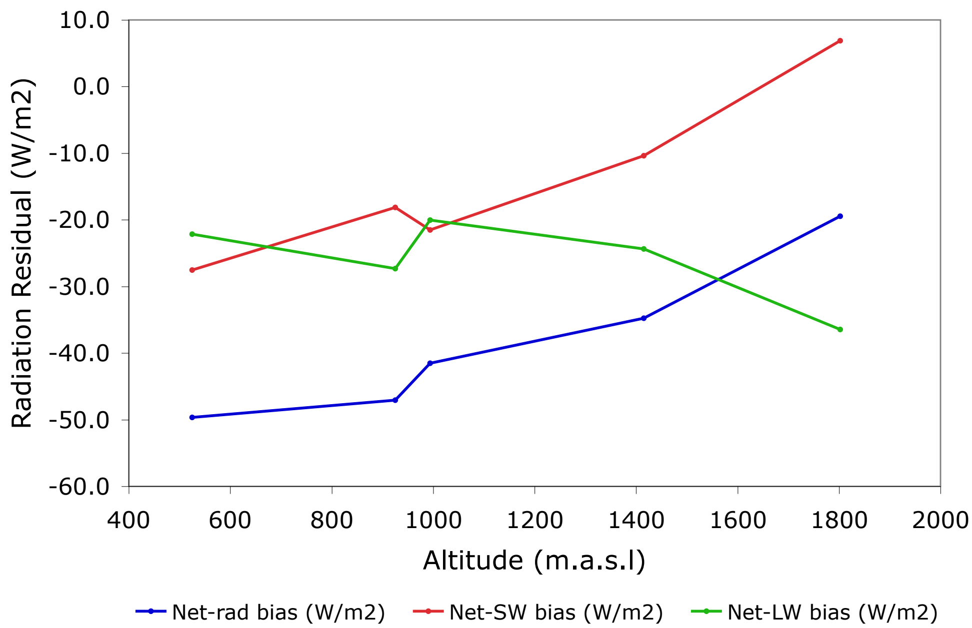

Figure 2.3: Mean bias between Polar MM5 and AWS observations (PMM5-AWS) for the summer 2008. Mean biases of net radiation, net shortwave radiation and net longwave radiation are plotted against altitude (m.a.s.l) for the 5 AWS locations.

Figure 2.3 displays the relationship between the mean residuals in NSW, NLW and NAW energy fluxes and elevation. The magnitude of the mean residual in NAW decreases with increasing elevation, indicating that melt volume predictions from Polar MM5 will be less accurate at lower elevations than at higher elevations. There is greater range in the mean NSW bias (36 W m^{-2}) than in the mean NLW bias (16 W m $^{-2}$) across the five sites (Figure 2.3). The variation in NSW bias fluctuates from negative values at low elevations, to positive values at high elevations. This is a predictable consequence of the model α being set to a constant value of 0.8. At high elevations, the average α may be slightly higher than this constant value, meaning that the model will absorb an excess of SW radiation and therefore have a positive bias in NSW. Conversely, at low elevation there will be periods of melt, during which snow metamorphism will cause α to drop far below the constant value of 0.8. This will cause the model to underestimate absorbed solar radiation and therefore the NSW, causing a negative bias. The mean NSW and NAW biases have an r^2 of 0.94 with each other, whereas the mean NLW and NAW biases have an r^2 of 0.64 with one another. This implies that most of the variance in the mean NAW bias elevation profile is accounted for by variance in the mean NSW bias. Therefore, we assume that minimising bias in the NSW flux will help to minimise bias in the NAW flux.

To further investigate the relationship between NAW, NSW and NLW residuals, we look at the daily timeseries for each of the five sites (Figure. 2.4). It is apparent that the NAW residuals co-vary most strongly with the NLW residuals at high elevation, and with the NSW residuals at lower elevation. The correlations between NSW residuals and NAW residuals, and NLW residuals and NAW residuals at the 5 AWS sites support this assertion (Table 2.3).

Table 2.3 clearly demonstrates that at lower elevations, where the majority of the melt takes place, it is the NSW residuals that control the NAW residuals. NSW residuals are affected by residuals in both SW↓ and SW↑. Errors in cloud cover are the most likely explanation for residuals in SW↓. However, a

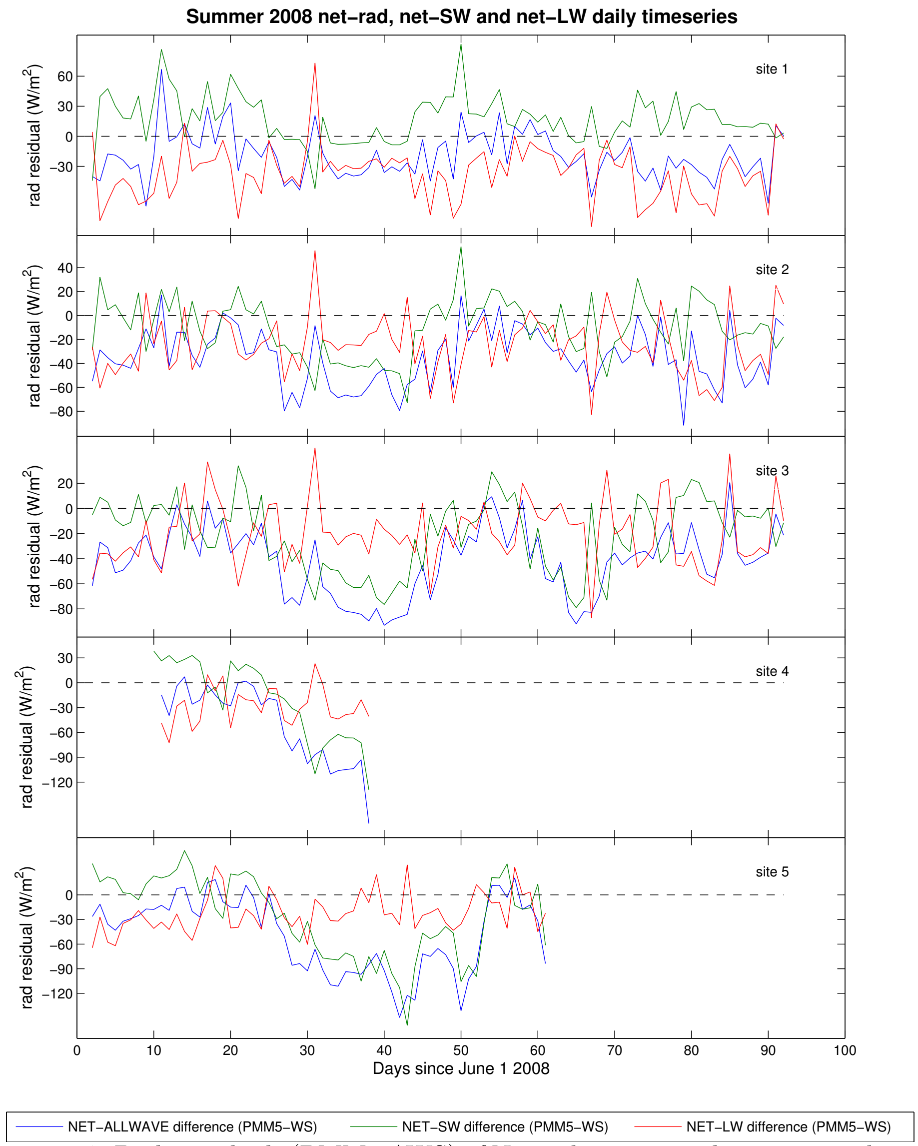

Figure 2.4: Daily residuals (PMM5-AWS) of Net radiation, net shortawave radiation and net longwave radiation for summer 2008 at 5 AWS sites (indicated in each figure panel).

generally high on-glacier α (for now, ignoring errors in α), means that errors in SW$\downarrow$ are modulated by opposite sign errors in SW$\uparrow$. In reality, there are large errors in using a fixed value of 0.8 for α. These differences in α affect

Table 2.3: Correlation coeficients for net short-wave residuals (PMM5-AWS) vs. Net all-wave residuals, and net long-wave residuals vs. net all-wave residuals.

	site 1	site 2	site 3	site 4	site 5
site elevation (m.a.s.l)	1802	1415	994	925	525
ρ, NSW residual, NAW residual	0.36	0.48	0.60	0.89	0.88
ρ, NLW residual, NAW residual	0.57	0.51	0.39	0.19	0.10

and cause error in the reflected SW radiation. Depending upon the sign and magnitude of the residual of incoming SW radiation, errors in α might act to accentuate or reduce and partly cancel the overall residual in the NSW. Thus, at low elevations, errors in α and cloud cover both affect errors in the NAW flux. In this study we have not characterized the magnitude of the relative contributions from the two factors. However since any error in SW$\downarrow$ is regulated by the factor $1 - \alpha$, and α is crudely assigned by the model, we conclude that α has a significant effect upon the modelled NAW flux.

2.3.2 Temperature Dependence

If the surface temperature reaches the pressure melting point, then melt can take place. Melting conditions increase the rate of snow metamorphism, which causes α to drop, due to changes in snow grain size, exposure of glacier ice, and pooling of water among other processes. Such drops in albedo increase the absorption of solar radiation, and thus change (increases in this case) the NSW radiation. Increases in NSW will lead to increases in NAW, unless there is a corresponding decrease in NLW.

During the summer of 2008, only three of the five AWS had useable near surface temperature (referred to as T2, because it is compared to model 2m

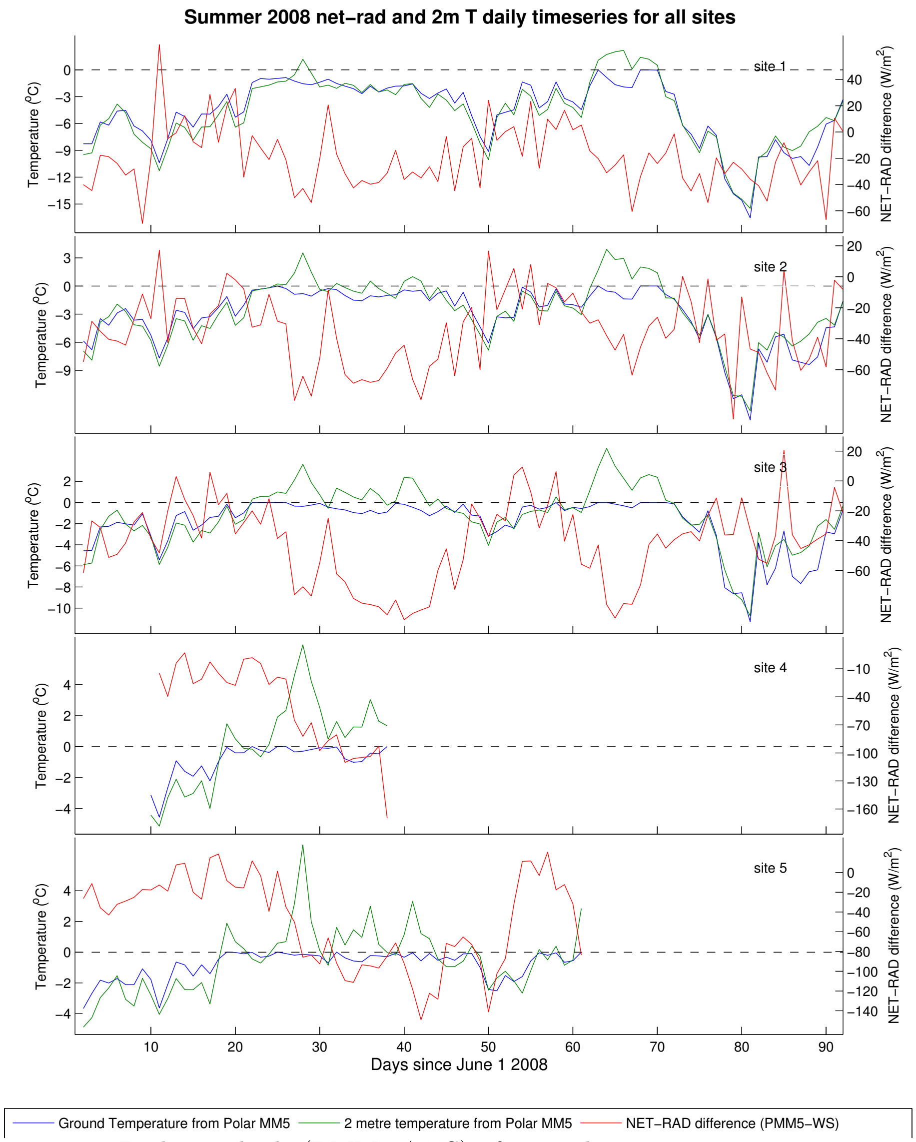

Figure 2.5: Daily residuals (PMM5-AWS) of ground temperature, 2m air temperature and net radiation for summer 2008 at 5 AWS sites (indicated in each figure panel).

temperature) records. At each of these sites, the modelled vs. measured RMSE for T2 was between $2°C$ and $3°C$, with a negative mean bias in each case (Table 2.2). The model under-predicts temperature at all sites, and the magnitude of the discrepancy is greater at lower elevations.

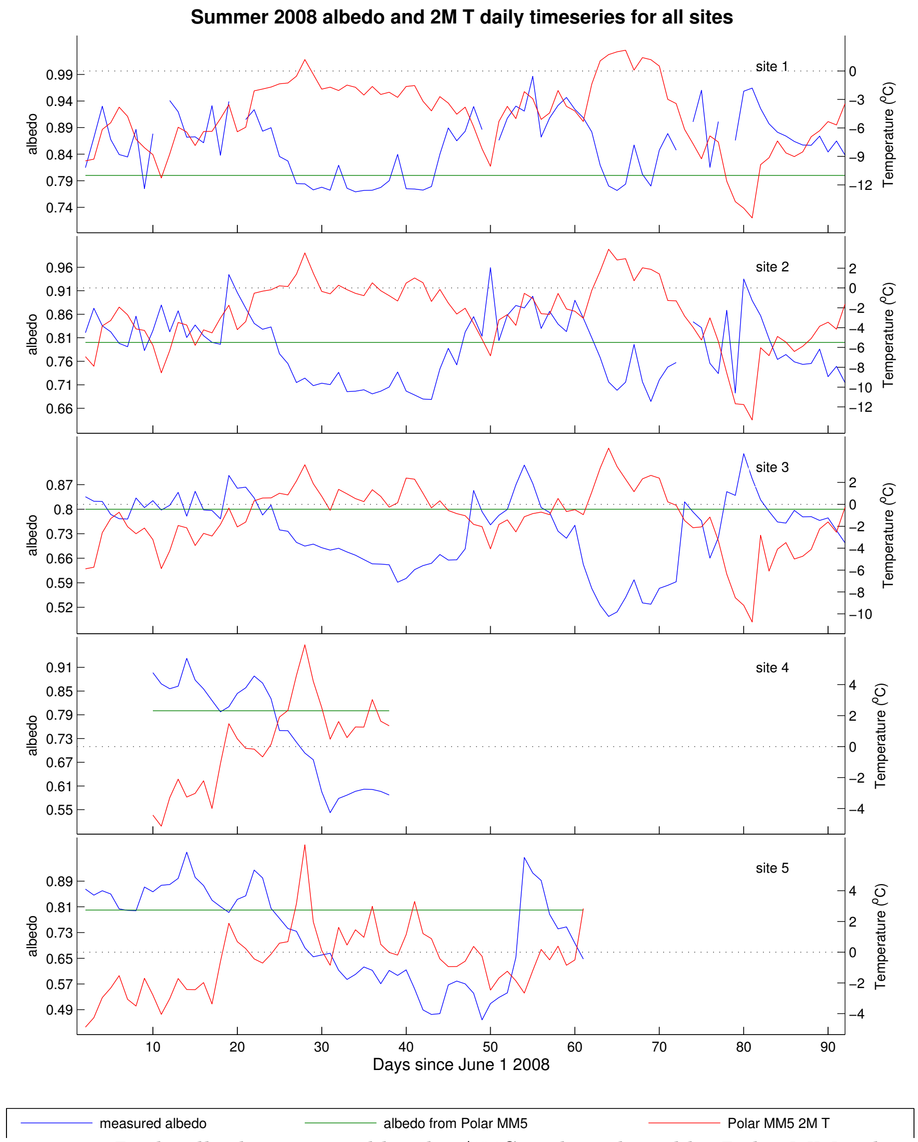

Figure 2.6: Daily albedo measured by the AWS and predicted by Polar MM5 plotted alongside 2m T predicted by Polar MM5.

Figure 2.5 illustrates NAW residuals (Polar MM5 - AWS) alongside both the Polar MM5 predicted ground and 2m air temperatures. When the temperature reaches zero (i.e. conditions where melt may occur), Polar MM5 significantly underestimates the NAW.

Figure 2.6 compares daily averaged T2 with the measured solar index weighted daily averaged α, ($\bar{\alpha}$), where:

$$\bar{\alpha} = \frac{\sum_{i=1}^{24} \mathrm{SW}_i^{\downarrow} \alpha_i}{\bar{\mathrm{SW}} \downarrow} \tag{2.4}$$

$\bar{\mathrm{SW}} \downarrow$ is the daily average incoming solar radiation, and $\mathrm{SW}_i^{\downarrow}$ and α_i are the incoming solar radiation and α at hour i respectively. This may be simplified to:

$$\bar{\alpha} = \frac{\bar{\mathrm{SW}}^{\uparrow}}{\bar{\mathrm{SW}}^{\downarrow}} \tag{2.5}$$

where $\bar{\mathrm{SW}}^{\uparrow}$ is the daily mean outgoing solar radiation. The solar index weighted method for obtaining α daily averages is used because the CNR-1 net radiometer instrument is known to perform poorly when the sun is at high zenith angles (i.e. close to the horizon). This may not be a significant concern for this study, since the majority of melt occurs at times of low zenith angle, but we use the solar index weighted method nonetheless.

It is clear from Figure 2.6 that when the temperature approaches zero, α drops dramatically at all sites (around day 28-29). This drop in α marks the onset of melt, and appears to occur at the same time at all the sites. The sudden onset for melt at all AWS sites corroborates observations made on the ice cap surface for that period of time, when melt was triggered at all elevations by one large high pressure system that engulfed the ice cap (Duncan (2011)).

Comparing Figure 2.6 to Figures 2.4 and 2.5, it is noted that for lower elevations, (sites 3, 4 and 5), changes in α coincide with changes in the NSW residuals (as expected, since model α is fixed at 0.8), and consequently the NAW residuals change. We conclude that α is an important factor in the radiation budget. Since α is so crudely assigned in Polar MM5, it is an obvious area in which to improve the model. In the next section we will explore further the relationship between T2 and α, and suggest a temperature dependent α parameterization suitable for programming in-line into Polar MM5.

2.3.3 Albedo Parameterization

Without utilizing a satellite derived α product such as that employed by (Box et al., 2004), the Polar MM5 default simply uses a constant α of 0.8 for all areas of the ice cap, at all times. In order to improve the treatment of albedo in Polar MM5, two α parameterizations that rely, at most, upon the previous day's mean T2 as an input, are compared offline, to the use of a constant albedo. We choose to use only T2 in order to i) avoid having to create new variables within the complex structure of Polar MM5, ii) avoid programming the model to read and write such variables, and iii), avoid having each run rely on the results of the previous run, as this poses difficulties when running a long continuous run. If the parameterization is programmed inline into Polar MM5, it is envisaged that the parameterization will not run during the 24 hour spinup (for which there is no previous day mean T2). It will run in the 48 hour run that follows each model spinup, using the spinup mean T2. By using the daily mean T2, as opposed to instantaneous values of T2, we do not risk introducing an unrealistic diurnal cycle in α.

We recognize that α relies on the evolution of the snowpack over the course of an entire season, and thus do not expect our parameterization to be completely accurate. However, we suspect that even a simple temperature based α parameterization will be an improvement over a constant value. Figure 2.7

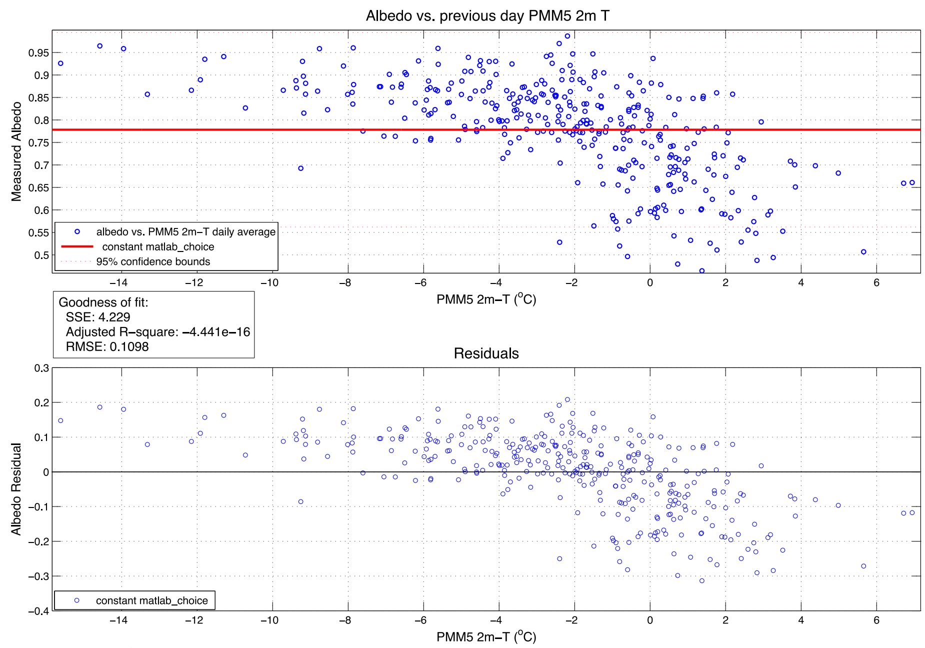

Figure 2.7: Scatter plot of measured daily average α vs. previous day 2m T, with a constant value fit (upper pannel). The lower panel plots residuals between the constant value of albedo.

shows daily average α measured at the AWS, plotted against the previous day's average T2 predicted by Polar MM5 (all days at all of the sites are included in the plot). Overlaid is the Polar MM5 parameterization for α (a constant value of 0.8). The residual plot indicates that the Polar MM5 method of assigning a constant value for α generally underestimates α at low temperatures, and overestimates α at high temperatures.

Figure 2.8 displays the same plot, but overlaid with linear fit between α, and

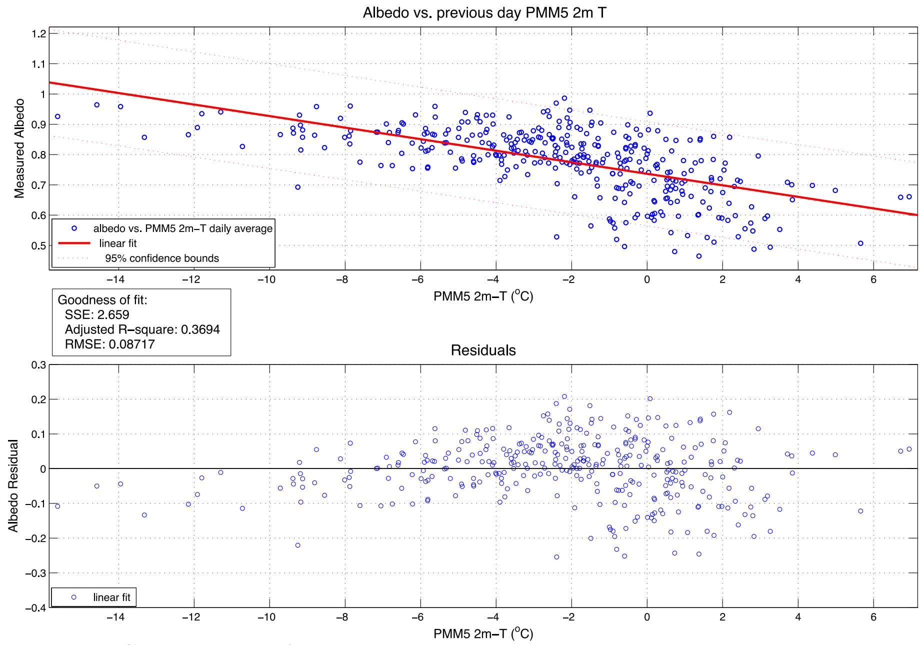

Figure 2.8: Scatter plot of measured daily average α vs. previous day 2m T, with a linear fit.

T2:

$$\alpha = a\mathrm{T2} + b \tag{2.6}$$

The constants a and b are determined through a least squares linear regression. The fit is an improvement, with RMSE of 0.087 compared to 0.11 for $\alpha = 0.8$, but the model now over-predicts α at low temperature, and although it does better at higher temperatures, it cannot replicate the step in α around T2 $= 0°C$. Another problem is that such a parameterization would predict $\alpha > 1$ for T2 $< -14°C$, and $\alpha < 0$ at very high T2, although such high temperatures are not seen on an ice cap).

A sigmoidal function (Figure 2.9) is suggested as a viable model to fit α as a function of T2. It addresses the apparent step in α centred near T2 $= 0$°C by

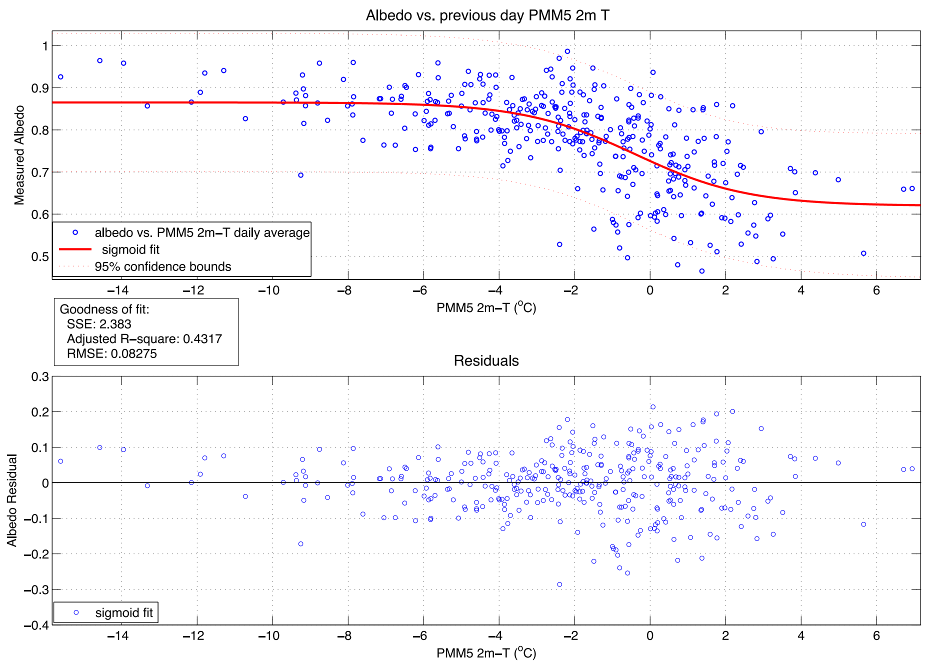

Figure 2.9: Scatter plot of measured daily average α vs. previous day 2m T, with a sigmoidal fit.

gradually shifting between a mean α for temperatures below zero and a lower mean α for temperature above zero. The sigmoidal curve is described by the following equation:

$$\alpha = \frac{(\alpha_l - \alpha_h)}{1 + e^{-\frac{(T-To)}{w}}} + \alpha_h \tag{2.7}$$

The 4 constants, α_l, α_h, T_0 and w, are calculated using a least squares regression. α_l and α_h are the limits for α at low and high temperatures respectively. T_0 is the temperature offset for the position of the centre of the curve inflection. w is a measure of the horizontal stretch of the curve.

The sigmoidal parameterization slightly improves the RMSE with respect to observations when compared to the linear fit albedo case (0.083 compared to 0.087 respectively), and also slightly improves the adjusted R-squared value (0.43 vs. 0.37) compared to the linear fit, but these improvements are small. However the sigmoidal curve captures the step nature of the change in α with respect to air temperature, and also gives a better distribution of residuals. Furthermore, α is bounded by $0.61 < \alpha < 0.88$ (Fig. 2.9), and so α cannot become unphysical (outside the range $0 < \alpha < 1$) at any temperature.

Figure 2.10 illustrates the effect upon NAW residuals of applying the sigmoidal parameterization offline to the energy balance. It is evident that at each site apart from site 1, the NAW is improved, although there are still major discrepancies. These discrepancies are likely due to cloud errors and deficiencies in the sigmoidal parameterization. It is possible, however, that running the parameterization inline will further improve predicted NAW through feedback between α and the model climate. For example, a small increase in modelled NAW could lead to an increase in modelled T2. This increase in T2 could feedback by lowering modelled α, which would further increase NAW. However, it is not possible to measure this process without programming the parameterization into Polar MM5.

2.4 Conclusions

The regional climate model Polar MM5 was run at 3km resolution over the Devon ice cap for the summer of 2008. The radiation budget components and air temperature were compared with measurements at five separate AWS on the ice cap, at altitudes from 525m to 1802m in altitude.

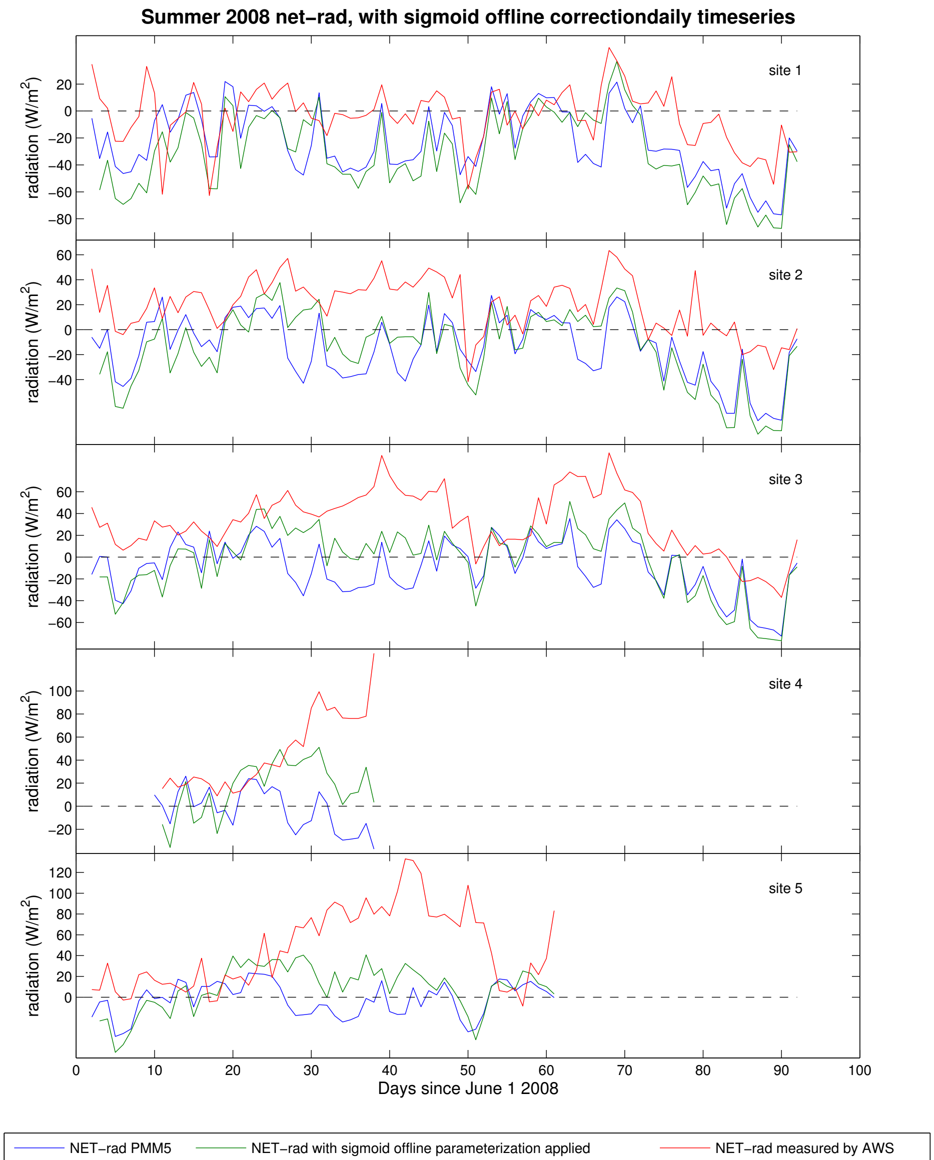

Figure 2.10: NAW with and without sigmoidal paraeterization. AWS NAW also plotted

The model under-predicted T2 at all elevations, with larger discrepancies occurring at lower elevations. This supports the hypothesis that the crude assignment of model $\alpha = 0.8$ is severely over predicting α under melting conditions. In reality, snow metamorphism causes α to decrease, which increases the absorption of SW radiation and thus the near surface temperature. At lower elevations, where melting conditions occur more frequently, it is not surprising that the model under-predicts near surface temperature.

The energy budget drives the near surface temperature. In this study we focused on the incoming and outgoing SW and LW radiation components of the energy budget. We assert that deficiencies in model prediction of both cloud and α contribute to discrepancies in the NAW energy flux. At high elevations NLW residuals primarily drive variability in NAW residuals, whereas at lower elevation, NSW residuals dominate and drive variability in NAW residuals. Although not conclusive, this suggests that at high elevations it is errors in cloud prediction that drive errors in NAW, whereas at low elevations it is errors in α that drive errors in the NAW.

Finally, given that i) α appears to be the primary driver of errors in NAW, and ii), α is so crudely assigned for glaciated grid cells in Polar MM5, we suggest a simple α parameterization for use in Polar MM5. This parameterization is a simple function of T2, and does not require a memory from previous model timesteps. This simplifies the task of programming the parameterization into Polar MM5 because each 48 hour time-slice can be initiated and run without the requirement for values of variables from the previous run. It is recognized that the suggested parameterization is an oversimplification, because albedo does not respond to air temperature on a daily timescale. However, the method proposed has the distinct advantage of being in a form that could be programmed in-line in Polar MM5.

When used off-line, the sigmoidal α parameterization was able to improve model predictions of NAW radiation at four of the five AWS sites. The improvements were relatively small, compared to the overall residuals in NAW radiation. However, we predict that running the parameterization inline within Polar MM5 would lead to feedbacks with the modelled climate, which could further improve prediction of NAW.

Despite the logistical advantages of the temperature dependent α parameterization, it is a statistical parameterization, and has very little physical basis. With the deficiencies in Polar MM5 albedo treatment as motivation, future objectives should strive to program an albedo parameterization in-line within the model. If it were possible to overcome the logistical challenges, it would be preferable to write a more physically based parameterization in which the snow surface is allowed to evolve over an entire season. A simple example is that of Oerlemans and Knap (1998), whereas a more complex example is developed by Bougamont et al. (2005).

Bibliography

Alt, B. "Synoptic climate controls of mass-balance variation on Devon Island ice cap.." *Arctic and Alpine Research* 10 (1978): 61–80.

Bougamont, M, J Bamber, and W Greuell. "A surface mass balance model for the Greenland Ice Sheet." *Journal of Geophysical Research* 110 (2005).

Box, J. E., D. H. Bromwich, and L.S. Bai. "Greenland ice sheet surface mass balance 1991–2000: Application of Polar MM5 mesoscale model and in situ data." *Journal of Geophysical Research* 109 (2004).

Box, J. E., D. H. Bromwich, B. A. Veenhuis, L. S. Bai, J. C. Stroeve, J. C. Rogers, K. Steffen, T. Haran, and S. H. Wang. "Greenland ice sheet surface mass balance variability (1988-2004) from calibrated polar MM5 output." *Journal of Climate* 19 (Jun 2006): 2783–2800.

Bromwich, D. H., J. J. Cassano, T. Klein, G. Heinemann, K. M. Hines, K. Steffen, and J. E. Box. "Mesoscale modeling of katabatic winds over Greenland with the Polar MM5." *Monthly Weather Review* 129 (2001): 2290–2309.

Burgess, D and M Sharp. "Recent changes in thickness of the Devon Island ice cap, Canada." *Journal of Geophysical Research* 113 (2008).

Burgess, D. O., M. J. Sharp, D. W.F. Mair, J. A. Dowdeswell, and T. J. Benham. "Flow dynamics and iceberg calving rates of Devon Ice Cap, Nunavut, Canada." *Journal of Glaciology* 51 (2005): 219–230(12).

Cassano, J. J., J. E. Box, D. H. Bromwich, L. Li, and K. Steffen. "Evaluation of polar MM5 simulations of Greenland's atmospheric circulation." *Journal of Geophysical Research* 106 (Dec 2001): 33867–33889.

Colgan, W., J. Davis, and M. Sharp. "Is the high-elevation region of Devon Ice Cap thickening?." *Journal of Glaciology* 54 (2008): 428–436(9).

Dowdeswell, J. A., T. J. Benham, M. R. Gorman, D. Burgess, and M. J. Sharp. "Form and flow of the Devon Island Ice Cap, Canadian Arctic." *Journal of Geophysical Research* 109 (2004).

Dowdeswell, J.A., J.O. Hagen, H. Bjornsson, A.F. Glazovsky, W.D. Harrison, P. Holmlund, J. Jania, R.M. Koerner, B. Lefauconnier, C.S.L. Ommanney, and R.H. Thomas. "The Mass Balance of Circum-Arctic Glaciers and Recent Climate Change." *Quaternary Research* 48 (07 1997): 1–14(14).

Duncan, A. Spatial and Temporal Variations of the Surface Energy Balance and Ablation on the Belcher Glacier, Devon Island, Nunavut, Canada. Master's thesis, University of Alberta, 2011.

Fettweis, X, H Gallée, L Lefebre, and J.P van Ypersele. "Greenland surface mass balance simulated by a regional climate model and comparison with satellite derived data in 1990-1991." *Climate Dynamics* (2005): 623–640.

Gallée, H. and P. G. Duynkerke. "Air-snow interactions and the surface energy and mass balance over the melting zone of west Greenland during the

Greenland Ice Margin Experiment." *Journal of Geophysical Research* 102 (1997): 13813–13824.

Gardner, A. S., G. Moholdt, B. Wouters, G. J. Wolken, D. O. Burgess, M. J. Sharp, G. Cogley, C. Braun, and C. Labine. "Sharply increased mass loss from glaciers and ice caps in the Canadian Arctic Archipelago." *Nature* 473 (April 2011): 357–360.

Gardner, A. S., M. J. Sharp, R. M. Koerner, C. Labine, S. Boon, S. J. Marshall, D. O. Burgess, and D. Lewis. "Near-Surface Temperature Lapse Rates over Arctic Glaciers and Their Implications for Temperature Downscaling." *Journal of Climate* 22 (2011/11/04 2009): 4281–4298.

Grell, G. A. "Prognostic Evaluation of Assumptions used by Cumulus Parameterizations." *Monthly Weather Review* 121 (03 1993): 764–787.

Grell, G A, J Dudhia, and D R Stauffer. A description of the fifth generation Penn State/NCAR mesoscale model (MM5). Technical report, NCAR, Natl. Cent. for Atmos. Res., Boulder, Colo, 1994.

Guo, Z. C., D. H. Bromwich, and J. J. Cassano. "Evaluation of Polar MM5 simulations of Antarctic atmospheric circulation." *Monthly Weather Review* 131 (Feb 2003): 384–411.

Hack, J. J., B. A. Boville, B. P. Briegleb, J. T. Kiehl, P. J. Rasch, and D. L. Williamson. Description of the NCAR community vlimate model (CCM2). Technical Report NCAR/TN-382+STR, NCAR, 1993.

Hines, K. M., D. H. Bromwich, and Z. Liu. "Combined global climate model and mesoscale model simulations of Antarctic climate." *Journal of Geophysical Research* 102 (Jun 1997): 13747–13760.

Holmgren, B. "Climate and energy exchange on a sub-polar ice cap in summer, Arctic Institute of North America Devon Island Expedition 1961–1963, Part E, Radiation climate.." *Meddelande No. 111, Department of Meteorology, Uppsala University, Uppsala, Sweden* (1971).

Janjic, Z. I. "The Step-Mountain Eta Coordinate Model: Further Developments of the Convection, Viscous Sublayer, and Turbulence Closure Schemes." *Monthly Weather Review* 122 (May 1994): 927–945.

Koerner, R. M. "Devon Island Ice Cap: Core Stratigraphy and Paleoclimate.." *Science* 196 (04 1977): 15–18.

Mair, D., D. Burgess, and M. Sharp. "Thirty-seven year mass balance of Devon Ice Cap, Nunavut, Canada, determined by shallow ice coring and melt modelling." *Journal of geophysical research* 110 (2005).

Manning, K.W. and C. A.A. Davis. "Verification and Sensitivity Experiments for the WISP94 MM5 Forecasts." *Weather and Forecasting* 12 (December 1997): 719–735.

Monaghan, A. J., D. H. Bromwich, H. L. Wei, A. M. Cayette, J. G. Powers, Y. H. Kuo, and M. A. Lazzara. "Performance of weather forecast models in the rescue of Dr. Ronald Shemenski from the South Pole in April 2001." *Weather and Forecasting* 18 (04 2003): 142–160.

Oerlemans, J. and W.H. Knap. "A 1 year record of global radiation and albedo from the ablation zone of the Morteratschgletscher, Switzerland." *Journal of Glaciology* (1998).

Reisner, J., R. M. Rasmussen, and R. T. Bruintjes. "Explicit forecasting of supercooled liquid water in winter storms using the MM5 mesoscale model." *Quarterly Journal of the Royal Meteorological Society* 124 (Apr 1998): 1071–1107.

Shepherd, A., D U Zhijun, T. J Benham, J. A Dowdeswell, and E. M. Morris. "Mass balance of Devon Ice Cap, Canadian Arctic." *Annals of Glaciology* 46 (2007): 249–254(6).

Van Den Broeke, M., P. Smeets, J. Ettema, and P. Kuipers Munneke. "Surface radiation balance in the ablation zone of the west Greenland ice sheet." *J. Geophys. Res.* 113 (2008).

Van Lipzig, N.P.M, E. Van Meijgaard, and Oerlemans. J. "Evaluation of a Regional Atmospheric Model Using Measurements of Surface Heat Exchange Processes from a Site in Antarctica." *Monthly Weather Review* 127 (1999): 1994–2011.

CHAPTER 3

Development of an ice sheet albedo parameterization for use in Polar WRF [1]

3.1 Introduction

The cryosphere is responding dramatically to climate warming (Bindoff et al. (2007)). Marked increases in surface melt of the Greenland Ice Sheet, and many other glaciers and ice caps have contributed to global sea level rise (Dyurgerov et al. (2002, 2005); Jacob et al. (2012)). Recent acceleration of glacier melt has led scientists to search for positive feedback mechanisms that accentuate climate warming and ice melt (e.g. Zwally et al. (2002)).

A key quantity in determining the contribution of an ice sheet or glacier to sea level rise is the climatic balance. This quantity is defined as the change in thickness of a column of ice over a specific time period, ignoring thickness changes due to ice dynamics, and accumulation or ablation at the base of the

[1] A version of this chapter is being prepared for journal submission with the author list: Benjamin Gready, Jason Box, Martin Sharp, Andrew Bush and David Bromwich

column (Cogley et al. (2011)). Climatic balance is determined by, and therefore represents the direct influence of, the climate on an ice mass. Climatic balance is a major term in the mass budget of an ice sheet. Furthermore, it serves as an upper boundary condition and driving term for dynamical ice sheet models.

Despite many efforts to quantify climatic balance through field and modelling studies, it remains a difficult quantity to determine for several reasons, including (i) the large spatial variability which exists over ice sheets, and (ii) processes that determine climatic balance (e.g. precipitation, snow surface evolution, and melt) are challenging to model. Climatic balance depends upon meteorological conditions at the surface of the ice, and thus its prediction requires careful consideration of micro-to-meso scale meteorology.

In the last decade, regional climate models (RCMs) have been used to estimate atmospheric conditions over entire ice sheets (Bromwich et al. (2001); Cassano et al. (2001); Guo et al. (2003); Hines et al. (1997); Van Lipzig et al. (1999); Hines and Bromwich (2008)). RCM output has been used to estimate surface mass balance over Greenland and Antarctica (Box et al. (2004, 2006); Bromwich et al. (2001); Ettema et al. (2009); Fettweis et al. (2005)). This method provides high resolution estimates of meteorological conditions, and ultimately climatic balance, over ice sheets at approximately 10-km resolution. While representing a major step forward in climatic balance modeling, these models still have shortcomings. A primary limitation has been the simplified treatment of ice sheet albedo in the Polar MM5 and Polar WRF regional climate models. Until release 3.2.1 of Polar WRF, albedo on glaciers was simply set as a constant, precluding any feedback with the modelled climate.

Recently, Livneh et al. (2010) introduced a snow surface albedo parameterization (Engineers (1956)) inline within WRF. While the parameterization is an improvement from a constant albedo, it has not been optimized for use on glaciers.

This study presents a simple, glacier - specific, albedo parameterization that is implemented inline within Polar WRF. The parameterization allows the albedo to evolve over the course of a season as a function of the snow depth, temperature and age. Calibration and validation are performed using the MODIS MOD10A1 albedo product, which allows comparisons over large areas. The introduction of this parameterization allows feedback between the modelled albedo and the modelled climate in Polar WRF. This is a vital feedback in the overall surface energy budget, and therefore the work promises to improve predictions of melt energy and therefore climatic balance based on Polar WRF output.

3.2 Methods

The overall objective of this study is to implement an inline albedo parameterization within the RCM, Polar WRF. Before running the parameterization within Polar WRF, we use satellite derived albedo measurements to calibrate the free variables in the parameterization. The calibrated albedo parameterization is then run within the model, and model performance is assessed by further comparison with satellite derived albedo measurements for three summers (two of which were not used for the calibration).

In addition to assessing the accuracy of the albedo parameterization, we investigate the extent to which inclusion of the parameterization inline within Polar WRF affects the modelled climate. These effects are investigated by comparing modelled surface variables from running two different calibrations of the parameterization inline in Polar WRF. By examining model output for an example transect (spanning a wide range in altitude (990-3040m.a.s.l)), we explore the differences in energy balance and mass balance components between the two calibrations. Using these comparisons, we aim to characterize the extent to which the inline parameterization generates feedback with the modelled climate, and how this varies along the transect.

3.2.1 Study Area

The study area considered is the western margin of the Greenland Ice Sheet (Figure 3.1). We chose this region for several reasons: (i) other modelling studies using RACMO2 (Ettema et al. (2009)) and previous versions of Polar WRF and MM5 (Box et al. (2004), Bromwich et al. (2001), Hines and Bromwich (2008))) have used this region, (ii) there is a large range in ice elevations (sea level to >3000 m), which covers all facies zones of the ice sheet, and (iii) there are processed and validated MODIS daily albedo data (MOD10A1), with validated cloud masks over the domain (personal communication with David Decker), for use in model calibration and validation.

3.2.2 Polar WRF

The Polar version of the Weather Research and Forecast model (Polar WRF) was run on a 25km resolution gridded domain coupled to a 75km resolution

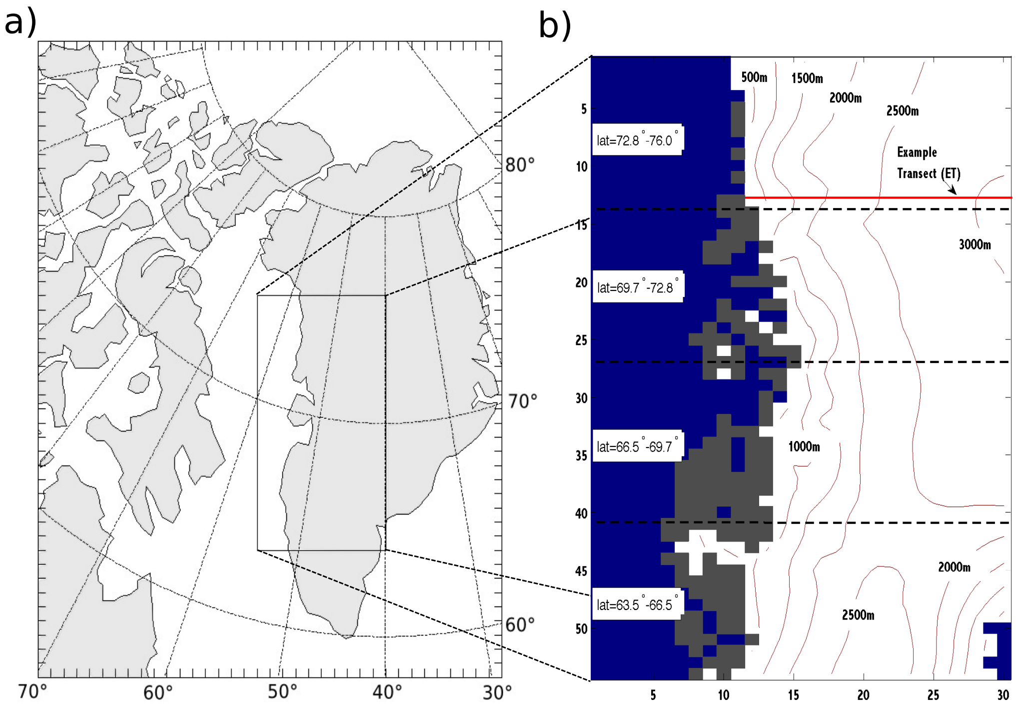

Figure 3.1: (a) The two domain setup for Polar WRF is shown. The outer domain has a grid resolution of 75km. The inner domain (indicated by the rectangle) has a grid resolution of 25km. (b) An expanded map of the 25km inner domain. Ocean and lakes are blue, non glaciated land is dark grey, and glaciated land is white. The contours indicate ice surface elevation. The black dotted lines show the approximate boundaries between four latitude bands used in the study to investigate spatial dependency of albedo parameterization. The example transect (ET) investigated later in the study is shown as the red line.

outer domain located over Western Greenland (Figure 3.1). The outer domain had horizontal dimensions ($N_x \times N_y$ grid points in E-W and N-S directions respectively) 37×46 with a time step of 180s. The inner domain had horizontal dimensions of 31×55 with a time step of 60s. Both domains had 28 terrain following vertical sigma coordinates, with a constant upper level of 10 hPa.

Polar WRF was run in “forecast” mode, in which the model output consists of many short separate forecasts. Each short forecast consists of a 24 hour spinup, followed by a 48 hour run, after which the model is reinitialized. By using many model restarts, model drift is prevented. However, a consequence of reinitializing every 48 hours, is that the model lacks any history greater than 1-2 days. The lack of longer term history prevents the use of a time-dependent albedo parameterization, because albedo varies over time scales greater than 48 hours. We therefore initialize each 48 hour run with results obtained from the previous run for several surface variables pertaining to the albedo parameterization. Allowing these surface variables to evolve over multiple model restarts allows the snow albedo to evolve on timescales greater than a single 48 hour forecast.

Polar WRF is initialized and nudged at the lateral boundary of the outer domain at 6 hourly intervals using data from the National Centers for Environmental Prediction (NCEP) FNL (Final) Operational Global Analysis, which are available on a 1x1 degree grid, at six hourly temporal resolution.

3.2.3 Modis MOD10A1 Daily Albedo

We use the MOD10A1 daily albedo product from the MODIS instrument on the Terra AM satellite to calibrate the albedo parameterization, and to validate the results from runs of Polar WRF with the albedo parameterization running inline. The MOD10A1 product has been tested against in-situ observations from five automatic weather stations in Greenland (Stroeve et al. (2006)), and shown to track the seasonal progression of albedo. It was, however, also shown to have an unrealistically high temporal variability, due to a number of sources of uncertainty. Stroeve et al. (2006) overcame this issue by taking 16 day averages of MOD10A1. In this study, we overcome the issue of high temporal variability by taking monthly and seasonal averages for all comparisons.

3.2.4 Albedo

Until recently, albedo over terrestrial ice was represented in Polar MM5/WRF either by declaring a constant albedo and correcting the net energy balance offline using monthly averaged satellite albedo products (e.g. Box et al. (2004)), or by using daily or monthly averaged satellite albedo products inline within the RCM (e.g. Box et al. (2006)). Release 3.0.11 of Polar WRF includes a simple time dependent albedo parameterization (Engineers (1956), Livneh et al. (2010)).

This study develops and implements a glacier-specific albedo parameterization for the NOAH land surface scheme, which runs inline in Polar WRF. Snow properties used in the parameterization, such as water equivalent snow depth(d) and snow surface albedo (α_{snow}), are taken from the end of each 48 hour output, and used as the input at the start of the next 48 hour run. This allows the albedo parameterization to operate with a memory that exceeds a single 48 hour model run, and permits more realistic seasonal evolution of the albedo within Polar WRF.

The parameterization is based upon that of Oerlemans and Knap (1998), in which the overall albedo, α, is a function of the Polar WRF prognostic variables α_{snow} and d. d is the water equivalent snow depth. α_{snow} is a new variable introduced to WRF, which tracks the snow surface albedo, neglecting the influence of the underlying ice. To find the resulting surface albedo (α), the following equation is used:

$$\alpha = \alpha_{snow} + (\alpha_{ice} - \alpha_{snow})\mathrm{e}^{-\frac{d}{d^*}} \tag{3.1}$$

The underlying ice albedo (α_{ice}, a constant), influences the overall albedo exponentially, according to a critical snow depth (d^*, also a constant). If d=0, equation 3.1 sets $\alpha = \alpha_{ice}$. The snow surface albedo decreases with time according to the following equation, where t^* (a constant) is the timescale for snow metamorphosis, and α_{os} is a constant describing the albedo of old snow (snow that has undergone extensive metamorphism and has an albedo that is no longer significantly decreasing):

$$\frac{d\alpha_{snow}}{dt} = \frac{-(\alpha_{snow} - \alpha_{os})}{t^*} \tag{3.2}$$

This equation is solved numerically for each model timestep as follows:

$$\alpha_{snow}(t + dt) = \alpha_{snow}(t) - dt\frac{(\alpha_{snow}(t) - \alpha_{os})}{t^*} \tag{3.3}$$

When new snow falls, the albedo increases, rather than decreases. In the Oerlemans and Knap (1998) study, α_{snow} was simply reset to the fresh snow albedo (α_{fs}) after every snowfall event in which snow depth increased by more than 2cm in 24 hours. This method proved problematic to implement in this study because of the small model timestep in Polar WRF (typically 180s). With such a short timestep it is not possible within the model framework to ascertain whether snowfall is part of a large enough event to have an impact upon the albedo, or a small event with insufficient accumulation to have an impact. When testing, we found that simply reseting α_{snow} to α_{fs} after every snow event, no matter how small, caused the overall albedo to be unrealistically high.

To combat this problem, we employed an incremental method to increase α_{snow}, dependent upon the snowfall rate, h, and the critical snowfall depth h^*.

$$\alpha_{\text{snow}}(t+dt) = \min \begin{cases} \alpha_{\text{snow}}(t) + hdt\frac{(\alpha_{fs} - \alpha_{\text{snow}}(t))}{h^*} \\ \alpha_{\text{fs}} \end{cases} \tag{3.4}$$

Albedo decrease due to snow surface evolution is characterized by t^*, which is assumed to be constant by Oerlemans and Knap (1998). However, snow surface evolution is complex, and the rate of evolution of the snow surface is dependent upon the temperature and water content of the snow pack (amongst other factors). Bougamont et al. (2005) took this into account by making t^* a function of both snow surface temperature and water content. In this study we prescribe t^* as:

$$t^* = \begin{cases} t_{\text{warm}} & T_{\text{ground}} = 0 \\ K|T_{\text{ground}}| + t_{\text{cold}} & -10°C < T_{ground} < 0°C \\ 10|T_{\text{ground}}| + t_{\text{cold}} & T_{\text{ground}} \leq -10°C \end{cases} \tag{3.5}$$

Where T_{ground} is the snow surface temperature ($°C$), t_{warm} is the critical snow aging time for $T_{\text{ground}} = 0°C$, t_{cold} is the critical snow aging time for $T_{\text{ground}} < 0°C$, and K is a tuning parameter similar to that used by Bougamont et al.

(2005). Since our study does not incorporate an advanced snow pack model, we have not included an explicit treatment of albedo dependence upon water content.

It has been observed that the ice surface albedo on the western margin of the Greenland ice sheet is not uniform, but that there is a distinct "dark zone" first noted by Oerlemans and Vugts (1993). Wientjes and Oerlemans (2010) suggest that the dark zone is caused by outcropping of ice layers containing a high concentration of dust particles. This explanation implies that the albedo of the dark ice zone is independent of contemporary meteorological conditions. Spatial variations in albedo of the underlying glacier surface cannot, by definition, be characterized using any of equations 3.1 - 3.5, because we prescribe a constant value for α_{ice}. The effect could be accounted for by prescribing α_{ice} as a field, derived from satellite measurements (e.g. from MOD 10A1), instead of being prescribed as a constant. We did not attempt this here, because a goal of this study was to develop a parameterization that can be used in the future by the Polar WRF community. If the parameterization required the input of α_{ice} as a field, the results may be improved for specific cases, such as the Greenland ice sheet, but the overall usability of the model would be reduced, and would likely inhibit the adoption of the parameterization.

3.2.5 Offline Calibration

Due to computational constraints (excessive runtime), calibration of the albedo parameterization was performed offline. However, initial conditions for α and α_{snow}, and values for T_{snow}, d, and h at each timestep, were taken from a previously completed run of Polar WRF with its default settings. Calibration was performed for the summer 2005. The default setup of Polar WRF (without the albedo parameterization from this study), was run from Oct 2004-May 2005, in order to obtain initial conditions for d and α_{snow}. The run was continued for the period May 2005 - Oct 2005, to provide predictions of T_{snow}, d, and h to be used in the offline calibration. We note that the calibration would ideally be performed with the parameterization running inline within Polar WRF to allow feedback between the albedo and the modelled atmosphere, but that proved to be unrealistically computationally expensive. The free parameters

Table 3.1: Summary of free parameters for the two calibrations "Cal A" and "Cal B". The RMSE at the bottom refers to the best RMSE found during the calibration. It is noted that when the two calibrations were run inline, (WCA and WCB), the RMSEs changed.

	Cal A	Cal B
α_{fs}	0.853	0.85
α_{os}	0.36	0.35
α_{ice}	0.32	0.5
d^*	130	5
h^*	3	2.5
t^*_{warm}	1.0	0.45
t^*_{cold}	30	80
K	25	40
RMSE	0.033	0.24

are listed in Table. 3.1, along with 2 calibrated values (Cal A and Cal B), which will be explained later. An important feature of a glacier albedo parameterization is its ability to reproduce observed gradients in albedo at the margin of the glacier. In order to explicitly take this concern into account, "mean elevation transects" are compared in order to calibrate and validate modelled albedo with MODIS MOD10A1 remotely sensed albedo. A mean elevation transect is constructed by (i) taking the seasonal mean at each grid-point, and then (ii) averaging all of the grid-points into 100m interval elevation bins. This two step process is applied to both the modelled and MOD10A1 albedo fields, and then the RMSE between the resulting mean elevation transects for modelled and MOD10A1 albedo is calculated. This is the metric by which model performance is evaluated.

To calibrate the model, we varied each of the free parameters in turn over a range of values (explained below), holding the rest constant. For each combination of the free parameters, the albedo was calculated offline, using variables from a previous run of Polar WRF to drive the parameterization. From the resulting albedo, the mean albedo/elevation transect (as explained above) was calculated, and compared to the MOD10A1 albedo mean elevation transect using the RMSE. The value of the free parameter with the lowest RMSE was taken as the new value for that parameter. The process was repeated for each of the free parameters

The value of the free parameters were not constrained, but rather allowed to assume their optimum value, no matter whether it made physical sense or not. Using trial and error, the approximate value for each parameter was found. The process explained above was repeated several times for each of the parameters. With each iteration, the RMSE was improved, and the variables updated. The process was stopped when the improvement to the RMSE upon further iteration, was less than 0.005. The best values found for the parameters in the initial calibration are listed as “cal A ” in Table. 3.1. Figure 3.2 illustrates the variation of each parameter around its optimal value for Cal A. As explained above, Cal A was performed using variables from a previously

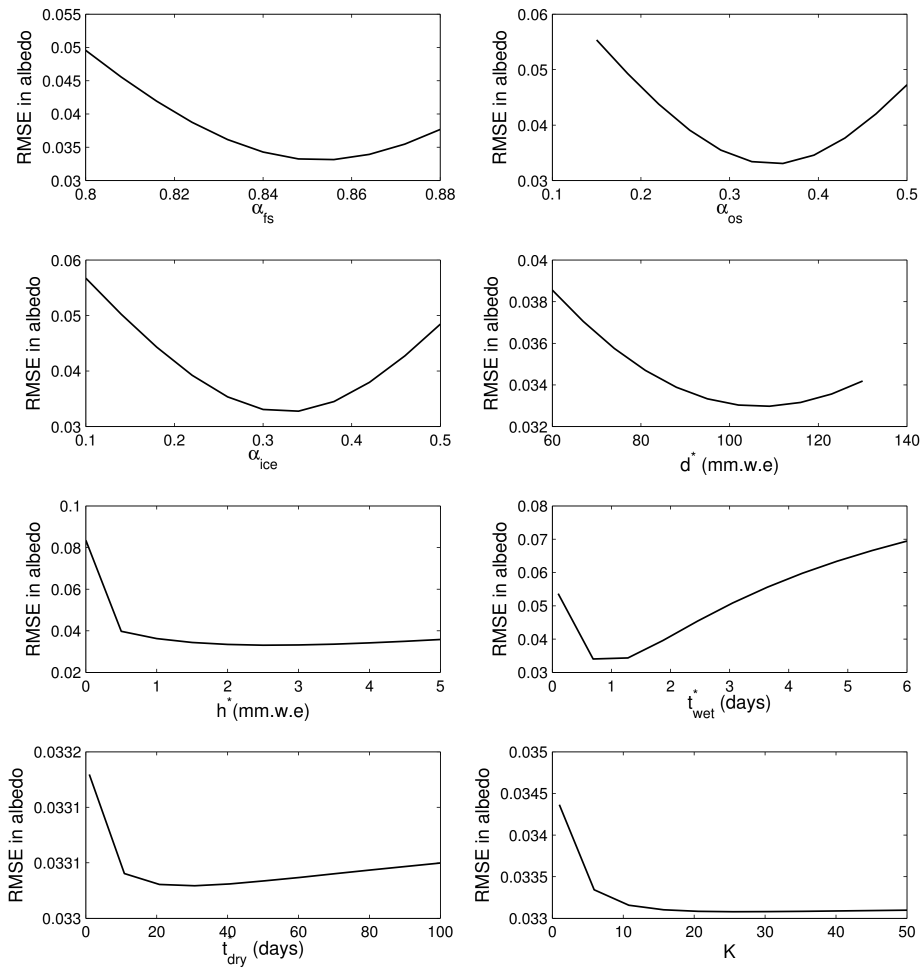

Figure 3.2: Calibration curves for WRF Calibration A. The calibration was carried out offline, and trial and error was used to find the optimum combination of free parameters. Using this optimum calibration, each individual parameter was varied around it's optimum value, and the RMSE of the elevation transect compared to MOD10A1 calculated for each instance. The variation of RMSE with each of the free parameters are plotted above.

completed Polar WRF run to drive the offline parameterization. The parameter values from this calibration were then used to run the parameterization inline within Polar WRF (for the summers of 2005 (the calibration year), 2001 (a cold year) and 2007 (a warm year) as validation years. These runs are referred to as WRF Cal A (WCA). (The results from these runs are presented later in the study).

As explained above, Cal A was performed using variable values from a previously completed Polar WRF run to drive the offline parameterization. The parameter values from this calibration were then used to run the parameterization inline within Polar WRF (for the summers of 2005 (the calibration year), 2001 (a cold year) and 2007 (a warm year) as validation years). These runs are referred to as WRF Cal A (WCA). The results from these runs are presented later in the study. A subsequent calibration referred to as "Cal B (explained in more detail later) was performed offline using the output WRF Cal A as input (Figure 3.3).

3.2.6 Uncertainty

Theoretically, if we knew all of the uncertainties in the input datasets, model uncertainty could be estimated by calculating the propagation of these uncertainties through the equations used in Polar WRF. However, this approach would soon become impractical due to the complexity of the model equations, the sheer number of input variables, and their corresponding uncertainties. Additional uncertainty is introduced by numerical rounding errors within the model, and the use of parameterizations that simplify many complex atmospheric phenomena (e.g. cloud parameterizations).

We therefore rely on measurements to assess the accuracy of the modelled

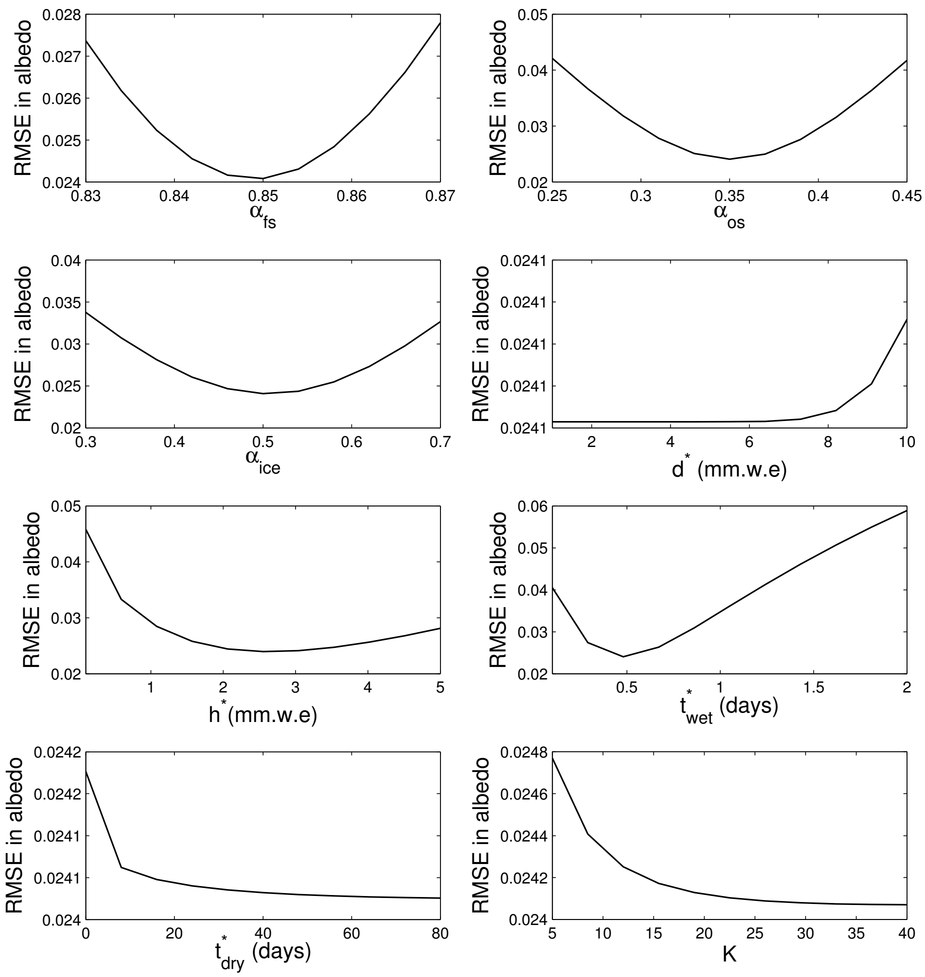

Figure 3.3: Calibration curves for WRF Calibration B. The calibration was carried out offline, and trial and error was used to the optimum combination of free parameters. Using this optimum calibration, each individual parameter was varied around it's optimum value, and the RMSE of the elevation transect compared to MOD10A1 calculated for each instance. The variation of RMSE with each of the free parameters are plotted above.

albedo. In situ measurements of albedo are very sparse, and are generally point measurements. To achieve suitable area coverage we use the MODIS

MOD10A1 daily albedo product. The 1.25km MOD10A1 albedo is re-gridded to mirror the 25km inner model domain allowing comparison with model output as described earlier. Validation of the MOD10A1 albedo is difficult, but Stroeve et al. (2006) compared it with albedo measurements at five weather stations on the western margin of the GIS, which span a range of elevations from the ablation zone to the ice sheet summit. Stroeve et al. (2006) calculated RMSEs for albedo in the dry snow, transitional, and ablation zones. Sources of uncertainty were associated with the use of a Bidirectional Reflectance Distribution Function (BRDF) correction, which corrects satellite albedo retrievals for errors caused by different viewing angles and solar illumination (Stroeve et al. (2006)). This correction is calculated using results from the DIScrete Ordinate Radiative Transfer model (DISORT), which also provides Anisotropic Reflectance Factors (ARFs) for each MODIS channel. The ARFs were used by Stroeve et al. (2006) to correct satellite retrievals to represent hemispheric albedo. DISORT was run for a single snow grain size (250μm), so variations in snow grain size will cause uncertainties in the ARFs. Additional uncertainty occurs because the ARFs were calculated ignoring diffuse radiation, and their magnitude will depend upon the ratio of direct to diffuse radiation. Further uncertainties in the MOD10A1 albedo come from slope effects, cloud detection errors, atmospheric corrections, and instrument calibration errors (Stroeve et al. (2006)).

In this study, we used the RMSEs calculated by Stroeve et al. (2006) as an estimate of the uncertainty in the MOD10A1 albedo. Since we compare mean elevation transects of MOD10A1 with the model output, the overall uncertainty of the MOD10A1 mean elevation must be calculated, by combining the uncertainties of each individual grid-point As explained earlier, the first step in calculating the seasonally averaged elevation transect of MOD10A1 is to average daily albedo values into 100m elevation bins. We conservatively predict that there is a high chance of systematic uncertainties during this spatial averaging step. During each particular satellite overpass, it is likely that large areas of the ice sheet (especially within the same elevation bin), will have similar illumination conditions, snow grain size, atmospheric conditions, viewing geometry and surface slope. Therefore, we take the more conservative approach of combining the MOD10A1 uncertainties as non-independent (rather than independent) when averaging into elevation bins.

The second step in calculating the seasonally averaged elevation transect of MOD10A1, is to average the albedo of each elevation bin for the entire season. Over the course of a melt season, illumination conditions, snow grain size, atmospheric conditions and viewing geometry will vary greatly. Since the variation of each of these factors is likely to be independent of the rest, we argue that their combined error will be randomized over time. Thus, we argue, the uncertainty of the MOD10A1 albedo at each location and time, is independent of the uncertainty of the MOD10A1 albedo at the same location, but at different times. Therefore, during the second step of calculating the seasonally averaged elevation transect of MOD10A1, the uncertainties for each elevation bin for each timestep (which were estimated (by combining as non-independent) in step one above), are combined independently (by adding the uncertainties in quadrature) while taking the seasonal average for each elevation bin.

Additional uncertainty originates from regridding MOD10A1 data from the native grid to the coarser model grid. The 25km model resolution does not accurately resolve the boundary of the ice sheet, yet the model does not allow for mixed glacier/non-glacier pixels (i.e. it considers a grid square to be either fully glaciated, or fully non-glaciated). There is therefore a high possibility that, around the ice sheet margin, we may be comparing a MODIS average albedo composed of some glaciated and some non-glaciated points, to the model albedo in a grid square that is specified as either purely glacial or purely non-glacial in Polar WRF. We account for this source of uncertainty (ϵ_{edge}), by considering the ratio of ice-edge grid cells (N_{edge}) to the total number of grid cells (N_{tot}) within each elevation bin, using the equation:

$$\epsilon_{\text{edge}} = \frac{1}{2}.\frac{N_{\text{edge}}}{N_{\text{tot}}}.(\bar{\alpha}_{\text{on}-\text{ice}} - \bar{\alpha}_{\text{off}-\text{ice}}) \tag{3.6}$$

Where $\bar{\alpha}_{\text{on}-\text{ice}}$ and $\bar{\alpha}_{\text{off}-\text{ice}}$ refer to the elevation bin seasonal mean albedos for on-ice grid cells and off-ice grid cells respectively. The factor of $\frac{1}{2}$ accounts for the fact that a Polar WRF grid cell at the edge of the ice sheet could be non-glaciated for up to half of its constituent area, but still be designated as glaciated. This therefore represents an upper bound for this source of uncertainty. Since off-ice grid cells have a lower average albedo than on-ice grid cells at the same elevation, we can be confident that this uncertainty is systematic, and can only act to lower the MODIS albedo in comparison to corresponding WRF predictions. We therefore only add this source of uncertainty to the upper bounds of uncertainty. Thus, we combine the uncertainty as follows:

$$\epsilon_{\text{upper}} = \epsilon_{\text{mod}} + \epsilon_{\text{edge}} \tag{3.7}$$

$$\epsilon_{\text{lower}} = \epsilon_{\text{mod}} \tag{3.8}$$

where ϵ_{upper} and ϵ_{lower} are the upper and lower bounds of uncertainty respectively.

3.3 Results and discussion

Two separate model calibrations, Cal A and Cal B, were performed offline for summer 2005. Cal A was obtained using the output (T_{ground}, d and h) from a previous Polar WRF run that used the default settings of the model (i.e. albedo was prescribed using the Engineers (1956) albedo parameterization) as input to the offline calibration. The parameterization with Cal A was run inline in Polar WRF for 2001 (a cold year), 2005 (to check the calibration) and 2007 (a warm year). This output is referred to as WCA. Although the parameterization had already been calibrated, the calibration process was repeated (Cal B) using the results from WCA for 2005 as input to the offline parameterization, instead of using results from the earlier default Polar WRF run. The results from Cal B were very different from those of Cal A, indicating that the inline parameterization used in WCA modified the model climate relative to that in the default simulation. Cal B was also run inline in Polar WRF, and a second set of output (WCB) was generated for 2001, 2005 and 2007. To clarify, “WCA” and “WCB” refer to the Polar WRF outputs with the albedo calibrations "Cal A" and "Cal B" respectively running inline.

3.3.1 Mean Elevation Transects

In this section, the skill of WCA and WCB at reproducing the MODIS MOD10A1 albedo vs. elevation profiles is examined. It will be demonstrated that (i) The new albedo parameterization improved upon the default albedo parameterization, (ii) WCB performed with more skill than WCA over the 3 years of comparison, and (iii) there is feedback between the albedo parameterization and the modelled climate.

WCA and WCB albedo vs. elevation profiles, are compared with MODIS MOD10A1 albedo vs.elevation profiles in Figure. 3.4. In 2005, the default Polar WRF albedo parameterization (Engineers (1956); Livneh et al. (2010)) vs. elevation is also compared. Both WCA and WCB performed with considerably lower RMSE (vs. MOD10A1 albedo) than the default Polar WRF albedo. Although the default albedo parameterization performed well at high elevation, it was unable reproduce the gradient of the MOD10A1 albedo with elevation, and performed poorly at low elevations. The overall RMSE of the default Polar WRF albedo was 0.12, compared to 0.0437 and 0.0442 for WCA and WCB respectively.

Both WCA and WCB performed with RMSE < 0.045 in each year, with the exception of WCA in 2001, for which the RMSE was 0.22. We investigate reasons for the poor performance of WCA in 2001 later in the study. The RMSEs of WCA and WCB compared to MODIS MOD10A1 in 2005 (both $\simeq$0.044) (Fig. 3.4), were considerably higher than those observed in the offline calibra-

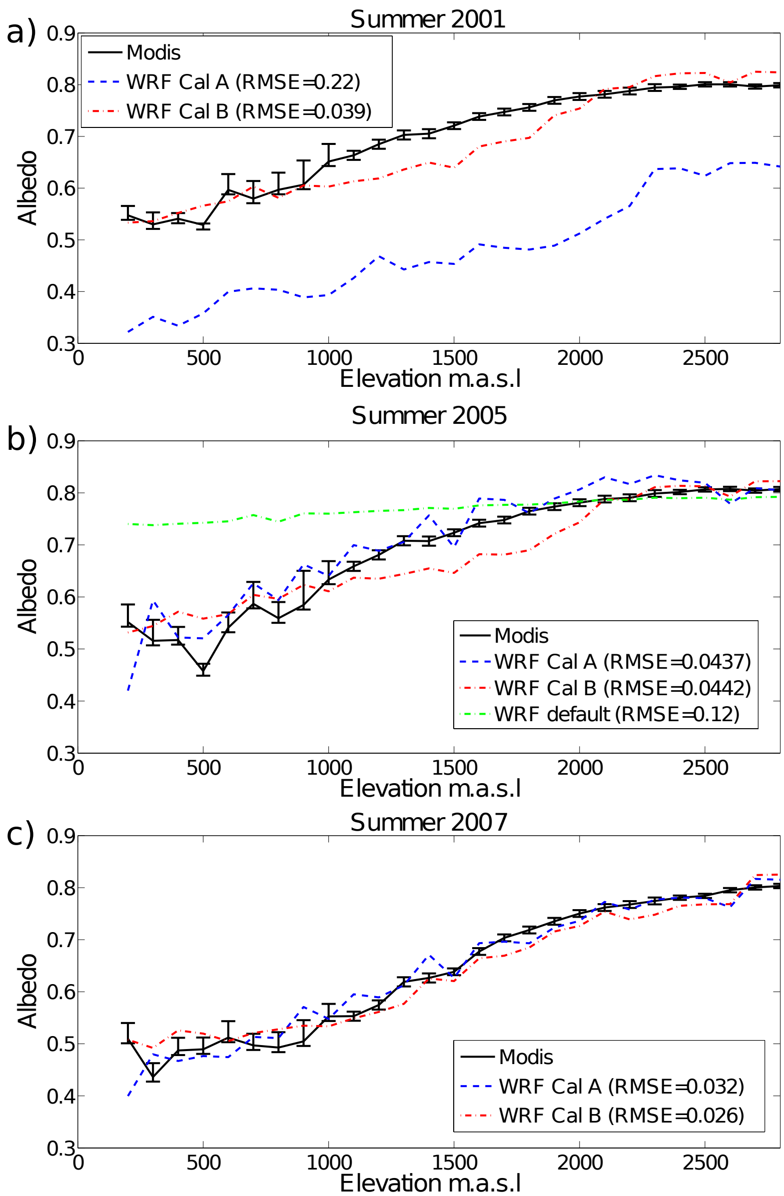

Figure 3.4: Mean elevation transect of albedo for the two calibrations alongside the MOD10A1albedo elevation profiles, for (top) 2001, (middle) 2005 and (bottom) 2007. In 2005, the mean elevation for the default Polar WRF albedo is also shown (green). Uncertainties for MOD10A1 are shown.

tions (0.033 for Cal A and 0.024 for Cal B) (Figures. 3.2 and 3.3). This could be explained by i) an error in either the offline or inline parameterization, or

ii) feedbacks between the albedo and modelled climate that change the input variables to the albedo parameterization in an appreciable manner. In order to rule out an error in either the inline or offline parameterizations, we compared the albedo predicted by WCA (running calibration A inline in Polar WRF), with the results of the offline parameterization, running Cal A and using WCA as input. The results were identical, indicating that the offline parameterization is working correctly. Therefore, the difference in the RMSE between the offline calibration and the the inline validation for 2005 implies that when run inline in Polar WRF, the albedo parameterization caused feedback between the modelled albedo and the modelled climate.

In 2005, both WCA and WCB reproduced the MOD10A1 albedo elevation profile with similar skill. WCB had a higher degree of skill at altitudes > 2000m, but it underestimated MOD10A1 between 1000m and 2000m (Figure. 3.4). Below 1000m WCB over-estimated MOD10A1 slightly. Although it produced a similar overall RMSE to WCB, WCA captured the overall shape of the MOD10A1 albedo profile more accurately - especially between 1000m and 2000m. The relatively high RMSE is attributed to the tendency of the RMSE to harshly penalize the highest residuals. Although WCA out-performed WCB in 2005, WCA produced a large negative residual at 200m elevation, which increased the RMSE to a level similar to that of WCB. In 2007, both calibrations of the parameterization worked effectively, with RMSE of 0.032 and 0.026 for WCA and WCB respectively. 2007 was chosen because it was a warm year, with a long melt season (Mote (2007)). For 2007, both WCA and WCB performed with lower RMSE than in 2005, the calibration year. 2001 was chosen as the second validation year because it was a cold year, with a short melt season (Mote (2007)). As noted earlier, WCA severely underestimated albedo at all elevations (RMSE=0.22) in 2001, while WCB performed well, with an RMSE of 0.039.

In summary, there was a feedback between the inline albedo parameterization and the modelled climate. When either Cal A or Cal B were run inline, the RMSE of the modelled albedo profile, compared to the MOD10A1 albedo profile, differed from the RMSE between the albedo profile generated in the offline calibration (Cal A or Cal B respectively), and the MOD10A1 albedo profile. The differences in RMSE between the inline and offline cases indicate that running the parameterization inline within Polar WRF, affects the modelled climate. The changes to the modelled climate, caused by the use of the inline albedo parameterization, include changes to the input variables of the albedo parameterization (snow depth, snow age, and surface temperature). These changes to the input variables cause the predicted albedo to be different from the value taken during the offline calibration. This demonstrates the feedback between the albedo parameterization and the modelled climate.

The feedbacks between the albedo and the model climate should be expected. However, the extent to which the calibrated albedo parameterization i) affects the model climate, and ii), is sensitive to the assignment of the free parameters, implies that the offline calibration method cannot produce a definitive “best” calibration for the inline version of the parameterization. Rather, the offline calibration provided “best guess” parameterizations (Cal A and Cal B), which were subsequently tested inline (WCA and WCB). WCB was shown to work well in three separate summers (2001, 2005 and 2007). With an RMSE < 0.05

in each case, we consider WCB to be the optimal calibration for use in this study.

3.3.2 Example Transect: Seasonal Evolution

In order to investigate the causes of the difference in performance of WCA and WCB in 2001, we sampled several variables from an example transect (ET) of the glaciated part of the model domain (Figure. 3.1). In the following section we investigate the behaviour of modelled ground and near surface air temperatures, snow depth, and terms in the surface energy budget along the ET. When distances are quoted, they refer to distances from the ice margin along ET.

Figure. 3.5(a) illustrates the seasonal evolution of albedo over the summer of 2001 at four distances along ET, according to the WCA and WCB model outputs. In each location, the WCB albedo was consistently higher than the WCA albedo for long time periods. The only occasion when the WCA albedo was higher than that of WCB was between day 15 and day 20 at 6km.

Fig. 3.5.b illustrates the seasonal evolution of d through the summer of 2001 for WCA and WCB. In each case, d has been normalised by the beginning of summer value of d. At 6km and 60km, the snow depths in WCA and WCB followed one another closely. However, at 24km and 42km from the ice margin, the snow depths in the two model runs diverged.

The only difference in setup between the WCA and WCB Polar WRF simulations is the calibration of the inline albedo parameterization. We observe that in the transect studied, changing the calibration dramatically changed the

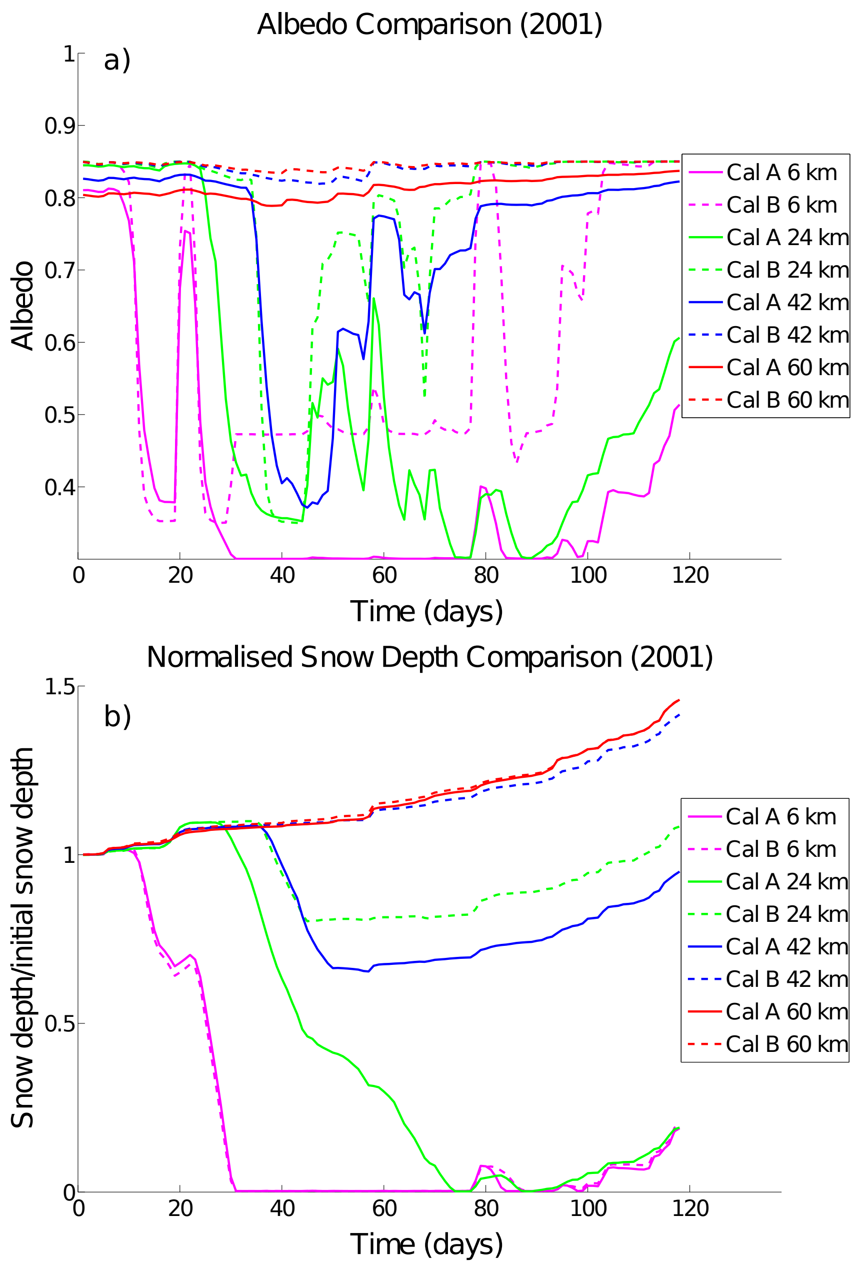

Figure 3.5: Comparison of a) albedo season evolution and b) snow depth seasonal evolution, at varying distances along ET from the ice margin for 2001. The distances indicated in the inset indicate distances from the ice margin along ET.

seasonal evolution of the modelled snowpack at 6km, 24km, and 42km, but it had little effect at 60km. Effectively, the end of summer snowline is moved further inland, and thus to a higher elevation, in the WCA simulation than in the WCB simulation. The dramatic difference of the snowpack evolution between WCA and WCB, is due to differences in the energy budget of the snowpack between the two simulations. These differences are entirely caused by the different albedo calibration used in each of the simulations. The objective of the next section is to investigate how the two differing calibrations of the albedo parameterization affected each of the terms in the energy budget in WCA and WCB.

3.3.3 Example Transect: Differencing WCA and WCB

In order to investigate the implications for the modelled climate of changing the calibration of the inline albedo parameterization, components of the energy and mass balance are examined. It was found that the differences in albedo between WCA and WCB changed the modelled energy balance significantly. In previous studies, such a change in the energy balance has been accounted for by applying a correction for albedo after the model was run (e.g. Box et al. (2004)). However, the changes to the energy balance in this study significantly affected all of the energy balance components, and demonstrated the importance of running an accurate albedo parameterization inline within Polar WRF. To demonstrate this point, we explore the differences between each of the energy balance components, as modelled in WCA and WCB. The differences (WCA-WCB) in the seasonal means of a range of variables, are presented in Figures. 3.6 and 3.7. The notation "Δ" is used to indicate such differences.

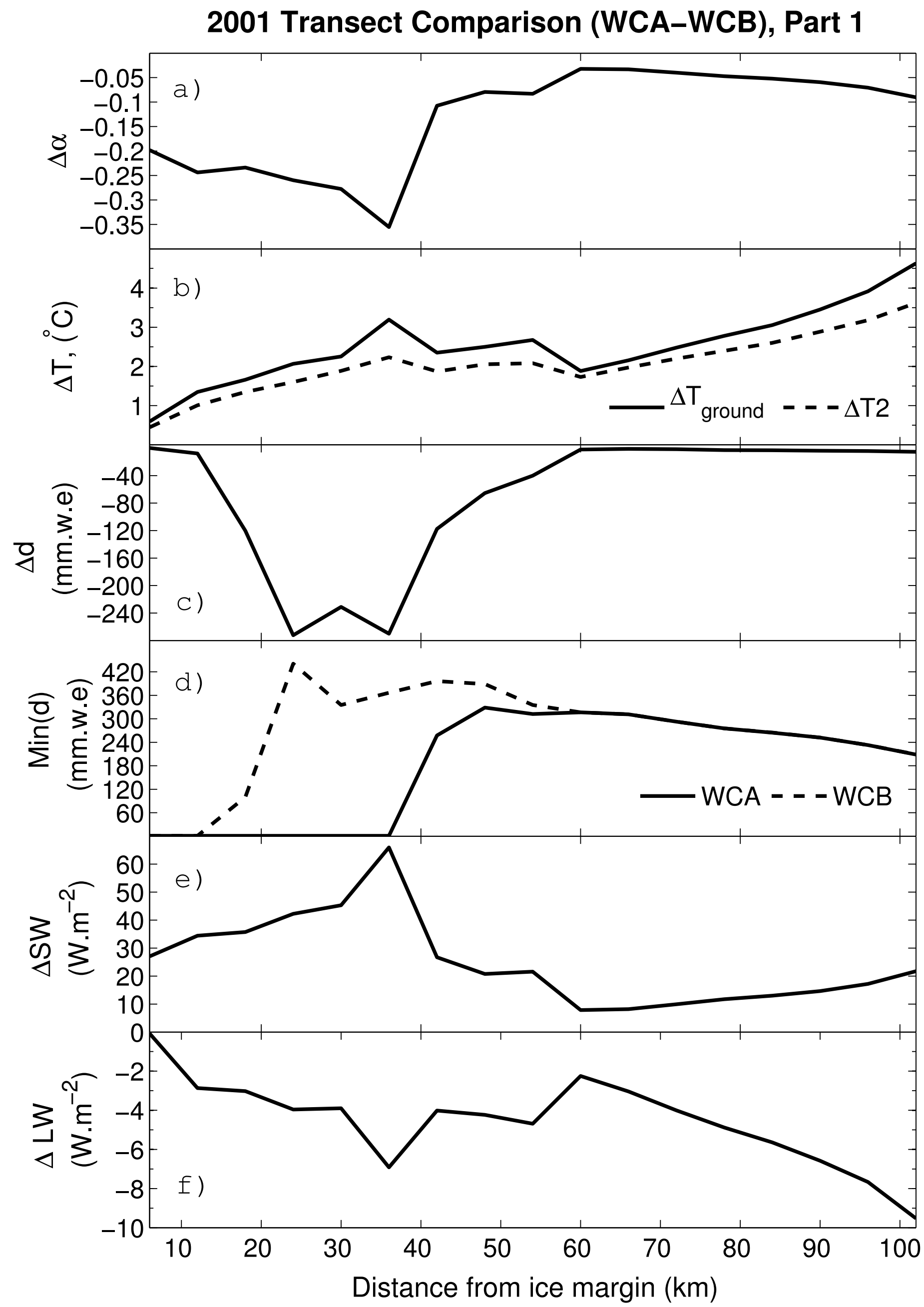

Figure 3.6: Summer mean differences (WCA - WCB) along ET, summer 2001, for: a) albedo, b) ground and 2m air temperature, c) water equivalent snow depth, e) net shortwave radiation flux, and f) net longwave radiation flux. d) illustrates the minimum snow depths for WCA and WCB along ET.

Albedo

The difference in summer mean albedo ($\Delta\alpha$) between WCA and WCB along ET (Figure. 3.6(a)) increases slowly in magnitude (absolute value decreases) from the ice margin to around 40km, at which point it decreases in magnitude sharply to -0.03 at 60km. Further inland, $\Delta\alpha$ increases in magnitude again, reaching -0.09 at 100km. The largest values of $\Delta\alpha$ occur mostly, but not exclusively, in regions where snow pack removal occurred earlier in the season in WCA than WCB. At 6km inland, snow removal occurred with similar timing in WCA and WCB, yet $\Delta\alpha$ was large (Figure 3.5(b)).

Temperature

The differences in surface temperature and two metre air temperature, (ΔT_{ground} and $\Delta T2$ respectively), increase with distance from the ice margin (Figure. 3.6(b)). In both cases, the difference is highest at 100km, but there is a localised maximum between 30km and 40km. Generally, as $\Delta\alpha$ increases in magnitude, so do $\Delta T2$ and ΔT_{ground}. Between 0-36km, $\Delta\alpha$ increased in magnitude, as did ΔT_{ground} and $\Delta T2$. This is also true for distances >60km along ET. However, between 40km-60km, this is reversed; the magnitude of $\Delta\alpha$ decreased, as did the magnitude of ΔT_{ground} and $\Delta T2$.

The difference in the modeled temperature between WCA and WCB is a manifestation of the differing climates in WCA and WCB. It is indicative of feedback between the modeled albedo and climate.

Snow Depth

The difference in d between WCA and WCB (Figure. 3.6(c)) was very small at distances greater than 60km. However, between 0km and 60km, there were significant differences. The largest difference in seasonal mean snow depth was $\sim$ 0.25 m.w.e between 24km and 36km. Either side of this region, the difference in snow depth decreased, and was negligible at the ice margin, and at >60km. The patterns seen in Figures. 3.6(c) and 3.5(b)) indicate that the two parameterizations yield very different end of summer snowline trajectories in this region of the ice sheet. This is confirmed by comparing the annual minimum snow depth along the transect (Figure 3.6(d)). The end of summer snowline location on the transect is distinguished by the location at which the entire snowpack is melted, exposing the end of summer surface of the previous year. In WCA, this occured 36km from the ice margin, whereas in WCB it occurs at just 12km from the ice margin. The change in seasonal averaged snow depth and position of the end of summer snowline between WCA and WCB, are again an indication of the impact of the calibration of the albedo parameterization, on the modelled climate. In the following sections, each component of the energy budget is presented in turn. It will be shown that the albedo parameterization does not just affect the net shortwave radiation, but that it causes significant changes to all of energy budget terms.

SW and LW Radiation Fluxes

Net shortwave (SW) and net longwave (LW) fluxes are calculated within the model as:

$$SW = (1 - \alpha)SW_{in} \tag{3.9}$$

$$LW = LW_{in} - \epsilon\sigma T^4_{ground} \tag{3.10}$$

Where SW_{in} and LW_{in} are the incoming shortwave and longwave fluxes respectively, ϵ is the surface emissivity, and σ is the Stefan-Boltzmann constant. The difference in seasonal mean net shortwave radiation, ΔSW, (Figure. 3.6(e)) is a direct response to $\Delta\alpha$. Such a response is expected because α directly determines the reflected shortwave radiation ($SW_{out} = \alpha SW_{in}$). ΔSW is positive throughout the transect (expected, because $\Delta\alpha < 0$ throughout the transect), and closely mirrors the shape of $\Delta\alpha$.

Less intuitive is the difference in the season mean net longwave radiation, ΔLW, (illustrated Figure. 3.6(f)). Outgoing longwave radiation is determined by the surface temperature through the Stefan-Boltzmann Law (Equation 3.10). The difference in ΔT_{ground} is illustrated in Figure. 3.6(b). The spatial pattern of ΔT_{ground} along ET, is negatively correlated with ΔLW. This may be understood, by considering that the second term in the right hand side of equation 3.10, is proportional to T^4_{ground}.

ΔLW, although not directly affected by $\Delta\alpha$, has been significantly affected by the change to the modelled temperature resulting from $\Delta\alpha$. It is a negative feedback, because it has opposite sign to ΔSW, the variable that is affected directly by $\Delta\alpha$. So lower albedo leads to an increase in SW which increased

T_{ground}. However, this is partially offset by the decrease in LW.

Overall, the shortwave and longwave fluxes responded to the changes in albedo between WCA and WCB with opposite sign. In the trivial case of the net shortwave radiation, the decrease in albedo in WCA compared to WCB caused more shorwave radiation to be absorbed by the surface, which increased the surface temperature, and thus further decreased the albedo through metamorphism. Thus there is a positive feedback mechanism between the albedo and net shortwave radiation flux. In the case of the net longwave radiation, the increase in surface temperature caused by the decreased albedo in WCA compared to WCB, caused an increase in outgoing longwave radiation in WCA compared to WCB. As a result, the net longwave radiation flux decreases, which negatively feeds back on the surface temperature. Thus, there is a negative feedback between albedo and net longwave radiation flux, although feedback is less than the feedback between albedo and net shortwave radiation.

Turbulent Fluxes

The sensible heat flux (Q_H) and latent heat flux (Q_L) are both lower in WCA than in WCB (Figure. 3.7(a)). The season mean differences, ΔH and ΔL follow similar patterns to one another. These patterns are attributed to changes in the near surface temperature lapse rate ($\beta_s = \frac{\partial T}{\partial z}$), and the near surface vertical gradient of water vapor pressure ($e' = \frac{\partial e}{\partial z}$, where e is the water vapor pressure) (expanded upon later in this section).

H, defined as positive towards the surface, is modelled as conduction, with

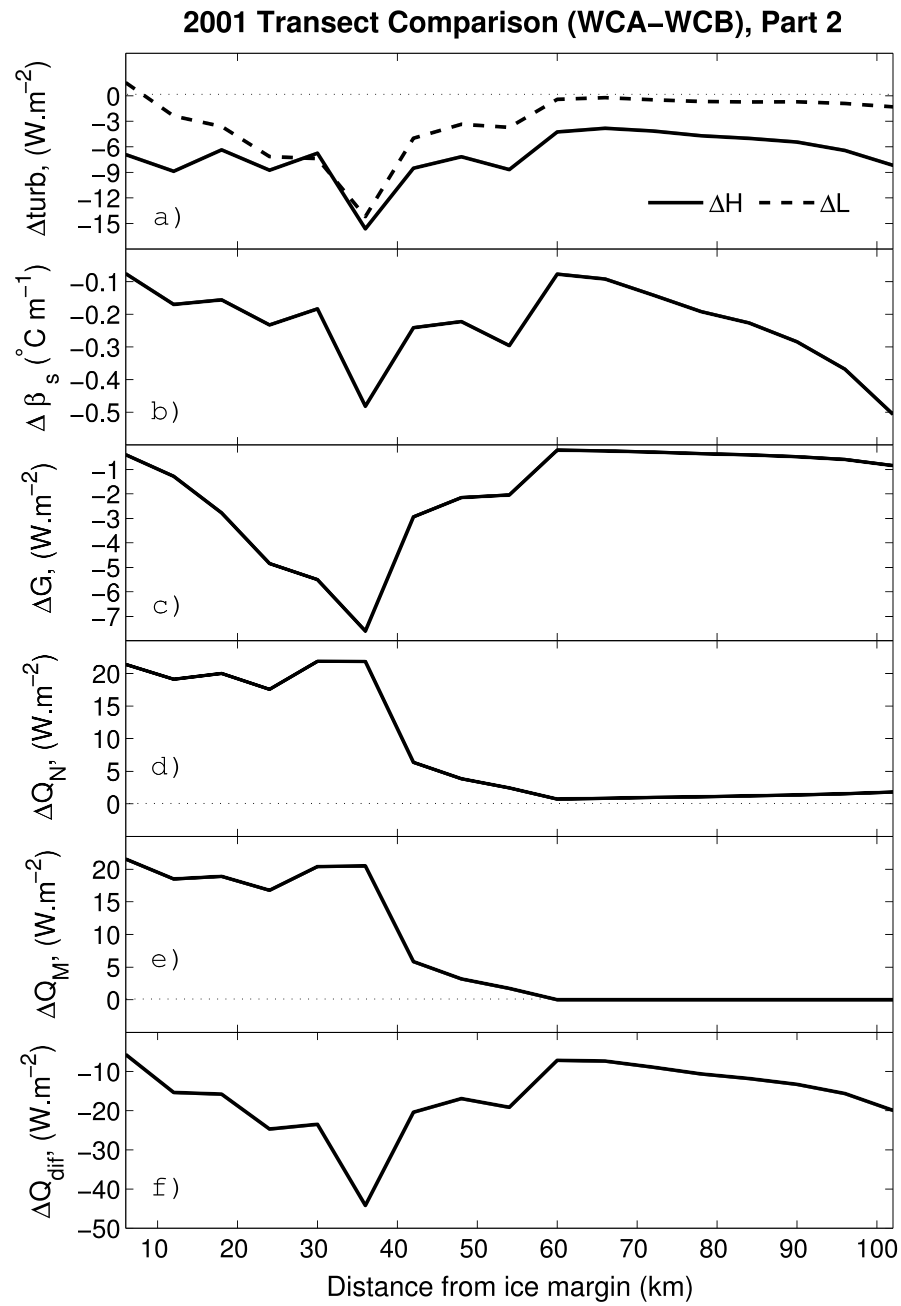

Figure 3.7: Summer mean differences (WCA - WCB) along ET, summer 2001, for: a) Sensible and Latent heat fluxes, b) Near surface temperature lapse rate, c) ground heat flux, d) net energy flux, e) melt energy flux and f) energy flux available for changing surface layer temperature (calculated as $Q_N - Q_M$).

eddies taking the place of molecules (Paterson (1994), page 60):

$$Q_H = K_h \rho c_p \frac{\partial T}{\partial z} \tag{3.11}$$

Where K_h is the eddy diffusivity for heat, c_p is the specific heat capacity at constant pressure, and ρ is air density. Q_H is dependent upon β_s, and therefore it is not surprising to see that the lower β_s found in WCA compared to WCB (Figure. 3.7(b)) causes the decrease in H. The shape of ΔH closely resembles that of $\Delta\beta_s$.

Q_L, the heat flux due to the vertical flux of water vapor (E), is dealt with similarly to Q_H, with the mass of water vapor per unit volume, m, taking the place of the of heat energy per unit volume ($\rho c_p T$) (Paterson (1994), page 60-61):

$$Q_L = -L_v E = L_v K_w \frac{\partial m}{\partial z} = L_v K_w \left(\frac{0.622\rho}{P}\right) \frac{\partial e}{\partial z} \tag{3.12}$$

L_v is the latent heat of vaporization, K_w is the eddy diffusivity of water vapor and P is atmospheric pressure. Q_L depends on e'; lower values of e', (positive gradient is defined as increasing vertically upward), lead to higher values for Q_L. e' is proportional to the difference between the water vapor mixing ratio at 2m and at the surface. There was no difference between modelled e at 2m in WCA and WCB. Therefore, any differences in e', are due to differences in e at the surface. It was noted earlier that T_{ground} is higher, and that far more of the snowpack melts in WCA than in WCB (Figures. 3.6 (b),(c) and (d)). Also, at many locations along ET, melt onset occurred earlier in WCA than WCB (Figure. 3.5 (b)). As a result of the increased melt duration, e at the surface is higher in WCA than in WCB. Therefore, e' is lower (more negative) in WCA compared to WCB, and this is reflected in ΔL, which is negative in the areas where there was more/earlier snow removal in WCA than WCB. At distances greater than 60km from the margin, ΔL was zero. This coincides with regions of the transect where there was no difference in the melt produced in WCA and WCB. We note that ΔH and β_s are negative in this region, indicating that the surface temperature was higher in WCA than in WCB, but not sufficiently to cause melt, and make significant changes to Q_L.

Overall, the response of both turbulent fluxes to the change in albedo in WCA compared to WCB was negative. This shows that the changes in the turbulent fluxes diminish the additional energy absorbed by the surface due to the lower albedo in WCA compared to WCB. Therefore, both turbulent fluxes feed back negatively on albedo.

Ground Heat Flux

Q_G is the ground heat flux. Positive values of Q_G indicate upward heat flux (warming the surface). Q_G is dependent upon the vertical gradient of temperature in the modelled subsurface ($\beta_g = \frac{\partial T_{sub}(z_g)}{\partial z_g}$, where $T_{sub}(z_g)$ is the subsurface temperature at depth z_g below the surface), and on the thermal conductivity of the subsurface (K_{th}):

$$Q_G = K_{th} \frac{\partial T_{sub}(z_g)}{\partial z_g} \tag{3.13}$$

Positive β_g (defined as T_{sub} increasing vertically downwards), leads to positive values of Q_G, which imply a positive heat flux in the upward direction, thus heating the surface.

The difference between season mean ground heat flux (ΔG) in WCA and WCB is illustrated in Figure. 3.7(c). ΔG is negative throughout the domain, and peaks between the end of summer snowline positions of WCA and WCB (Figure. 3.6 (d)). This is due to differences in β_g and K_{th} between WCA and WCB, which are now discussed.

In Polar WRF, the temperature of the lowest subsurface layer is held constant in time. Therefore, changes to T_{ground} are proportional to changes to β_g. Since T_{ground} is warmer in WCA than WCB, β_g is less in WCA than WCB. This is true at all locations along ET, and leads to the negative value of ΔG. The maximum magnitude of ΔG is located 36km inland, in the region between the end of summer snowline positions for WCA and WCB. This particular location makes sense, because $Q_G \propto K_{th}$, and K_{th} is almost 10 times larger for ice ($K_{th} \sim$ 2.10 - 2.75 Wm^{-2} (Yen (1981))), than for snow ($K_{th} \sim$ 0.3 - 0.6 Wm^{-2} (Van Dusen (1929); Schwerdtfeger (1963))). In other words, ice is a far more effective conductor of heat than snow. Snow has the effect of thermally insulating the surface, and minimizing Q_G. In the region between the end of summer snowline positions of WCA and WCB, where ΔG is largest, WCA loses all of its snow to melt, whereas WCB does not. Since snow is such as effective insulator, the ground heat flux in WCB is subdued compared to WCA. In WCA, the snow was removed in this region, and hence the magnitude of the ground heat flux was greatly increased.

Similar to the net longwave radiation, and the turbulent energy fluxes, the response of the ground heat flux to the increase in albedo in WCA compared to WCB is negative. The presence of the ground heat flux in the model, when the albedo was lowered in WCA, reduced the overall increase of radiation at the surface in WCA compared to WCB. Thus the ground heat flux has a negative feedback on albedo.

Net Energy Flux

The net energy flux (Q_N) is calculated as:

$$Q_N = SW + LW + Q_H + Q_L + Q_G + Q_R \tag{3.14}$$

Q_R is the latent heat due to the freezing of liquid rain within the snow-pack, which is very similar in WCA and WCB, with $-0.05Wm^{-2} < \Delta Q_R < 0.2Wm^{-2}$, and is therefore not discussed in detail. The difference in net energy flux (ΔQ_N) between WCA and WCB is illustrated in Figure. 3.7(d). Each of the components of ΔQ_N contributed significantly to the overall value, indicating that the albedo parameterization has a significant impact on many aspects of the model climate. While ΔSW was large enough to cause ΔQ_N to increase significantly, we have seen that each of the other components in the energy budget (LW, Q_H, Q_L and Q_G) diminished the impact of the ΔSW, by assuming the opposite sign. The overall magnitude of this will be examined below. However, in the next section, it is shown that most of ΔQ_N was used to perform additional melting of snow or ice.

Energy Flux for Melting

The net surface energy flux is used to heat the surface of the glacier when the surface temperature is below the melting point. If the surface is at the melting point, the net surface energy flux is used to melt snow or ice.

ΔQ_M (illustrated in Figure. 3.7(e)) follows ΔQ_N very closely, indicating that most of the excess Q_N found in WCA compared to WCB, is used to perform additional melting in WCA. There is a clear step in ΔQ_M. At distances $\leq$40km inland, ΔQ_M is large, indicating much more energy was used for melting in WCA than in WCB. This excess melt energy is responsible for the difference in end of season snowline position between WCA (40km inland) and WCB (12km inland), and responsible for excess ice melting at distances $\leq$12km inland. At distances >40km inland, ΔQ_M is very small, because there was little melt in either WCA or WCB, because T_{ground} never reached the pressure melting point.

The difference, $\Delta Q_{surf} = \Delta Q_N - \Delta Q_M$ (not shown graphically), is the additional energy used to heat the surface in WCA compared to WCB. Below 60km from the ice margin, ΔQ_{surf} is very small compared to ΔQ_M. This implies that very little additional energy was used for heating the surface in WCA compared to WCB. This is logical, since the same energy is required to heat the surfaces to the melting point in WCA and WCB, since both model runs were initiated with identical initial conditions. The small value of ΔQ_{surf} below 60km is associated with the difference in surface temperature cooling between WCA and WCB, after the end of the melt season. At distances further than 60km inland, no melt occurs in either WCA or WCB. In this region, all of ΔQ_N (which is small) is used solely for additional heating of the surface.

Non - Shortwave Energy Flux

As has been discussed earlier, the only surface energy flux to which the albedo is directly related is the shortwave flux. However, this study has shown that changing the calibration of the inline albedo parameterization within Polar WRF had significant effects on all of the energy balance components. To illustrate this point, Figure 3.7(f) shows the summer mean difference between WCA and WCB, for the sum of all the surface energy fluxes except the net shortwave energy flux ($\Delta Q_{dif} = \Delta Q_N - \Delta SW$). ΔQ_{dif} represents the combined effect of changes in the longwave, turbulent, and ground energy fluxes on the surface energy balance that result from the changes to the calibration of the inline albedo parameterization. ΔQ_{dif} ranges from -7.1Wm^{-2} to -44.4 Wm^{-2}, and is a significant proportion of ΔSW. This is an important result, because it demonstrates that the parameterization of albedo significantly affects all of the energy balance components, and not just the (obvious) shortwave flux, with which it has a direct relation. In the most extreme case, at 36km inland, ΔSW = 66 W m^{-2}, but $\Delta Q_{dif} = -44.2$ W m^{-2}, more than two thirds the magnitude of ΔSW, leaving the resultant change to the net energy balance, $\Delta Q_N = 21.8$ W m^{-2}. The net effect of ΔQ_{dif} is to reduce the overall net energy balance in WCA compared to WCB. This implies, that if the feedbacks were not present, and the effect of changing albedo was simply to change the net shortwave radiation, the resulting net energy balance would be unrealistically high. In other words, the feedback of the albedo on the other energy balance components causes the effect of changing the albedo on the net energy balance to be diminished.

Previous studies have corrected for an inaccurate albedo parameterization with a post-run correction to the net shortwave energy flux (e.g. Box et al. (2004)). This study suggests that this method would lead to an over-estimation of the net energy balance, and therefore an over-estimation of melt (assuming that the albedo was overestimated, as is the case with the default albedo parameterization in this study (figure 3.4(b))).

In summary, although the model setup for WCA and WCB was identical apart from the calibration of the albedo parameterization, the modelled surface variables changed significantly between the two model runs. This was manifest in the changes to the modelled near surface air temperature, surface temperature, end of summer snowline position, and all of the energy budget terms. Despite the similar model setups, all of the differences (WCA-WCB) in the energy budget components (apart from latent heat due to freezing rain), at their respective maximums along ET, varied within one order of magnitude of each other, (high 10^0 to mid 10^1 Wm^{-2}).

While the shortwave energy flux was, predictably, higher due to the increase in albedo in WCA compared to WCB, all of the other surface energy components were lower. In some locations, the change to the longwave, turbulent and ground energy fluxes, was over 65% of the change to the shortwave radiation. This leads us to the conclusion that a reliable albedo parameterization must be run inline within Polar WRF in order to accurately predict the net energy balance. If, instead of running an albedo parameterization inline, a post-run correction for albedo were applied to the net shortwave radiation (e.g Box et al. (2004)), there would be considerable inaccuracies in Q_N, and therefore the Q_M. This would have implications for modelling climatic balance, as melt calculations are a core objective of such studies.

3.4 Conclusions

This study has presented a glacier and ice sheet albedo parameterization that has been programmed inline into the NOAH land surface scheme within the Polar WRF regional climate model. This represents a step forward for running Polar WRF over glaciated regions, because it allows the modelling of albedo without a requirement for an additional dataset, and provides the opportunity for an albedo - climate feedback.

In previous studies using Polar WRF/MM5 albedo has either been prescribed as a constant, (which is highly inaccurate and precludes any feedback on the modelled atmosphere), or as a field of monthly satellite derived albedos (Box et al. (2004); Bromwich et al. (2001)), which although more accurate, precludes the climate feeding back on albedo, and requires an additional input dataset.

Due to computational constraints, the parameterization used here had to be calibrated offline, using previously produced Polar WRF output as the input for the offline version of the parameterization. We found that i), the offline parameterization used for calibration was sensitive to changes in the input, and ii), when running a calibration inline within Polar WRF, the presence of the inline parameterization had a sufficiently strong effect on the modelled climate that the variables needed for the albedo parameterization itself, were significantly altered. As a result, we found that the optimum offline calibration from one Polar WRF output, when run inline in a new Polar WRF simulation, produced a modelled climate in which the same calibration for the albedo parameterization was no longer optimal. In other words, although the offline calibration method generated calibrations that produced good results when run inline, it was not possible to find a definitive "best" calibration for the parameterization. If we were able to perform the calibrations inline, it would be possible to find the "best" calibration. However, this is computationally unrealistic, because it would involve re-running the entire Polar WRF simulation for each combination of model parameters)

Working with the limitations described, we calibrated the model for the summer of 2005. We presented two calibrations (Cal A and Cal B) of the model which were run inline within Polar WRF for the summers of 2001 (a cold year), 2005 (the calibration year) and 2007 (a very warm year). The model outputs, WCA and WCB, of albedo were both successful for 2005 and 2007, with RMSE$<$0.045 in each case. However, in 2001, WCA performed poorly (RMSE=0.22), whereas WCB performed similarly well to the other years, with RMSE=0.039. We conclude that WCB, (Polar WRF with Cal B running inline), was able to successfully reproduce gradients of ice sheet albedo along the western side of the Greenland Ice Sheet, for both the calibration summer (2005), and two additional summers (2001 and 2007) with contrasting air temperature conditions.

Feedbacks between albedo and the modelled climate were investigated by studying the differences in energy and mass budget components generated by WCA and WCB along an example transect from the model domain for

2001. All components of the energy budget were affected by the differences in the albedo parameterization, and the responses were of a similar order of magnitude to one another (apart from latent heat of freezing rain, which showed a very small response). The response of the longwave, turbulent, and ground energy fluxes to the changing albedo was oppositeto that of the net shortwave flux. While the shortwave flux exhibited a positive feedback with albedo, all of the other energy balance components showed a negative feedback. The additional energy absorbed by the surface as a result of reducing the albedo, was significantly reduced (by up to two thirds) by the combined negative feedbacks involving the longwave, turbulent, and ground energy fluxes. In addition to the energy balance components affected by the albedo parameterizations, it was observed that the surface temperature, near surface air temperature, and position of the end of summer snowline were also affected.

From these results, it is concluded that (i) the inline albedo parameterization had significant feedback with many aspects of the model climate and (ii) it is necessary to have the parameterization running inline in the model. In some previous studies (e.g. Box et al. (2004)), albedo was set as a constant (0.8) in the RCM during the run, and a post run correction for the reductions in albedo during the melt season was applied to the net-shortwave flux after the run was completed. The results of this study suggest that the increases to the net energy balance from applying such a correction, would be an overestimate, because they would not account for the negative feedbacks involving the longwave, turbulent, and ground energy fluxes.

In conclusion, this study represents a step forward in the evolution of Polar

WRF in modelling climate over land ice, since (i) it allows the model to capture the basic elevation profile of albedo on the Greenland Ice Sheet, without relying on an additional input dataset, and (ii) it allows full feedback between albedo, and the modeled climate, while also being computationally efficient. Eventually a full multi layer snow/firn model should be integrated inline into Polar WRF. If such a model integrated more realistic snow physics, such as temperature diffusion and melt water percolation and refreezing, it could allow climatic balance to be calculated inline in Polar WRF, and for more realistic feedbacks between glaciated surfaces and the modelled climate.

3.5 Acknowledgements

The Polar WRF boundary conditions used in this study are from the Research Data Archive (RDA) which is maintained by the Computational and Information Systems Laboratory (CISL) at the National Center for Atmospheric Research (NCAR). NCAR is sponsored by the National Science Foundation (NSF). The original data are available from the RDA (http://dss.ucar.edu) in dataset number ds083.2.

Bibliography

Bindoff, N., J. Willebrand L., V. Artale, A. Cazenave, J. Gregory, S. Gulev, K. Hanawa, C. Le Quéré, S. Levitus, Y. Nojiri, C. K. Shum, L. D. Talley, and A. Unnikrishnan. 2007 : 384–432.

Bougamont, M, J Bamber, and W Greuell. "A surface mass balance model for the Greenland Ice Sheet." *Journal of Geophysical Research* 110 (2005).

Box, J. E., D. H. Bromwich, and L.S. Bai. "Greenland ice sheet surface mass balance 1991–2000: Application of Polar MM5 mesoscale model and in situ data." *Journal of Geophysical Research* 109 (2004).

Box, J. E., D. H. Bromwich, B. A. Veenhuis, L. S. Bai, J. C. Stroeve, J. C. Rogers, K. Steffen, T. Haran, and S. H. Wang. "Greenland ice sheet surface mass balance variability (1988-2004) from calibrated polar MM5 output." *Journal of Climate* 19 (Jun 2006): 2783–2800.

Bromwich, D. H., J. J. Cassano, T. Klein, G. Heinemann, K. M. Hines, K. Steffen, and J. E. Box. "Mesoscale modeling of katabatic winds over Greenland with the Polar MM5." *Monthly Weather Review* 129 (2001): 2290–2309.

Cassano, J. J., J. E. Box, D. H. Bromwich, L. Li, and K. Steffen. "Evaluation of polar MM5 simulations of Greenland's atmospheric circulation." *Journal of Geophysical Research* 106 (Dec 2001): 33867–33889.

Cogley, J.G., R. Hock, L.A. Rasmussen, A.A. Arendt, A. Bauder, R.J. Braithwaite, P. Jansson, G. Kaser, M. Möller, L. Nicholson, and M. Zemp. "Glossary of Glacier Mass Balance and Related Terms." *IHP-VII Technical Documents in Hydrology.* 2011.

Dyurgerov, M., M. Meier, and R. Armstrong. "Glacier Mass Balance and Regime: Data of Measurements and Analysis." *University of Colorado Institute of Arctic and Alpine Research Occasional Paper 55* (2002).

Dyurgerov, M., M. Meier, and R. Armstrong. "Mass Balance of Mountain and Sub-Polar Glaciers Outside the Greenland and Antarctic ice sheets.." *Supplement to the M. Dyurgerov Occasional Paper 55, 2002.* (2005).

Engineers, US Army Corps Of. Summary Report of the Snow Investigations - Snow Hydrology. Technical report, North Pacific Division, Corps of Engineers, U.S. Army, Portland, Oregon, 1956.

Ettema, J, M R. van den Broeke, E van Meijgaard, W Jan van de Berg, J L. Bamber, J E. Box, and R C. Bales. "Higher surface mass balance of the Greenland ice sheet revealed by high-resolution climate modeling." *Geophys. Res. Lett.* 36 (06 2009).

Fettweis, X, H Gallée, L Lefebre, and J.P van Ypersele. "Greenland surface mass balance simulated by a regional climate model and comparison with satellite derived data in 1990-1991." *Climate Dynamics* (2005): 623–640.

Guo, Z. C., D. H. Bromwich, and J. J. Cassano. "Evaluation of Polar MM5 simulations of Antarctic atmospheric circulation." *Monthly Weather Review* 131 (Feb 2003): 384–411.

Hines, K M. and D H. Bromwich. "Development and Testing of Polar Weather Research and Forecasting (WRF) Model. Part I: Greenland Ice Sheet Meteorology.." *Monthly Weather Review* 136 (2008): 1971–1989.

Hines, K.M., D.H. Bromwich, and R.I. Cullather. "Evaluating moist physics for Antarctic mesoscale simulations." *Annals of Glaciology* 25 (1997): 282–286.

Jacob, T., J. Wahr, T. Pfeffer, and S. Swenson. "Recent Contributions of Glaciers and Ice Caps to Sea Level Rise." *Nature* 10847 (2012).

Livneh, B, Y Xia, K E. Mitchell, M B. Ek, and D P. Lettenmaier. "Noah LSM Snow Model Diagnostics and Enhancements." *Journal of Hydrometeorology* 11 (2010): 721–738.

Mote, T. L. "Greenland surface melt trends 1973–2007: Evidence of a large increase in 2007." *Geophysical Research Letters* (2007).

Oerlemans, J. and W.H. Knap. "A 1 year record of global radiation and albedo from the ablation zone of the Morteratschgletscher, Switzerland." *Journal of Glaciology* (1998).

Oerlemans, J. and H. F. Vugts. "A Meteorological Experiment in the Melting Zone of the Greenland Ice Sheet.." *Bulletin of the American Meteorological Society* 74 (March 1993): 355–366.

Paterson, W. S. B. *The Physics of Glaciers (3rd edn. ed.)*. Pergamon, Oxford, 1994.

Schwerdtfeger, P. "Theoretical Derivation of the Thermal Conductivity and Diffusivity of Snow." *IASH* 61 (1963): 75–81.

Stroeve, J C., J E. Box, and T Haran. "Evaluation of the MODIS (MOD10A1) daily snow albedo product over the Greenland ice sheet." *Remote Sensing of Environment* 105 (2006): 155 – 171.

Van Dusen, M.S. "Thermal conductivity of non-metallic solids." *International Critical Tables of Numerical Data, Physics, Chemistry and Technology. 216–217.* . McGraw-Hill, New York: Washburn, E.W. (Ed.),, 1929. 216–217.

Van Lipzig, N.P.M, E. Van Meijgaard, and Oerlemans. J. "Evaluation of a Regional Atmospheric Model Using Measurements of Surface Heat Exchange Processes from a Site in Antarctica." *Monthly Weather Review* 127 (1999): 1994–2011.

Wientjes, I. G. M. and J. Oerlemans. "An explanation for the dark region in the western melt zone of the Greenland ice sheet." *The Cryosphere Discussions* 4 (2010): 163–181.

Yen, Y.C. "Review of Thermal Properties of Snow, Ice and Sea Ice." *CRREL Report* (1981).

Zwally, H. J, W Abdalati, T Herring, K Larson, J Saba, and K Steffen. "Surface Melt-Induced Acceleration of Greenland Ice-Sheet Flow." *Science* 297 (2002): 218–222.

CHAPTER 4

Simulating 8 years of Climatic and Total Mass Balance in the Canadian High Arctic using Polar WRF [1]

4.1 Introduction

One of the challenges posed by recent climate warming is the uncertainty associated with the potential contribution of glacier wastage to sea level rise. Terrestrial ice loss through meltwater runoff and iceberg calving, is thought to currently be the largest contributor to sea level rise (Church (2001); Jacob et al. (2012)). To date, a large proportion of this contribution is thought to have come (and is predicted to continue to come) from smaller ice masses and glaciers, (Meier et al. (2007); Bindoff et al. (2007)), although the ice sheet contribution is growing (Jacob et al. (2012)). As the Canadian Arctic Islands (CAI) contains the largest concentration of terrestrial ice (~160,000km^2) outside the two major ice sheets (Dyurgerov et al. (2005, 2002)), characterization

[1] A version of this chapter is being prepared for journal submission with the author list: Benjamin Gready, Alex Gardner, James Davis, Martin Sharp, Jason Box and Andrew Bush

of the glacier mass balance in this critical region is essential in order to obtain accurate estimates of the potential contribution of the World's glaciers to global sea level change.

Regional estimates of mass balance in the CAA for the period 1995-2000 have been obtained from repeat airborne laser altimetry surveys (Abdalati et al. (2004)). Estimates for 2004-2009 have been obtained using repeat satellite gravimetry (GRACE), repeat satellite laser altimetry (ICESat), and a mass budget model (Gardner et al. (2011)). Results suggest that the CAI is losing ice at an accelerating rate, with the rate increasing from 31±8 Gt yr^{-1} in 2004-2006 to 92±12 Gt yr^{-1} in 2007-2009. Mass balance records from the Devon, Meighen and Melville South ice caps, and White Glacier in the CAI date back to the late 1950s/early 1960s, with a common record dating back to 1963. Sharp et al. (2011) showed that 30-48% of the total mass loss from these 4 glaciers since 1963, has occurred since 2005.

While estimates of mass balance in the CAI have been largely based on ground or satellite observations, or derived using statistically based Temperature Index (TI) models (Cogley and Adams (1998); Koerner (2005); Mair et al. (2005); Shepherd et al. (2007); Colgan et al. (2008); Burgess and Sharp (2008); Gardner et al. (2011); Sharp et al. (2011)), researchers have applied physically based mass balance models to other regions. For instance, regional Climate Models (RCMs) have been used to generate high resolution meteorological fields for use with energy budget mass balance models in order to estimate the climatic balance of the Greenland ice sheet (Box et al. (2004, 2006); Fettweis et al. (2005); Ettema et al. (2009)).

This study uses the Regional Climate Model (RCM) Polar WRF to dynamically downscale low resolution meteorological fields to a high resolution grid over the Queen Elizabeth Islands (QEI) in the CAA. Results from the model are used to drive 2 separate climatic balance models. Climatic balance is combined with estimates of iceberg discharge to the ocean (derived from satellite remote sensing) to produce the first physically based, high resolution, regional scale mass balance estimates for glaciers in the QEI. The recent mass balance histories of the seven major icecaps in the QEI are investigated by resampling the model output over these regions.

4.2 Methods

The RCM Polar WRF is used to generate high resolution meteorological fields over the QEI. Climatic mass balance (B_{clim}) is estimated from these fields using 2 different approaches (a temperature index model (TI), and an energy balance model (EB)), both of which use output from Polar WRF as input. Regional mass balance for both approaches is estimated by summing B_{clim} over the entire model domain, and combining it with an estimate for total ice discharge by iceberg calving into the ocean.

4.2.1 Polar WRF

We used the polar optimized version of the Weather Research and Forecasting model (Polar WRF), version 3.2.1, to obtain estimates of meteorological parameters over a 6km resolution grid covering all the ice caps in QEI, (Figure 4.1). The simulation used 2 coupled domains, with horizontal resolutions of

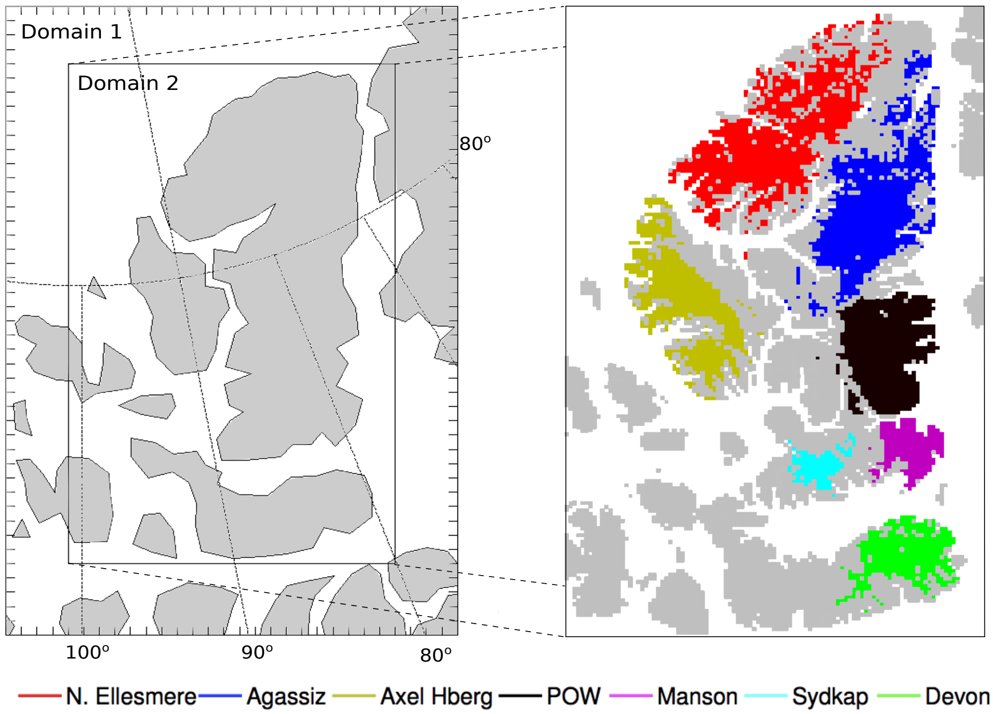

Figure 4.1: Left: 2 Domain setup for Polar WRF. Domain 1 has resolution of 30km x 30km. Domain 2 has resolution of 6km x 6km. Right: Major ice caps of the QEI. From North to South, Northern Ellesmere, Agassiz, Axel Heiberg Island, Prince of Wales, Manson, Sydkap, and Devon. The colour scheme used for the ice caps here, is used in figures later in the study.

30km (30×45 grid points with a time step of 150s) and 6km (30×45 grid-points with a time step of 150s) respectively (Figure 4.1). Both domains had 28 terrain following vertical sigma coordinates, with a constant upper level of 10 hPa. In an effort to combat model drift, Polar WRF was run in a configuration known as "forecast mode". In this mode, the model is restarted every 48 hours, using a 24 hour spin-up. The resulting 48 hour "time slices" are combined to create a continuous record. Land surface variables pertaining to the albedo parameterization (Thesis chapter 2) are passed from the end of each run into the next. Due to computational constraints, is was not possible to simulate the entire 8 year period. In the QEI, the majority of interannual variability in climatic balance comes from variations in summer melt (Koerner (2005)). Simulations were therefore performed for each summer season (June-September), and estimates of winter snow accumulation derived by Gardner et al. (2011) were used for the remainder of each year.

Input datasets

Initial conditions and nudging at the lateral boundary of the outer domain at 6 hourly time intervals, are provided by the 1×1 degree resolution NCEP FNL Operational Model Global Tropospheric Analyses. Static terrestrial data are provided by the USGS 24 category landuse and 2m topography datasets.

Physical Parameterizations

The Noah land surface model (Chen and Dudhia (2001)) was used to parameterize land surface physics. This included an ice sheet specific albedo parameterization (Thesis chapter 3). Shortwave and Longwave radiation physics are calculated using the RRTMG scheme (Iacono et al. (2008)), an updated version of the Rapid Radiative Transfer Model (RRTM), which rectifies a deficit in clear sky incoming longwave radiation noted in previous parameterizations (Mlawer et al. (1997)). Planetary Boundary Layer physics are prescribed by the MYNN2 scheme (Nakanishi and Niino (2006)), microphysics by the Morrison 2-mom scheme (Morrison et al. (2009)), and cumulus physics by the Grell-Devenyi scheme (Grell and Dévényi (2002)).

Polar WRF has been tested using a similar setup for Greenland by Hines and Bromwich (2008), using a 24km resolution grid. We use a higher resolution (6km) grid in this study in order to capture the more complex topography of the QEI ice caps.

4.2.2 Climatic Mass Balance

The often confusing terminology used in mass balance studies has recently been clarified and updated by Cogley et al. (2011). This study uses the definitions proposed in that work. *Climatic balance* at a point location, b_{clim} (kg m^{-2}), often referred to as *surface mass balance* in other studies, is the sum of the surface balance and the internal balance (surface and internal balances, refer to the difference between accumulation and ablation, at the surface, and within the snow/firn pack respectively). As its name suggests, the climatic balance reflects the influence of the climatic conditions at the glacier surface on the glacier mass balance. Ignoring ice thickness changes due to changes in ice dynamics and the basal balance (the latter of which is thought to be negligible in the CAA), the climatic balance represents the change in thickness of a vertical column of ice over a determined period of time due to climatic influences (Hock (2005)). If b_{clim} is summed over an area such as an ice cap, or for all of the ice caps in the QEI, the result is the climatic balance of that region, which is referred to as B_{clim}.

At each point, b_{clim} is a function of precipitation P, runoff R, surface water vapor flux, E, and blowing snow sublimation and redistribution, Q_S. In this case, and unless stated, P, R, E and Q_S refer to point location values (units kg m^{-2}), however the same symbols will be used to denote totals over an area (units kg) when indicated.

$$b_{clim} = P + R + (E + Q_S) \tag{4.1}$$

$$R = M(1 - P_r) \tag{4.2}$$

M is surface melt and P_r refers to a potential meltwater retention factor (introduced in more detail later). In this study, each of the terms in (4.1) and (4.2) refer to annual values, because Pr is calculated on an annual timestep, and explained in detail below. Since Polar WRF was only run for the summer months of each year, it was necessary to use alternative methods to estimate values for the winter months. During the winter, we assume R=0, and winter accumulation, $(P + E + Q_s)$, is derived from Gardner et al. (2011) as is explained in more detail below. The convention is used that terms with positive signs indicate positive contributions to b_{clim}, thus P is always positive, whereas R is ≤ 0. E and Q_s can be either positive or negative terms in the mass balance.

In this study, we compare 2 methods for computing melt from the Polar WRF output; an Energy Budget (EB) method and a Temperature Index (TI) method. b_{clim} is calculated in the same manner (using equations 4.1 and 4.2) for both methods, except that, for the TI method, the effects of E and Q_s are ignored. This is to conform with the methods used in Gardner et al. (2011), allowing comparisons to be made with the results of that study. The following sections explain each of the terms used in equations 4.1 and 4.2.

Precipitation

For summer months (June-Sept) when Polar WRF was run, we use the precipitation generated by Polar WRF as P. For the winter months, we use the precipitation fields generated by Gardner et al. (2011) using the National Centers for Environmental Prediction (NCEP) / National Center for Atmospheric Research (NCAR) Reanalysis 1 (R1) precipitation (Kalnay et al. (1996)), which they downscaled to a 500m resolution grid, and bias corrected using in-situ observations (Gardner et al. (2011)). We resampled their 500m resolution precipitation fields to the 6km resolution grid used in this study, and assumed that P is equal to accumulation. The end of winter accumulated precipitation is used as an estimate of snow depth at the beginning of each summer season, an initial condition for Polar WRF.

Melt Water Retention

In polar ice masses, a cold snow and firn pack causes a significant fraction of melt water to refreeze as internal accumulation during the early melt season, thus reducing runoff. It is important to quantify this process for an accurate assessment of the climatic balance. Following Box et al. (2004), we use the Pfeffer et al. (1991) model for meltwater retention. This model calculates the potential meltwater retention factor, P_r using an annual timestep. P_r is the fraction of the total melt that is refrozen in the snowpack in a year.

$$P_r = \left[\frac{c}{L_f}\bar{T}\frac{d}{P} + \left(\frac{C-M}{P}\right)\left(\frac{\rho_e}{\rho_0} - 1\right)\right] \tag{4.3}$$

Where c is the specific heat of ice, ρ_e is the density of water saturated snow, ρ_0 is the average density of dry firn (found to be 353kg^{-1}m^{-3} in west Greenland (Box and Steffen (2001)), $\bar{T}$ is the annual mean temperature, M is the annual volume of snow melt, P is annual precipitation, d is the water equivalent depth of the annual accumulation, and C is the annual dry snow accumulation calculated as:

$$C = P + E + Q_S - \text{liquid precipitation} \tag{4.4}$$

where liquid precipitation is calculated internally in Polar WRF, as the sum of precipitation at times when 2m temperature is $> 0°C$.

Annual runoff is calculated as $R = M(1 - P_r)$, and annual internal accumulation is calculated as MP_r. A weakness of this approach is that runoff can only be calculated in annual timesteps.

Blowing Snow Sublimation and Transport

Blowing snow sublimation and transport can be an important term in the surface mass budget (Pomeroy and Essery (1999); Bintanja (2001); Déry and Yau (2001b,a)). It has been recognized as one of the major uncertainties in estimates of the climatic balance of Antarctica (Turner et al. (2002)). The effect of blowing snow on the climatic balance is given by

$$Q_S = Q_{sub} + Q_D \tag{4.5}$$

where Q_{sub} is blowing snow sublimation, and Q_D is blowing snow redistribution (Déry and Yau (2002)).

Q_{sub}, is calculated using a parameterization derived from a double moment model (PIEKTUK-D) (Déry and Yau, 2001a):

$$\begin{aligned} Q_{sub} &= (a_0 + a_1\xi + a_2\xi^2 + a_3\xi^3 + a_4U_{10} + a_5\xi U_{10} \\ &\quad + a_6\xi^2U_{10} + a_7U_{10}^2 + a_8\xi U_{10}^2 + a_9U_{10}^3)/U' \end{aligned} \tag{4.6}$$

U_{10} is the magnitude of the 10m wind field, a_0 - a_9 are constants (Déry and Yau (1999)), and ξ is a thermodynamic term with units of $-1 \times 10^{12} m^2 s^{-1}$, which is a function of relative humidity with respect to ice (RH_i), ice density ρ_i. The terms F_K and F_d, represent conductivity and diffusion during sublimation.

$$\xi = \frac{(RH_i - 1)}{2\rho_i(F_k + F_d)} \tag{4.7}$$

$$Fk = \frac{L_s^2}{RvKT^2} \tag{4.8}$$

$$Fd = \frac{R_vT}{De_i} \tag{4.9}$$

Here, L_s is the latent heat of sublimation, R_v is the individual gas constant for water vapor, K is the thermal conductivity of air, D is the coefficient of diffusion of water vapor in air, and e_i is the saturation vapor pressure of ice.

Potential blowing snow transport, Q_{TP} (kg m^{-1} s^{-1}) is calculated using the following approximation (Tabler (1991); Budd et al. (1966); Déry and Yau

(2002)):

$$Q_{TP} = aU_{10}^{b} \tag{4.10}$$

where a and b are constants that have been given several values in the literature (Box et al. (2004); Déry and Yau (2002)). Snow transport is only allowed to occur when U_{10} exceeds a temperature dependent limit, U_t given by

$$U_t = U_{t_0} + 0.0033(T_a + 27.27)^2 \tag{4.11}$$

where $U_{t_0} = 6.975\text{ms}^{-1}$ is the minimum velocity for the onset of blowing snow that is reached at $-27.27°C$ (Déry and Yau (1999)). Below this temperature, U_t is held constant as done by Box et al. (2004). Like Box et al. (2004), we define snow availability, A, as a function of time since the last snowfall event, t (hours):

$$A = \frac{1}{1.038 + 0.0378t + 0.00014349t^2 + 1.911315e^{-7}t^3} \tag{4.12}$$

Actual blowing snow transport is then calculated as, $Q_{TA} = AQ_{TP}$ (Box et al. (2004)). The redistribution is calculated through the divergence of Q_{TA}:

$$Q_D = -\frac{1}{\rho}\nabla \cdot Q_{TA} \tag{4.13}$$

Thus, areas of accelerating winds will be sources and areas of decelerating winds will be sinks for blowing snow redistribution.

Surface Melt: Energy Budget Method

Melt rates are computed from energy budget closure at the surface. Any energy imbalance will either cause the surface temperature to change, or ice to melt. If there is excess energy, the surface will heat to an upper limit of $0°C$, after which, any excess energy will be used for melting (Male and Granger (1981)).

$$Q_N = -(Q_{RAD} + Q_H + Q_E + Q_G + Q_R) \tag{4.14}$$

The residual of the energy budget used for melting is Q_N or changing snow/ice temperature, Q_{RAD} is the net radiative energy flux (longwave and shortwave), Q_H is the sensible heat flux and Q_E is the latent heat flux. Net shortwave radiation is calculated internally in Polar WRF using the glacier specific albedo parameterization presented in Thesis chapter 3. Q_G is the conductive heat flux into the snow/ice, and Q_R is the energy flux from liquid precipitation (rain) (Box et al. (2004); Hock (2005)). Melt, M, is computed within Polar WRF from Q_N for each time interval Δt, whenever $T_{surface} > 0°C$.

$$M = Q_M \Delta t (L_f \rho)^{-1} \tag{4.15}$$

Here, L_f = 384 kJ kg^{-1} is the latent heat of fusion, and ρ = 917 kg m^{-3} is the density of ice.

Surface Melt: Temperature Index Method

In order to compare climatic balance estimates derived using output from Polar WRF with estimates from Gardner et al. (2011) (who use a TI model to estimate melt), we ran a TI model using 2 metre temperatures (T2) from Polar WRF as the input. In this method, melt is calculated as:

$$M = \sum_{i=\text{melt days}} \bar{\mathrm{T}}_i.\mathrm{K}_i \tag{4.16}$$

Where, on day i, $\bar{\mathrm{T}}_i$ is the mean temperature and K_i is the degree day factor respectively. The sum is calculated over all days with positive $\bar{\mathrm{T}}_i$. We utilize the Pfeffer et al. (1991) melt water retention scheme (described above) in the TI model. K_i assumes a value of 4.7 $\pm$ 1.5 kg m^{-2} d^{-1} $°C^{-1}$ for snow and 8.1 $\pm$ 2.6 kg m^{-2} d^{-1} $°C^{-1}$ for ice.

4.2.3 Iceberg Calving

Regional estimates of iceberg calving fluxes (D) for the QEI were provided by James Davis (personal communication). Mass change (loss) due to iceberg calving of an ocean terminating glacier, is considered through two processes: (i) the flux of ice through a cross sectional area located at the glacier terminus (referred to as "ice discharge", always negative) and (ii) the flux of ice due to advance or retreat of the glacier front (referred to as "retreat flux", positive for advance, negative for retreat). This method was used to estimate the iceberg calving flux from 26 glaciers located in the QEI for each year in the period 2001-2010. In order to obtain regional estimates of iceberg calving flux, mean flux estimates, for the period 2001-2010, from the 26 studied glaciers, were regressed against the basin (catchment area of each outlet glacier) integrated precipitation totals (generated by Gardner et al. (2011), explained earlier) for the same time period. Using the relationship derived between basin total precipitation and calving flux, the 2001-2010 mean calving flux from all of the QEI ocean terminating glaciers was estimated. Inter-annual variability of the regional calving flux was estimated as being in equal ratio to that of the inter-annual variability of the 26 outlet glaciers studied in detail. More details of these methods may be found in Davis (2012).

4.2.4 Annual Total Mass Balance

Total climatic balances, B_{clim}, for the entire QEI, and for individual ice caps within the QEI, are computed using both the EB and TI methods. This is done by summing b_{clim} over each region of interest for each season (Figure. 4.1). Total mass balance for each year, ΔM is computed as

$$\Delta M = B_{clim} + D \tag{4.17}$$

where D is the iceberg calving flux.

4.2.5 Hypsometry

A potential source of model uncertainty comes from the accuracy of the ice-mask used in Polar WRF. In Figure 4.2 we compare the icemask used by Polar WRF in this study, with the more accurate icemask assembled by Gardner et al. (2011) using data from the Global Land Ice Measurements from Space (GLIMS) project (for ice outlines on Axel Heiberg Island, and the Prince of Wales, Manson and Sydkap ice caps), Burgess and Sharp (2004) (for Devon ice cap), and using a normalized-difference snow index applied to Landsat-7 (ETM+) imagery from 1999-2003. Overall, Polar WRF predicts a total

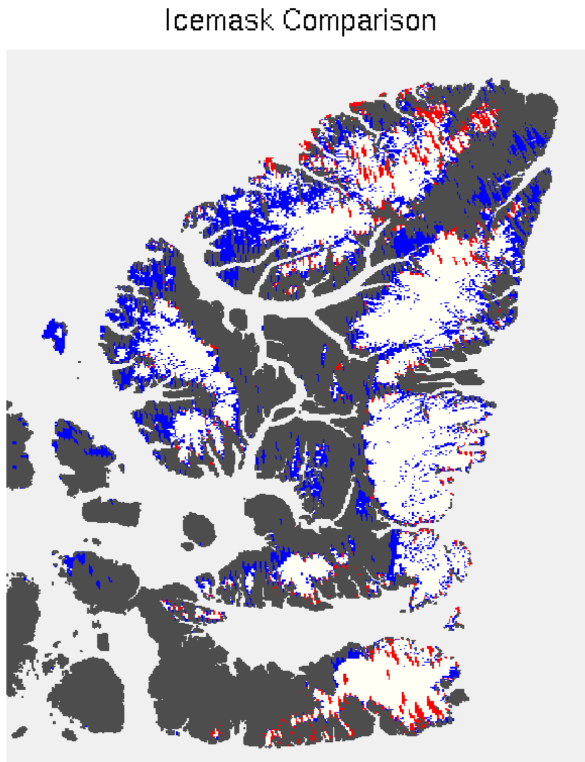

Figure 4.2: Comparison of icemasks from this study, and Gardner et al. (2011). White areas indicate areas that are ice in both icemasks. Blue areas are specified as ice in Polar WRF, but are ice-free in Gardner et al. (2011). Red areas are ice-free in Polar WRF, but specified as ice in Gardner et al. (2011).

ice covered area of 149000km^2, whereas the more accurate ice area used by Gardner et al. (2011) is just 106000km^2. Figure 4.2 demonstrates that the additional ice area predicted by Polar WRF is largely concentrated around the perimeters of many of the ice caps. Visually, the extra ice appears to be distributed evenly around the domain, although it is notable that Polar WRF under-predicts the areal coverage of Devon ice cap, and also misses many areas of ice in the northern section of the Grant ice cap, Ellesmere Island.

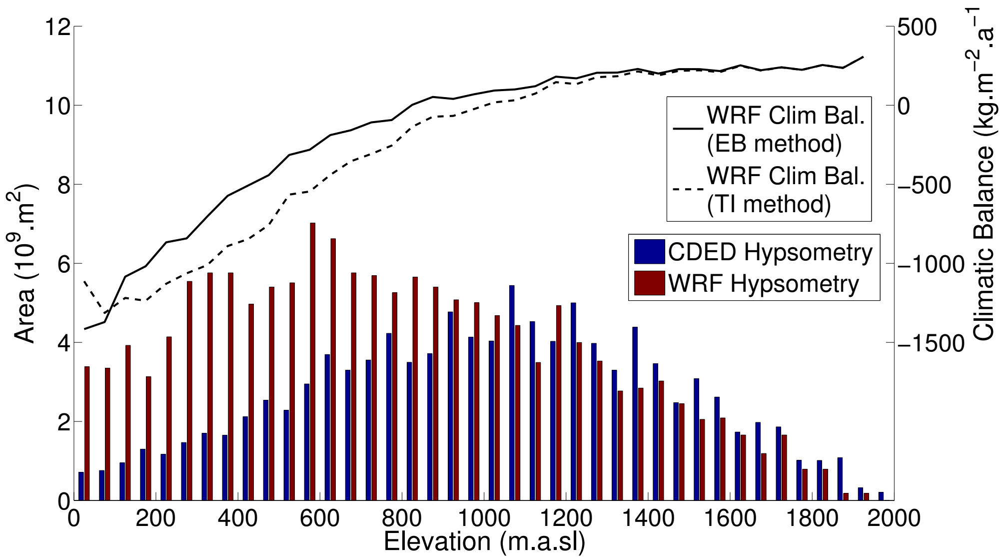

Figure 4.3: The bar chart illustrates the on-ice hypsometric profiles from Polar WRF (red) and CDED (Gardner et al. (2011)) (blue). Below 1000m Polar WRF has far too much ice covered area, whereas above 1000m both hypsometries are similar. Climatic balance for the EB and IT methods are plotted to demonstrate that the large discrepancies in hypsometry occur at elevations where the climatic balance is predominantly negative. Climatic balance results will be presented more thoroughly later in the study.

Figure. 4.3 illustrates the hypsometry of the glaciated regions in the domain, derived from the Polar WRF icemask and DEM, alongside hypsometry derived from the Canadian Digital Elevation Data set (CDED) by Gardner et al. (2011). At high elevations, where climate balance estimates are positive, the model hypsometry matches well with Gardner et al. (2011). As expected from the spatial distribution of the excess model ice (illustrated in Figure. 4.2), the extra ice area (43000km^2) is located at low elevations (below 1000m.a.sl), where the climate balance estimates are largely negative.

It is little surprise that the model hypsometry is more consistent with CDED at high elevations (although it is is cautioned that the accuracy of CDED is questionable at high elevations, due to lack of contrast of images in those areas). High elevations are generally the flat tops of ice caps, whereas low elevation regions are generally located in a complex array of steep sided valleys containing outlet glaciers. At 6km resolution, many outlet glaciers are not resolved by the model grid and, since "mixed" grid cells are not possible, errors are inevitable. Ideally such inaccurate grid points would be included as ice, or non-ice, in a manner that conserves the overall ice volume for the entire gridded domain. However, Figure. 4.3 clearly demonstrates this not to be the case, and a systematic bias by which too many grid points are interpreted as ice is present in Polar WRF (specifically, this is generated in the preprocessing program, "geogrid").

We correct for the inaccurate icemask for all variables (e.g. climatic balance) in the study that are integrated to find a regional total. This is achieved by splitting the region of interest into 50m elevation intervals, ranging from sea level, to the highest point in the region. For each elevation interval, the mean value of the variable in question (e.g. climatic balance) is calculated (units per m^2). This creates a "mean elevation profile" for the region of interest, for the variable in question. Meanwhile, the physical area (m^2) for each elevation interval is estimated from the CDED DEM, and the result is a "CDED area-elevation profile" for the region of interest. The regional total for the variable in question, is obtained by multiplying the mean elevation profile of the variable in question, by the CDED area-elevation profile, and summing over all of the elevation bins. In this study, any value that does not have units of "per m^2" has had the hypsometric correction applied, unless it is otherwise stated.

Table 4.1: Root mean square error and mean error for the radiation budget components, 2 metre temperature, and positive degree days/day.

	RMSE	mean bias
SWin (Wm^{-2})	45.8	3.9
SWout (Wm^{-2})	47.3	6.6
LWin (Wm^{-2})	22.1	-9.3
LWout (Wm^{-2})	9.2	-5.1
Net-rad (Wm^{-2})	29.8	-7
Net-SW (Wm^{-2})	33.1	-2.7
Net-LW (Wm^{-2})	18.5	-4.3
T2 (no bias correction) ($°C$)	3.12	-1.8
T2 (with bias correction) ($°C$)	2.84	-0.18
pdd/day (no bias correction) ($°C$.day^{-1})	0.498	-0.294
pdd/day (with bias correction) ($°C$.day^{-1})	0.5319	0.167

4.3 Results and Discussion

4.3.1 Comparison with in-situ Observations

2 Metre Temperature

Near surface temperature records are available for 69 locations spanning 6 distinct areas on 4 separate icefields in the QEI. We compare Polar WRF T2 to these observations. Relative to these observations, Polar WRF T2 exhibits a root mean square error (RMSE) of 3.17$°C$ and a mean bias of -1.83$°C$. Part of the discrepancy is due to differences in model and measured elevation at the observation sites. Figure 4.4 illustrates the frequency distribution of the elevation discrepancies. The distribution is wide, indicating that there are often large errors in the model DEM, and this is reflected in the RMSE of 202m. However the distribution is centred close to zero, with a mean bias of +4.5m. This indicates that although there may be some very large model errors due to differences between model and true elevation for individual AWS

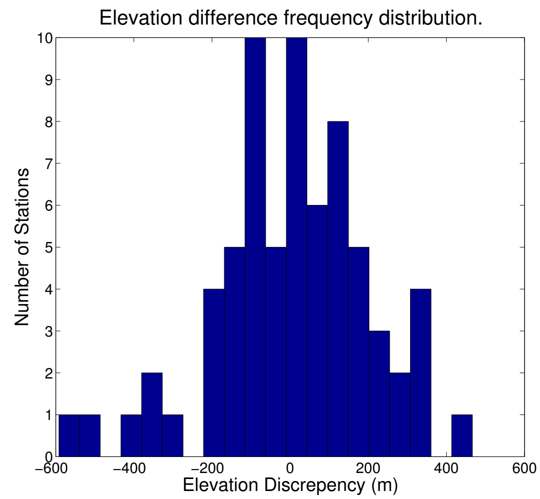

Figure 4.4: Histogram illustrating the frequency distribution of elevation discrepancies. The pattern reflects the small overall bias, yet high RMSE.

sites, the errors are randomly distributed around zero for the 69 AWS sites. Furthermore, the small bias suggests that that for the purposes of comparing Polar WRF T2 to AWS observations, we are justified in making a correction for elevation errors in Polar WRF. We correct for elevation discrepancies by applying a constant lapse rate of -6.5°C.km^{-1} to the elevation difference between model DEM and that measured at each AWS site. Figure 4.5 compares elevation corrected Polar WRF T2 with corresponding AWS observations for all of the 69 locations. With the elevation corrections applied, Polar WRF exhibits RMSE = 3.12°C and mean bias of -1.80°C. Figure 4.5 also illustrates the best fit linear regression best fit between Polar WRF and AWS T2. We apply the inverse of the this linear regression as a bias correction to Polar WRF T2 and by doing this, reduce the RMSE to 2.84°C and the mean error to -0.18°C. This bias correction is used for the TI method of calculating melt. It cannot be applied for the EB method, because all of the energy balance

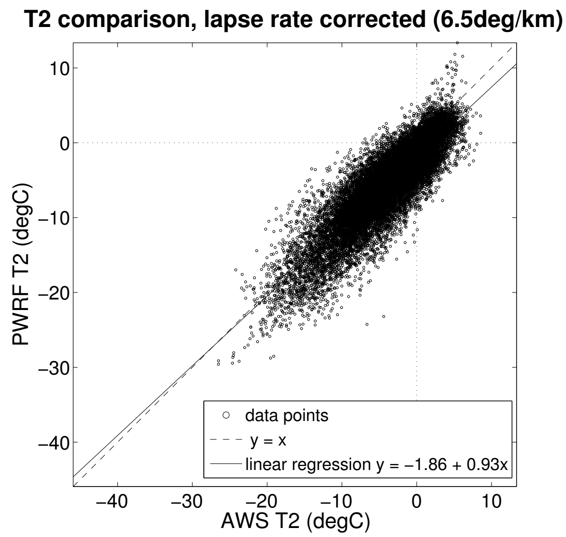

Figure 4.5: T2 from PWRF, corrected for elevation differences using a constant lapse rate of -6.5°C.km^{-1}, plotted against T2 from corresponding observations at 69 AWS sites in the CAA.

components are computed inline in Polar WRF.

Positive Degree Days

When using the TI method for calculating ablation, daily melt is proportional to the daily mean T2 when the daily mean T2 is above freezing (this is referred to as a "daily degree day total"). Figure 4.6 compares the mean daily degree day totals predicted by Polar WRF and AWS, at each of the 69 locations, for the non bias corrected (a) and bias corrected (b) cases. We compare the mean daily degree day totals rather than the sum of positive degree days, because there is high variability in the length of the T2 records from the 69 AWS locations. Some of the records span multiple seasons, whereas others cover only a fraction of a single season. By comparing the mean daily positive degree days, we are normalizing the sum of the positive degree days by the

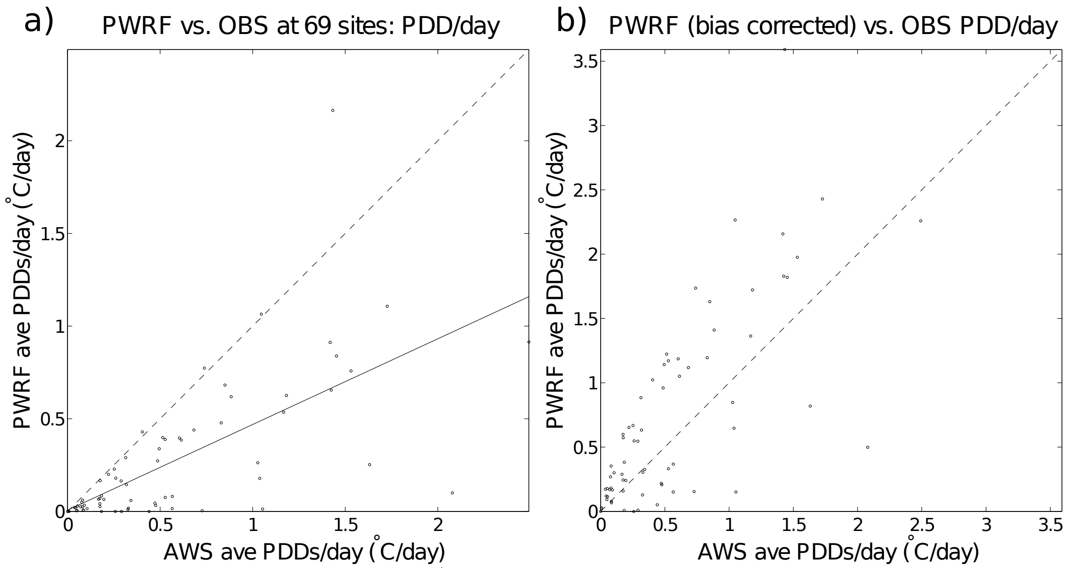

Figure 4.6: Comparison of PDD/day from observations at 69 AWS locations with PDD/day from Polar WRF, a) without the inverse linear regression bias correction applied, and b), with the inverse linear regression bias correction applies. PDD/day is simply the sum of the PDDs for the entire set of observations at each AWS, divided by the number of days for which there were measurements.

length of each record, allowing values to reflect the relative intensity of melt at each location, rather than the length of the respective record. Without the bias correction, Polar WRF underestimates mean daily positive degree days (mean error -0.29 PDD/day). This is no surprise given that Polar WRF exhibits a negative T2 bias. With the bias correction applied, Polar WRF exhibits a mean bias of +0.17 PDD/day, which indicates that Polar WRF will slightly over estimate melt with the bias correction applied. However, the magnitude of the mean error is less than half of the mean error for the non bias corrected Polar WRF T2.

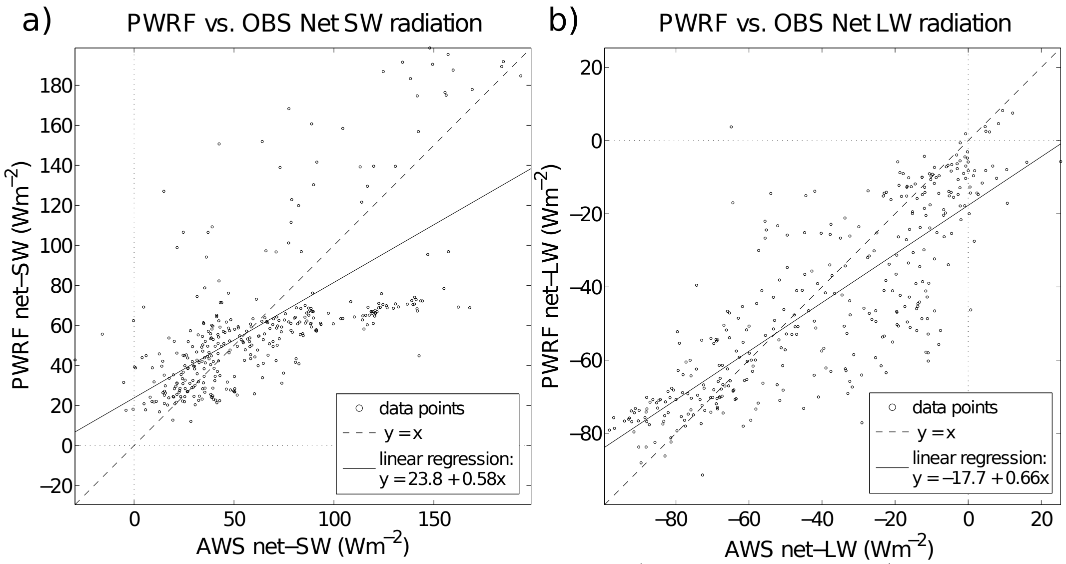

Figure 4.7: Comparison of PWRF and observed a)net shortwave and b) net longwave radiation fluxes at 5 AWS located on Devon ice cap. Daily averages are computed for comparison. Measurements span the summer of 2008.

Radiation Budget

Radiation budget measurements are available for summer 2008 at 5 sites on Devon Island ice cap. Figures 4.7 (a) and (b) illustrate the performance of Polar WRF in estimating the net shortwave and net longwave components of the energy budget respectively. In both cases Polar WRF exhibited low mean error (net shortwave = -2.7 Wm^{-2}, net longwave = -4.3 Wm^{-2}), but relatively high values for RMSE (net shortwave = 33.1Wm^{-2}, net longwave = 18.5 Wm^{-2}). The mean error of net longwave radiation flux (-4.3Wm^{-2}) is consistent with the findings of Hines et al. (2011), who found a net bias of -9Wm^{-2}, which is a significant improvement on Polar MM5, with a net bias of -22.4Wm^{-2}.

Turbulent Fluxes

Duncan (2011) used measurements from 3 AWS on the Belcher Glacier, Devon Ice Cap, to estimate the turbulent fluxes on a high resolution grid covering the glacier. The study had a number of limitations however: The measurements were made at only a single height above ground level, and this height was assumed constant despite a changing effective height due to melt or snowfall events. The water vapour mixing ratio was assumed constant and took the value for a melting glacier surface, and constant surface roughness length was assumed. Due to these assumptions, the turbulent fluxes calculated by Duncan (2011) are not suitable for deriving an uncertainty in Polar WRF turbulent fluxes. It is therefore very difficult to assess model performance in simulating the turbulent fluxes. Hines et al. (2011) also had very few in situ turbulent flux measurements with which to validate Greenland simulations, (personal communication with Dr. Hines). Hines et al. (2011) found bias in the sensible heat flux of 12.3Wm^{-2} and in the latent heat flux of 1.8Wm^{-2}.

4.3.2 Climatic Balance Components

We use both the TI and EB approaches, driven by the Polar WRF output variables, to obtain two estimates of the climatic mass balance. We will present each of the mass balance components for the two methods, before computing a mass budget for the entire QEI. Finally, the model output is sampled for each of the 7 major icecaps in the QEI (Figure 4.1). A summary of model statistics is provided in Table 4.2, and statistics for each year are provided in Table 4.3.

		2001-2008			
		Sum	Mean	max	min
	Period	(Gt)	(kg m^{-2})		
clim bal (EB)	Annual	-41	-49	990	-2400
clim bal (TI)		-110	-130	990	-1800
clim bal (TI no bc)		110	130	990	-990
melt (EB)	Summer	-290	-350	0.00	-2600
melt (TI)		-370	-440	0.00	-2100
melt (TI no bc)		-130	-150	0.00	-1200
int acc (EB)	Annual	47	56	450	0.00
int acc (TI)		55	65	510	0.00
int acc (TI no bc)		33	38	360	0.00
runoff (EB)	Summer	-250	-290	0.00	-2400
runoff (TI)		-320	-370	0.00	-2000
runoff (TI no bc)		-96	-110	0.00	-1100
Q_D	Summer	-0.045	-0.053	34	-36
Q_{sub}		-0.80	-0.94	0.00	-13
$Q_S = Q_{sub} + Q_D$		-0.84	-0.99	28	-45
E		-1.7	-2.0	-0.10	-19
snow (summer)	Summer	84	99	430	1.4
rain (summer)	Winter	23	27	200	0.27
snow (winter)		100	120	830	7.4

Table 4.2: Polar WRF statistics for climatic balance, melt, internal accumulation, runoff, blowing snow sublimation, redistribution, surface water vapor flux, summer snowfall and rain, and winter snowfall. For the components that are calculated differently, values are given for the EB, TI and the TI method with no bias corrected (no bc) applied to the near surface temperature. The sum is the total ice discharge for the entire domain for 2001-2008. Mean, Max and Min values are in kg m^{-2}, and are also calculated over the entire domain for 2001-2008. The sum and mean values have had the hypsometric correction applied. The period, refers to the period, within each year, for which the variable in question is estimated.

		2001				2002				2003				2004			
		Sum	Mean	max	min	Sum	Mean	max	min	Sum	Mean	max	min	Sum	Mean	max	min
	Period	(Gt)	(kg m^{-2})			(Gt)	(kg m^{-2})			(Gt)	(kg m^{-2})			(Gt)	(kg m^{-2})		
clim bal (EB)		-2.9	-27	860	-2100	9.8	92	990	-2100	6.4	60	900	-2200	13	130	910	-1800
clim bal (TI)	Annual	-14	-130	700	-1300	8.7	82	990	-1300	-5.5	-52	850	-1500	14	130	910	-1200
clim bal (TI no bc)		14	130	860	-600	27	250	990	-520	21	200	900	-690	29	270	910	-400
melt (EB)		-34	-320	-2.7	-2300	-26	-250	-0.013	-2300	-31	-290	-0.00018	-2300	-22	-210	0.00	-2000
melt (TI)	Summer	-46	-430	-22	-1500	-28	-260	0.00	-1500	-45	-430	0.00	-1600	-23	-220	-2.0	-1400
melt (TI no bc)		-16	-150	0.00	-690	-7.0	-66	0.00	-700	-16	-150	0.00	-830	-5.1	-48	0.00	-550
int acc (EB)		6.0	56	270	2.7	5.0	47	220	0.013	5.7	54	320	0.00018	5.4	51	270	0.00
int acc (TI)	Annual	6.6	62	440	9.9	5.5	52	460	0.00	8.4	79	470	0.00	7.0	66	470	2.0
int acc (TI no bc)		4.9	46	320	0.00	2.6	24	200	0.00	5.0	47	340	0.00	3.2	30	210	0.00
runoff (EB)		-28	-260	0.00	-2200	-21	-200	0.00	-2100	-25	-230	0.00	-2200	-17	-160	0.00	-1900
runoff (TI)	Summer	-39	-370	0.00	-1500	-22	-210	0.00	-1400	-37	-350	0.00	-1500	-16	-150	0.00	-1300
runoff (TI no bc)		-11	-110	0.00	-670	-4.5	-42	0.00	-680	-11	-100	0.00	-770	-1.9	-18	0.00	-530
Q_D		-0.011	-0.10	9.6	-14	-0.013	-0.12	16	-21	-0.011	-0.10	9.8	-13	-0.0048	-0.045	11	-16
Q_{sub}	Summer	-0.089	-0.84	0.00	-7.5	-0.13	-1.2	0.00	-7.5	-0.17	-1.6	0.00	-6.8	-0.070	-0.66	0.00	-7.9
$Q_S = Q_{sub} + Q_D$		-0.100	-0.94	8.0	-20	-0.14	-1.3	13	-27	-0.18	-1.7	7.7	-18	-0.075	-0.71	7.4	-20
E		-0.18	-1.7	-0.23	-9.0	-0.19	-1.8	-0.22	-10	-0.24	-2.2	-0.30	-11	-0.14	-1.3	-0.14	-10.0
snow (summer)		9.4	88	300	7.0	14	140	430	14	15	140	410	4.7	14	130	360	25
rain (summer)	Summer Winter	3.7	35	170	2.6	3.8	35	200	0.82	2.4	22	160	0.27	2.5	24	140	0.64
snow (winter)		12	120	770	11	13	120	800	7.4	14	140	750	8.7	14	130	770	13

		2005				2006				2007				2008			
		Sum	Mean	max	min	Sum	Mean	max	min	Sum	Mean	max	min	Sum	Mean	max	min
	Period	(Gt)	(kg m^{-2})			(Gt)	(kg m^{-2})			(Gt)	(kg m^{-2})			(Gt)	(kg m^{-2})		
clim bal (EB)		-20	-190	860	-2300	5.6	53	930	-2200	-14	-130	660	-2400	-39	-370	470	-2300
clim bal (TI)	Annual	-25	-240	690	-1800	-6.1	-58	910	-1600	-32	-310	450	-1800	-48	-460	350	-1800
clim bal (TI no bc)		8.6	81	860	-950	19	180	930	-690	3.1	29	660	-990	-7.4	-70	450	-950
melt (EB)		-51	-480	-0.0010	-2600	-27	-260	-0.13	-2400	-40	-380	-0.0033	-2500	-64	-600	-15	-2500
melt (TI)	Summer	-57	-540	-2.0	-2100	-40	-380	0.00	-1800	-60	-560	0.00	-1900	-73	-690	-47	-2000
melt (TI no bc)		-19	-180	0.00	-1200	-13	-120	0.00	-840	-22	-200	0.00	-1100	-30	-290	-1.9	-1100
int acc (EB)		6.8	64	450	0.0010	5.9	55	240	0.13	6.2	58	290	0.0033	6.5	61	260	5.3
int acc (TI)	Annual	7.4	70	410	2.0	6.8	64	510	0.00	7.0	66	270	0.00	6.0	57	190	7.1
int acc (TI no bc)		3.8	36	340	0.00	4.4	41	360	0.00	4.5	42	330	0.00	4.3	40	250	1.9
runoff (EB)		-44	-410	0.00	-2400	-21	-200	0.00	-2300	-34	-320	0.00	-2400	-57	-540	0.00	-2400
runoff (TI)	Summer	-50	-470	0.00	-2000	-33	-310	0.00	-1800	-53	-500	0.00	-1900	-67	-630	0.00	-1900
runoff (TI no bc)		-16	-150	0.00	-1100	-8.4	-79	0.00	-810	-17	-160	0.00	-1100	-26	-250	0.00	-1100
Q_D		-0.0017	-0.016	34	-36	-0.0013	-0.012	18	-11	0.0012	0.011	27	-14	-0.0042	-0.039	21	-24
Q_{sub}	Summer	-0.11	-1.1	0.00	-13	-0.061	-0.57	0.00	-8.3	-0.067	-0.63	0.00	-13	-0.10	-0.97	0.00	-11
$Q_S = Q_{sub} + Q_D$		-0.12	-1.1	28	-45	-0.062	-0.58	14	-15	-0.066	-0.62	20	-21	-0.11	-1.0	16	-33
E		-0.24	-2.2	-0.10	-19	-0.18	-1.7	-0.12	-15	-0.22	-2.1	-0.21	-13	-0.28	-2.7	-0.31	-15
snow (summer)		9.0	85	320	3.5	9.5	90	270	1.4	5.0	47	180	3.7	7.9	74	320	4.3
rain (summer)	Summer Winter	2.5	24	160	0.49	3.2	30	160	2.0	1.4	13	93	0.64	3.5	33	100	3.7
snow (winter)		13	120	800	10	15	140	830	7.9	14	130	620	14	7.2	68	370	11

Table 4.3: Polar WRF statistics for climate balance components. Mean, Max and Min values are in kg m^{-2}, and the time period for each component is given in column 2. The sum and mean values have had the hypsometric correction applied. Max and min values are the extrema for the daily values, for entire domain, for each year. The sums are the totals for the entire domain and for the entire year (or summer/winter). The means are taken over the entire grid, for the year (or summer/winter) totals. Where appropriate, values are given for the EB and both the bias corrected and non bias corrected (no bc) versions of the TI method.

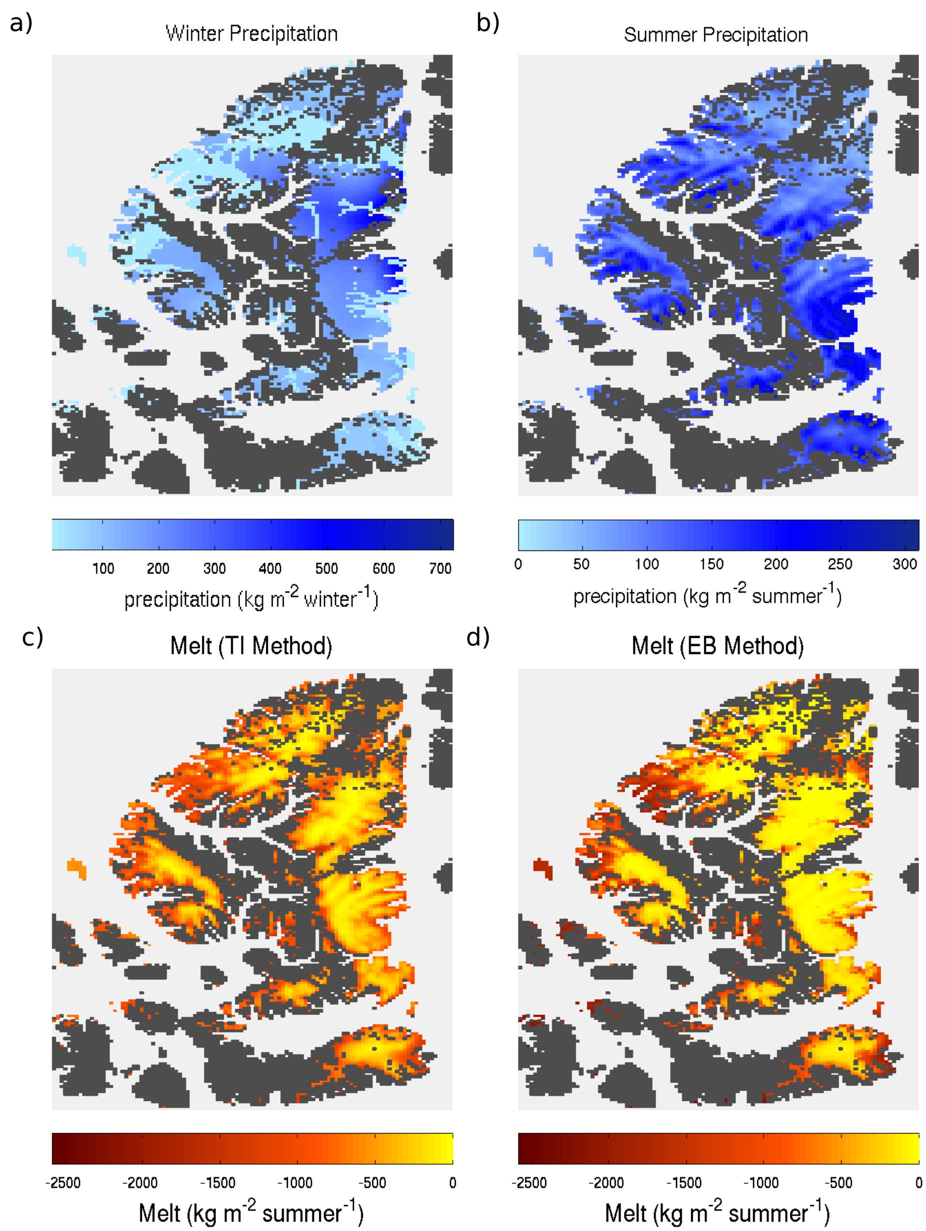

Figure 4.8: a) 2001 - 2008 mean of the winter (October-May) mean precipitation. The three remaining panels show the 2001 - 2008 mean of the summer mean values of: b) Precipitation predicted by Polar WRF, c) Melt,using the TI method, and d) Melt, using the EB method. Melt is displayed with units kg m^{-2} $summer^{-1}$, but since no melting occurs during winter, melt can equally be considered annual (units kg m^{-2} yr^{-1})

Precipitation

Summer and winter precipitation are illustrated in Fig. 4.8. (a) and (b). Since the model is only run for the summer months of each year, precipitation for the rest of the year (referred to as winter precipitation) is taken from Gardner et al. (2011). The modelled total contributions of summer and winter precipitation to the overall mass budget, in the period 2001-2008, are similar at 107 Gt (summer), and 100 Gt (winter) respectively. Frozen precipitation accounted for 75% of the summer precipitation, and rain accounted for the remaining 25% during the study period.

The winter precipitation exhibits artefacts from the higher resolution native grid of Gardner et al. (2011), which had to be resampled to the 6km grid scale of this study. The winter precipitation has distinct areas of high and low annual precipitation totals, with a maximum winter accumulation of 830 kg m^{-2} in 2003, and a minimum of 7.4 m^{-2} in 2002. Polar WRF summer snowfall varies from a minimum of 1.4 kg m^{-2} in 2006 to a maximum of 430 kg m^{-2} in 2002. Summer rain varied from a minimum of 0.27 kg m^{-2} in 2006 to a maximum of 200 kg m^{-2} in 2002. Summer precipitation is generally highest in the south east region of the domain, with particularly high values on the north side of Manson Icefield and south side of Prince of Wales Icefield.

Melt

Melt totals for both the TI and EB methods are illustrated in Figure. 4.8 (c) and (d) respectively. The TI and EB methods exhibit differing ranges in melt production, ranging from 0 kg m^{-2} (both methods, multiple summers) to

-2100 kg m^{-2} and -2600 kg m^{-2} for the TI and EB methods respectively (both in 2005). Although the extreme of melt for the TI method is 19% less than for the EB method, the total melt is 22% larger. This may be understood by examining the spatial distribution of melt in each method. In the TI method, the melt, although less near the glacier margins, extends much further into the interior of the ice caps than melt in the EB method. Melt predicted by the EB method is intense at the ice margins, but does not extend very far towards the centre of the ice caps. Overall, the larger melting area in the TI method, outweighs the higher maximum melt rates seen in the EB method, and more melt is produced by the TI method.

Blowing Snow Sublimation and Redistribution

Figure. 4.9 illustrates the average patterns of blowing snow sublimation and redistribution and of surface water vapour flux. The data are summed for each summer at each location in the model domain, and averaged for the summers of 2001-2008. Blowing snow sublimation is always negative, and ranges from 0 kg m^{-2} (2005) to a minimum of -13 kg m^{-2} (2007). Blowing snow redistribution, Q_D, varies from a maximum of +34 kg m^{-2} to -35 kg m^{-2}, with both extremes found in 2005 (Table. 4.3). Summer blowing snow redistribution has little effect on the overall mass budget of the glaciated regions of the domain, with a total contribution of -0.045 Gt between 2001 and 2008. Summer blowing snow sublimation, while smaller in magnitude at the extreme grid cells, has nearly 20 times the influence on overall mass balance, contributing -0.8Gt to the overall mass budget of the region between 2001 and 2008.

There are strong regional patterns of blowing snow sublimation and redistri-

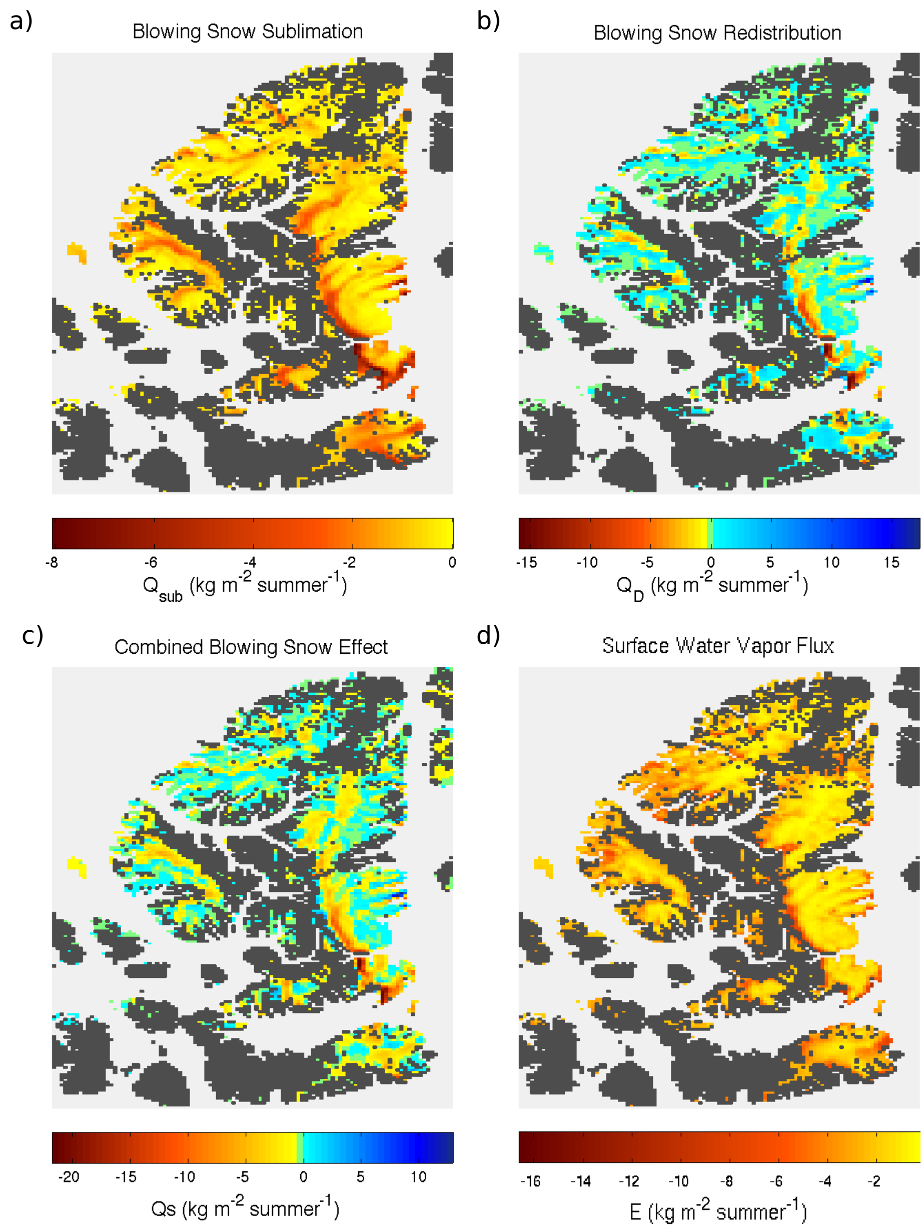

Figure 4.9: 2001 - 2008 mean of summer mean values of: a) Blowing snow sublimation, b) blowing snow redistribution, c) combined blowing snow sublimation and redistribution, and d) surface water vapour flux.

bution in summer, with a clear arc of high magnitude extending along the western sides of the Agassiz Ice Cap, Prince of Wales Icefield, and Manson

Icefield. Additional areas of high magnitude include North and central Devon Ice Cap, West Sydkap, and Northern Axel Heiberg (Müller ice cap). These areas are the windiest parts of the model domain.

Surface Water Vapor Flux

The effects of surface sublimation and evaporation are combined in the Surface Water Vapour Flux (SWVF). The mean summer SWVF which varied between -0.10 kg m^{-2} and -19 kg m^{-2} (both extremes were found in 2005). The summer SWVF represents over twice the combined mass loss due to blowing snow sublimation and redistribution, with a total contribution of -1.7 Gt to the mass budget between 2001 and 2008. The spatial distribution of the mean SWVF is illustrated in Figure. 4.9 (d). Generally, SWVF is low in the high elevation interior regions of the icecaps, which, because of low surface temperatures and lack of liquid water, are dominated by sublimation. SWVF is generally higher at lower elevations, typically around the margin of the icecaps where the majority of melt takes place. In these areas liquid water is available for evaporation. Since the latent heat of sublimation (2260 kJ kg^{-1}) is nearly 6.8 times the latent heat of fusion (334 k kg^{-1}) for water, it is not surprising that areas with greater potential for evaporation show higher values of SWVF.

Potential Melt Water Retention and Internal Accumulation

Maps of the potential meltwater retention and internal accumulation, averaged from 2001 to 2008 are presented in Figure. 4.10. P_r represents the proportion of the total melt that is retained by the snow pack and firn as internal accumulation, it varies from 0 to 1. P_r is generally high in the interior regions

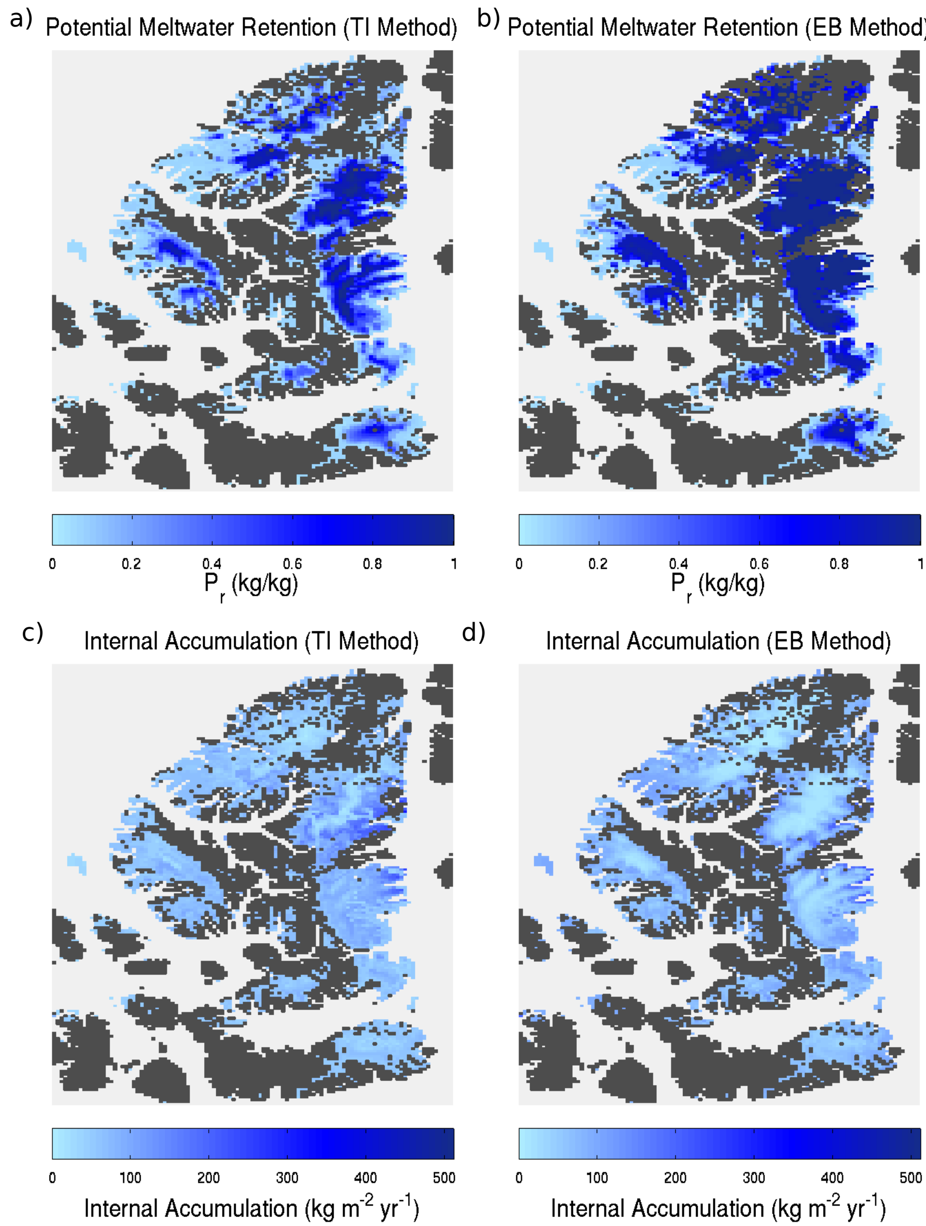

Figure 4.10: 2001 - 2008 mean of summer mean values of: a) Potential melt water retention factor for TI method, b) Potential melt water retention factor for EB method, c) Internal accumulation for the TI method, and d) Internal accumulation for the EB method.

of the ice caps, and decreases in the ablation areas at the ice cap margins. The EB method exhibits more extensive areas of high P_r than the TI method, for which high P_r is confined largely to ice cap interiors. Such differences are exclusively due to differences in melt, as it is the only term in (4.3) that differs between the two methods.

Internal accumulation for the TI and EB methods is illustrated in Figure. 4.10 (c) and (d). Internal accumulation represents a significant term in the overall mass budget, with totals of 47 Gt yr^{-1} and 55 Gt yr^{-1} for the EB and TI methods respectively between 2001-2008. Despite the comparatively large area of high P_r in the results from the EB method, the total internal accumulation is slightly less than in the TI method. This is because the vast majority of the areas with high P_r in the EB method are also areas of very low melt. Although values of P_r are generally lower for the TI method than for the EB method, and the region of high P_r is less extensive, meltwater production extends further inland, increasing the resulting meltwater retention.

Runoff and Climatic Balance

Figure. 4.11 displays the runoff and climatic balance, summed over all glaciated regions of the model domain, for 2001-2008, for both the TI and EB methods. Runoff is simply the melt minus the internal accumulation, and it displays a very similar pattern to that of melt.

Mean climatic balance is computed as the difference between accumulation and ablation at each location. Accumulation is primarily through precipitation, although blowing snow redistribution may be a source of accumulation in some

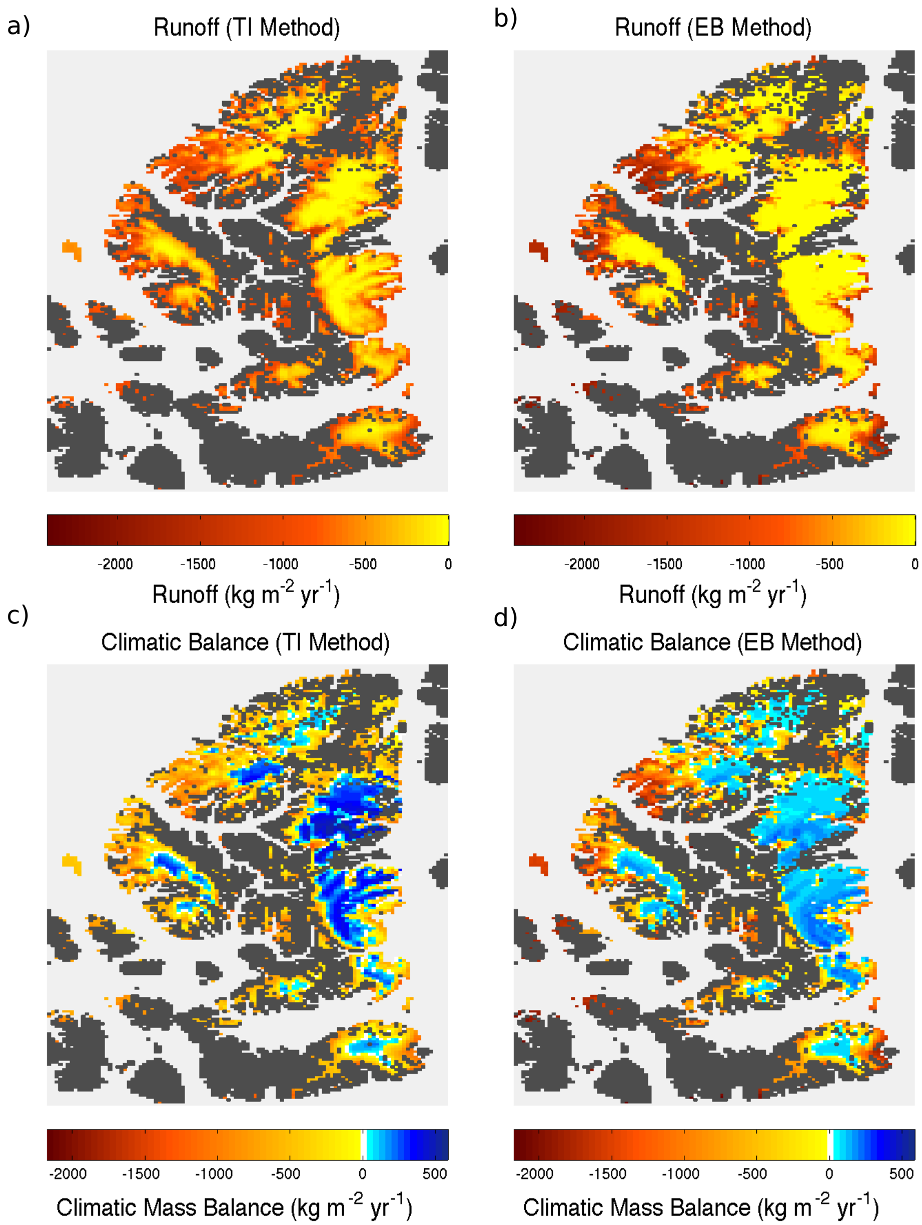

Figure 4.11: 2001 - 2008 mean of summer mean values of: a) Runoff, using the TI method, b) Runoff, using the EB method, c) Climatic balance, using the TI method, and d) Climatic balance, using the EB method.

locations. For the EB method, ablation is the sum of runoff (melt - internal accumulation), blowing snow sublimation and redistribution (when negative), and surface water vapor flux (when negative). For the TI method, ablation is simply the runoff. The total climatic balance from 2001 to 2008 is -41 Gt for the EB method, and is -110 Gt for the TI method. This difference is almost completely due to the difference in runoff computed by the two methods. For the TI method, climatic balance is characterized by large areas of (relatively) low intensity melt, and limited areas of positive balance. For the EB method, climatic balance is characterized by large areas of positive balance, surrounded by far smaller areas of (relatively) high intensity melt.

4.3.3 Temporal Variations

Figure. 4.12 illustrates the time evolution of several mass balance components over the 8 year study period. Each value is the total for all glaciated regions of the model domain, summed over the summer in the case of melt, and summed over the entire year in the case of precipitation, internal accumulation, calving and climatic balance. In the cases of melt, internal accumulation and climatic balance, we include results from the EB and TI methods, but also include results from the non bias corrected TI method as well (referred to as the NBCTI), to illustrate the necessity of performing a bias correction on temperature generated by an RCM in order for it to be useful as an input to a TI model. In each case (apart from calving flux), the hypsometric correction was applied to the model output, to correct for the inaccuracies in the Polar WRF elevation-area distribution.

Applying the bias correction increased the melt production by between 18Gt (2004) and 38Gt (2005). The difference brings melt production from the TI

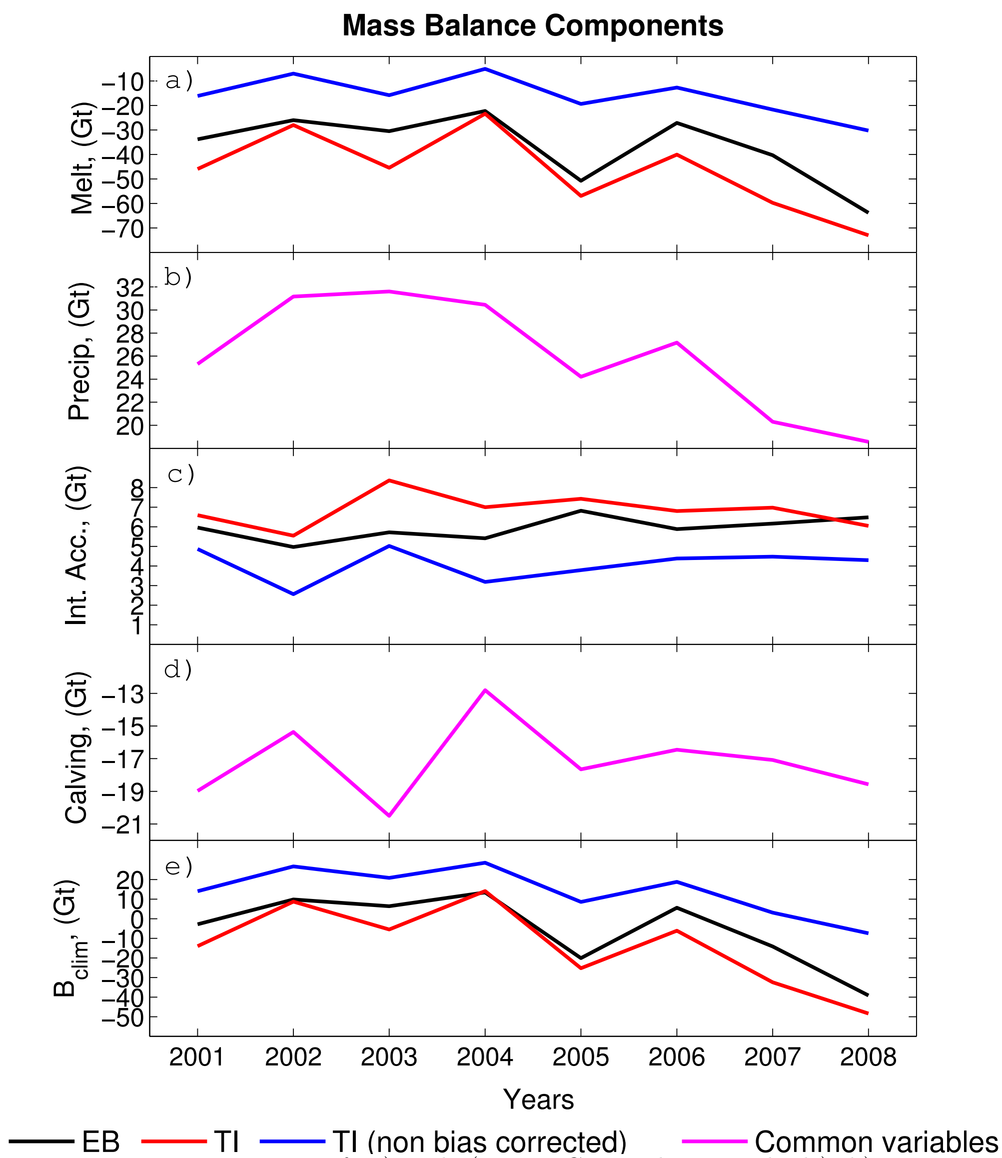

Figure 4.12: Timeseries of: a) Melt (TI, NBCTI and EB methods), b) Precipitation (common for all the methods), c) Internal Accumulation (TI, NBCTI and EB methods), d) Ice discharge through iceberg calving, and e) climatic balance (TI, NBCTI and EB methods).

method much closer to that of the EB method. The fact that the melt production of the bias corrected TI method agrees much better with the EB melt volume than the non bias corrected version did, indicates that either (i) the degree day factors being used are not accurate or (ii) the modelled near surface lapse rates are inaccurate, and thus so is the near surface air temperature, or (iii) the energy budget of the model is not coupled correctly with the surface temperature.

The TI method generates higher internal accumulation than the NBCTI method. Since all factors in the calculation of internal accumulation are the same, except for the calculation of melt, increased melt must be the cause of higher internal accumulation in the TI method. In areas where P_r, the potential meltwater retention factor, is equal to 1, all of the meltwater production is stored and re-frozen within the snowpack. In such cases, more melt would directly lead to more internal accumulation, until, (i) latent heat release by refreezing of meltwater within the snowpack overcomes the cold content of the annual accumulation, and (ii) additional melt water raises pore water content to the point that it is sufficient to overcome capillary forces and percolate down slope (Colbeck (1976); Pfeffer et al. (1991)).

Although internal accumulation somewhat compensates for the extra melt in the TI method compared to the NBCTI method, the overall climatic balance is consistently higher in the NBCTI method. The EB method is more similar to the TI method than the NBCTI method, but its results lies between the two in each of the study years.

Trends in each of the mass balance components displayed in Figure. 4.12 are estimated from linear regression, and summarized in Table. 4.4. Trends were initially calculated for the period 2001-2008 (the entire study period), with a

	2001-2008				2004-2008			
	Gradient ($Gt\ yr^{-2}$)	R^2	F	P-Value	Gradient ($Gt\ yr^{-2}$)	R^2	F	P-Value
melt (EB)	-3.57	0.38	3.69	0.103	-7.27	0.46	2.51	0.211
melt (TI)	-4.35	0.42	4.30	0.084	-10.21	0.71	7.18	0.075
melt (NBCTI)	-2.11	0.41	4.14	0.088	-5.26	0.77	10.00	0.051
precipitation	-1.44	0.51	6.29	0.046	-2.77	0.81	12.64	0.038
int acc (EB)	0.14	0.33	2.96	0.136	0.15	0.19	0.69	0.467
int ccc (TI)	-0.01	0.00	0.01	0.937	-0.24	0.54	3.57	0.155
int acc (NBCTI)	0.05	0.02	0.13	0.726	0.29	0.72	7.90	0.067
discharge	0.02	0.00	0.00	0.962	-1.10	0.61	4.74	0.118
clim bal (EB)	-4.88	0.44	4.67	0.074	-9.92	0.56	3.81	0.146
clim bal (TI)	-5.80	0.46	5.08	0.065	-13.20	0.74	8.76	0.060
clim bal (NBCTI)	-3.50	0.49	5.78	0.053	-7.74	0.77	10.31	0.049

Table 4.4: Linear trends for each of the balance components displayed in Figure. 4.12, for the periods 2001-2008, and 2004-2008 respectively. Trends that were not significant above the 90% level (using the F-test, indicated by P-value > 0.1) were considered insignificant, and are shaded grey above.

the null hypothesis that there is no trend, and the alternative hypothesis that a linear trend exists. Visual inspection Figure. 4.12 led to the hypothesis that trends in the balance components become more extreme after 2004. Therefore, trends were also calculated for 2004-2008, using the same set of hypotheses as above. In both cases, the null hypothesis for a balance variable is rejected, if a trend has significance above the 90% level, using the F-test. Otherwise, the null hypothesis is not rejected, and that balance component is assumed to have no significant trend. The TI and NBCTI methods exhibited accelerating melt rates over the study period (2001-2008). The acceleration of melt with the TI method, -4.4 Gt yr^{-2}, was greater than with the NBCTI method (-2.1Gt yr^{-2}), indicating that the bias correction increased not only the melt rate, but also the acceleration of melt over the study period. The acceleration of melt derived from the EB method (-3.6 Gt yr^{-2}), was not significant at the 90%

level. The acceleration of melt is higher after 2004 than before 2004 in the TI method (-10 Gt yr^{-2}) and NBCTI method (-5.3 Gt yr^{-2}). Again, there was no significant acceleration in the EB method derived melt estimates. The increased acceleration exhibited by the TI and NBCTI methods is consistent with the findings of Sharp et al. (2011), who infer dramatically increased melt over the 7 major icecaps of the QEI after 2005 from trends in 700hPa summer air temperatures taken from NCEP/NCAR R1 Reanalysis, MODIS MOD11A2 land surface temperatures, and increases in melt season duration, derived from the Ku-band SeaWinds scatterometer on QuickSCAT (Long and Hicks (2010)) and in situ climatic balance records.

The annual rate of precipitation decreased by 1.4 Gt yr^{-2} during the study period (2001-2008), and the rate of decrease increased to 2.8 Gt yr^{-2} for the period 2004-2008; As melt rates increased (according to the TI and NBCTI methods), precipitation rates decreased. This is somewhat contradictory to future projections from GCMs which indicate that in warming climate scenarios, precipitation at high latitudes will increase, due to increased capacity of warm air to transport moisture from mid to high latitudes (e.g. Manabe and Wetherald (1975)). There was no significant trend in the internal accumulation for any of the three methods, or in the iceberg calving rate over the study period 2001-2008. This is also true for the period 2004-2008, with one exception; the internal accumulation derived from the NBCTI method showed a significant, but small trend (0.29 Gt yr^{-2}).

The trend in climatic balance reflects the combined effect of the accelerating melt rates (for the TI and NBCTI methods) and decelerating precipitation rates over the study period. The climatic balance rate decreased by 3.5 Gt yr^{-2}, 5.8 Gt yr^{-2} and 4.9 Gt yr^{-2} according to the NBCTI, TI, and EB methods respectively (significance > 90%). The majority of the decrease occurred between 2004-2008, with climatic balance rates decreasing by 7.7 Gt yr^{-2}, 13.2 Gt yr^{-2} and 9.9 Gt yr^{-2} according to the NBCTI, TI, and EB methods respectively during this period (significance > 90%). This is consistent with the findings of Sharp et al. (2011) who found the mean rate of mass loss from 4 glaciers in the QEI, (Devon ice cap, Melville South ice cap, Meighen ice cap, and White Glacier) between 2005 and 2009 was nearly 5 times the 1963-2004 mean.

4.3.4 Net Mass Balance

Net mass balance for the entire study region for each year, is calculated by summing the specific climatic balance for each ice covered grid cell for each year, and adding it to the total iceberg calving mass loss (presented in Fig. 4.12).

Uncertainty

We are able to estimate model uncertainty in the net mass balance (ΔM) for the TI method at each point on the grid, by combining uncertainty estimates for each of the variables used in the calculation. Temperature uncertainty (taken as the RMSE value) was derived from comparison with observations in this study. Uncertainty in the positive degree day factor was derived in Gardner et al. (2011), and we use the same values (K_{ice}=8.1 $\pm$ 2.6 kg day^{-1}

$^{\circ}$C^{-1}, K_{snow}=4.7 ± 1.5 kg day^{-1} $^{\circ}$C^{-1}) here. Precipitation uncertainty is also taken from Gardner et al. (2011) for summer and winter (± 33%). In the winter, this is justified because we use winter values of precipitation taken from that study. In summer, there are estimates for on-glacier precipitation derived from sonic ranger measurements. However, these measurements do not detect rain, which made up 25% of summer precipitation in this study, and they are not well distributed over the glaciated regions of the domain. Thus, we apply the precipitation uncertainties derived by Gardner et al. (2011) to the summer recognising that it remains to be demonstrated that this is appropriate. With estimates for the daily uncertainty in climatic balance at each grid point, it is a challenge to combine the uncertainties in a meaningful way over the entire domain, and over an entire season. The uncertainty for the entire grid, for a season is obtained by summing the uncertainty at each grid cell over the entire grid, both spatially and temporally. The method used to sum the uncertainties however, depends on whether the uncertainties are considered to be *independent* (in which case they are summed in quadrature), or *non-independent* (in which case they are summed by simple addition).

If, taking one extreme, it was assumed that the uncertainty in climatic balance for each grid cell is *independent* of the uncertainty in climatic balance for each of the other grid cells (175 cells × 105 cells × 120 days), then the combined uncertainty in climatic balance for the entire grid, would certainly be an underestimate. It would be an underestimate because for spatially and temporally close (discussed below) locales, there is a high probability for similar errors between modelled and real climatic balance values between grid cells. This is because spatially and temporally close locations are likely to share similar driving conditions at the surface (e.g. cloud cover, albedo, altitude, slope and aspect, proximity to ocean). Therefore differences between modelled and real surface conditions are likely to have spatial and temporal cohesion over short length and time-scales, and are therefore unlikely to be *independent* on such scales.

If, taking the opposite extreme, it was assumed that the uncertainty in climatic balance for each grid cell is *non-independent* of the uncertainty for climatic balance in each of the other grid cells, then the combined uncertainty in climatic balance for the entire grid, would certainly be an overerestimate. It would be an overestimate because for spatially and temporally distant locales, there is a low probability for errors between the modelled and real values of climatic balance being systematic. This is because over large spatial and temporal scales, there is high variability (we argue) in the driving conditions at the surface (see above). Therefore, differences between modelled and real surface conditions are very unlikely to have spatial and temporal coherence over large length and time-scales. Therefore, it is likely that uncertainties are *independent* over large length and time-scales.

In an attempt to include such qualitative concerns, we consider that model errors could depend on one another within the spatial and temporal scale of a large mesoscale disturbance (10-50km, a few days), and within localized regions that are geographically similar (with respect to altitude, slope aspect, albedo, distance to ocean). For this, we consider a typical scale for the radius of a large ice cap in the CAA to be 50-100km, and that albedo can change over the timescale of hours to weeks. In order to account for these spatial

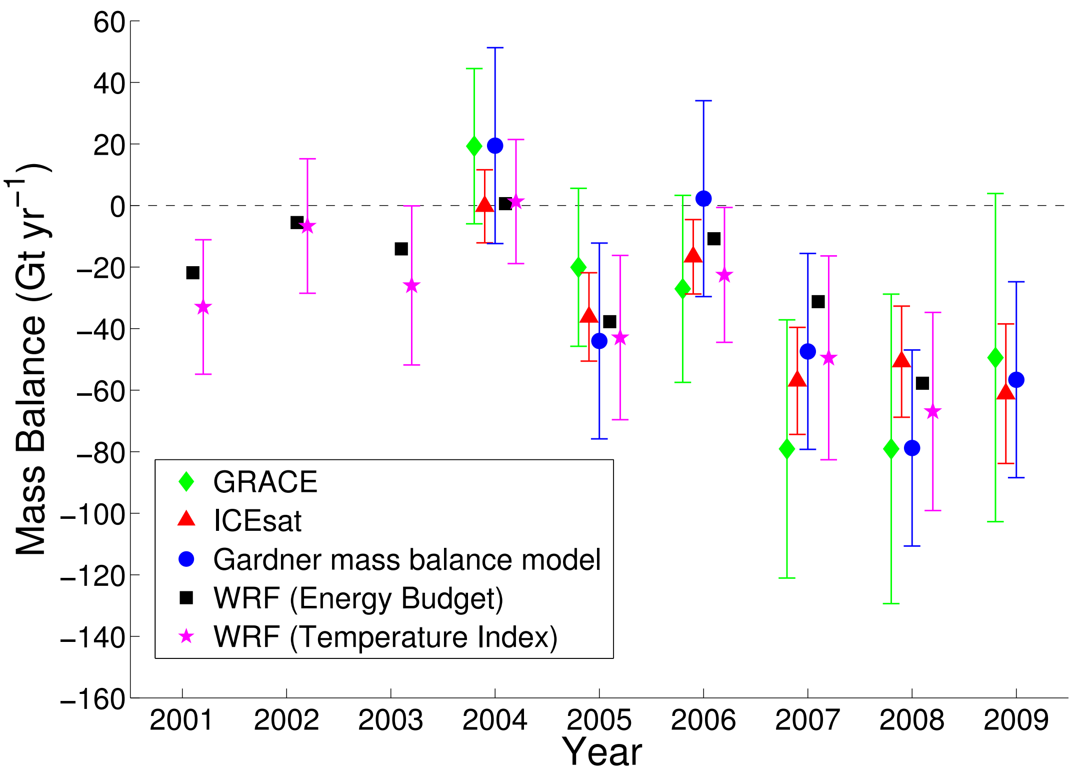

Figure 4.13: Comparison of mass balance totals derived in this study (2001 - 2008), with those reported by Gardner et al. (2011). Note that small gaps between measurements within each year are included for clarity, and are not indicative of specific timing within each year.

and temporal scales, we combine uncertainties as dependent over a length scale of 90km, and a timescale of 7 days. These dependent uncertainties are then further combined independently, to cover the entire domain and each summer. In order to do this, we simply split the domain into 90km×90km×7 day segments to compute non-independent uncertainties, and then combine the resulting blocks as independent uncertainties.

Although we were able to find uncertainties for the LW and SW components in the energy balance, there are other terms in the EB method for which there are too few in-situ measurements to allow us to derive meaningful uncertainty estimates. We did not therefore estimate the uncertainty for the EB method. This problem has been encountered in previous studies using RCM output to derive climatic balance, and these studies did not state uncertainties (Box et al. (2004, 2006)).

Annual Balance

Figure 4.13 illustrates the annual net mass balance estimates from the EB (ΔM_{EB}) and TI(ΔM_{TI}) methods. Annual net balance estimates from (i) repeat satellite gravimetry (GRACE), (ii) repeat satellite laser altimetry (ICESat) and (iii) a temperature index model, driven by 700mb air temperatures from the NCEP/NCAR R1 dataset (Kalnay et al. (1996)), downscaled by Gardner et al. (2009), are also included for comparison. It is noted that in the TI model of Gardner et al. (2009), a calving flux of 2.61 ± 1.92 Gt yr^{-1} was used, whereas in this study we use a much larger calving flux estimate (Davis (2012), Figure. 4.12).

Both the TI and EB methods estimate a strongly negative overall balance between 2001 and 2008, with the TI method total, $\sum \Delta M_{TI} = -139 \pm 73$Gt, being more than double that predicted using the EB method, $\sum \Delta M_{EB} = -63$Gt for the same period.

It has been established that the ice mask in the model produces too large a glaciated area (Figure. 4.2). The majority of this extra ice area was at low elevation, causing the overall melt sum to be too great. We therefore corrected for the error in hypsometry when calculating the annual net balance shown in

Figure. 4.13. However, since the model was run with too large an ice area, several climatic feedbacks would have operated within the model. In particular, increasing the ice area in the model has the effect of increasing the average albedo, which tends to cool the model atmosphere. Ice surface temperatures cannot rise above 0°C, which causes high temperature gradients to develop above the ice surface during melting. High temperature gradients lead to increased sensible heat flux towards the surface, again causing a cooling effect on modelled air temperature. In contrast, there is also the negative feedback of less outgoing longwave radiation. Overall, we suggest that the cooling effect of the ice-albedo and ice-sensible heat flux feedbacks outweigh the warming effect of the ice-longwave feedback, and that the simulated climate is cooled by the extra ice in the domain. This is consistent with the negative temperature bias found when modelled near surface temperatures were compared with in situ observations at 69 locations; The mean model error was -1.8 °C (Table. 4.1).

In every year except 2002 and 2004, ΔM_{TI} is more negative than ΔM_{EB}. This is expected, because Polar WRF air temperature was corrected for a negative bias, which would increase melt estimates from in the TI method. No such corrections were applied to Polar WRF variables used in the EB method since it was not possible to make meaningful comparisons between all of the components and in-situ observations.

Overall, the annual ΔM estimates in this study, from both the EB and TI methods, agree well with the three methods from Gardner et al. (2011). All estimates, except ΔM_{EB} in 2007, fell within the error bounds of estimates

	Grace	ICESat	Gardner TI model	WRF EB	WRF TI
Grace	-	19.05	20.36	27.09	19.43
ICESat	19.05	-	16.86	12.24	8.94
Gardner TI model	20.36	16.86	-	15.93	14.77
WRF EB	27.09	12.24	15.93	-	10.30
WRF TI	19.43	8.94	14.77	10.30	-

Table 4.5: Inter-comparison for the GRACE and ICESat geophysical estimates, and WRF EB, WRF TI and Gardner TI model estimates, of annual net mass balance for the QEI. The number in each cell is the RMSE (Gt yr^{-1}), calculated for the methods at the respective column and row headings. The RMSEs are calculating using the years in which the estimates from this study overlapped those from Gardner et al. (2011) (2004-2008).

from GRACE, ICESat and the TI model of Gardner et al. (2011). In 2007, ΔM_{EB} was narrowly outside the error bounds of GRACE and ICESat. The fact that ΔM_{EB} overestimated, rather than underestimated the mass balance estimated from GRACE and ICESat in 2007, is consistent with the fact the model produced an artificially cool climate, and this was in no way corrected for in the EB method.

It is difficult to quantify the relative quality of the five methods (three models, two geophysical methods), because there are only five years (2004-2008) of overlap between the time period of this study and that of Gardner et al. (2011). Table. 4.5 uses the RMSE to compare the five methods. The mean RMSE is 16.5 Gt yr^{-1} and the maximum RMSE is 27.09 Gt yr^{-1} for WRF EB vs. GRACE. The RMSE between the GRACE estimates and the estimates from each of the other methods is always less than the uncertainty of the

GRACE method in each case (GRACE uncertainty range is 25.2-53.3 Gt yr^{-1}, mean 34.7 Gt yr^{-1}). The RMSE between the ICESat estimates and the three models were 16.9 Gt yr^{-1} (Gardner TI model), 12.24 Gt yr^{-1} (WRF EB), and 8.94 Gt yr^{-1} (WRF TI). The ICESat uncertainty ranged from 11.9-22.6 Gt yr^{-1}, with a mean of 14.8 Gt yr^{-1}, indicating that the WRF EB and TI methods compared favourably with ICESat, showing RMSE of similar or less magnitude to the mean uncertainty of ICESat. Of the three models, WRF TI performed with the lowest RMSE against both GRACE and ICESat. However, with the large uncertainties in GRACE and ICESat, and with only five years of comparison, longer records are required to objectively compare the models.

The results presented here extend the regional mass balance estimates for the QEI back to 2001. Results indicate that 2001 and 2003 were negative balance years (although for 2003, the upper uncertainty limit for the TI method, was 0 Gt yr^{-1}). 2002 was predicted as slightly negative balance year by both the TI and EB methods respectively. Given that the uncertainty for the TI method overlaps with 0 Gt yr^{-1}, we cannot rule out the possibility that 2002 was a neutral or even slightly positive balance year.

Five year mean values of total mass balance of the QEI using GRACE were presented by Jacob et al. (2012). In table 4.6 the values of the Wahr method Jacob et al. (2012) are compared to those of Gardner et al. (2011) (GRACE, ICESat and TI model), and those of this study (WRF EB and TI methods). For the period 2003-2007 the EB method was within the uncertainty bounds of Wahr, the TI method uncertainty bounds overlapped with those of Wahr, and there were no values for the Gardner et al. (2011) as that study began

	2003-2007	2004-2008	2005-2009
Wahr	-12±9	-33±8	-42±8
WRF_EB	-14.7	-23.5	
WRF_TI	-24±12	-32±12	
GRACE		-37±16	-51±19
ICESat		-32±7	-44±7
Gardner TI		-30±14	-45±14

Table 4.6: Five year mean values of mean annual mass balance for the QEI (in Gt) for this study (WRF EB and TI methods), GRACE, ICESat and the TI method from Gardner et al. (2011), and values derived from GRACE by Jacob et al. (2012) (Wahr method).

in 2004. For the period 2004-2008, the EB method is outside the uncertainty bounds of the Wahr method, whereas the TI method agrees closely. In both the periods 2004-2008 and 2005-2009, the uncertainty bounds of all of the Gardner et al. (2011) methods overlap with the uncertainty bounds of Wahr in each case. However, this is not very surprising in the cases of the GRACE and TI method from Gardner et al. (2011), because the uncertainty bounds are large.

The results from this study are consistent with Sharp et al. (2011), in exhibiting significantly lower mass balance from the 2005-2008 period(-181±58Gt for the TI method and -138Gt for the EB method), compared to the 2001-2004 period (-64±45Gt for the TI method and -40Gt for the EB method).

4.3.5 Major Ice Caps

Ice Cap Balance Component Timeseries

In this section we present model output for the 7 major icecaps of the QEI (Figure. 4.1). Figure. 4.14 presents timeseries of the annual climatic bal-

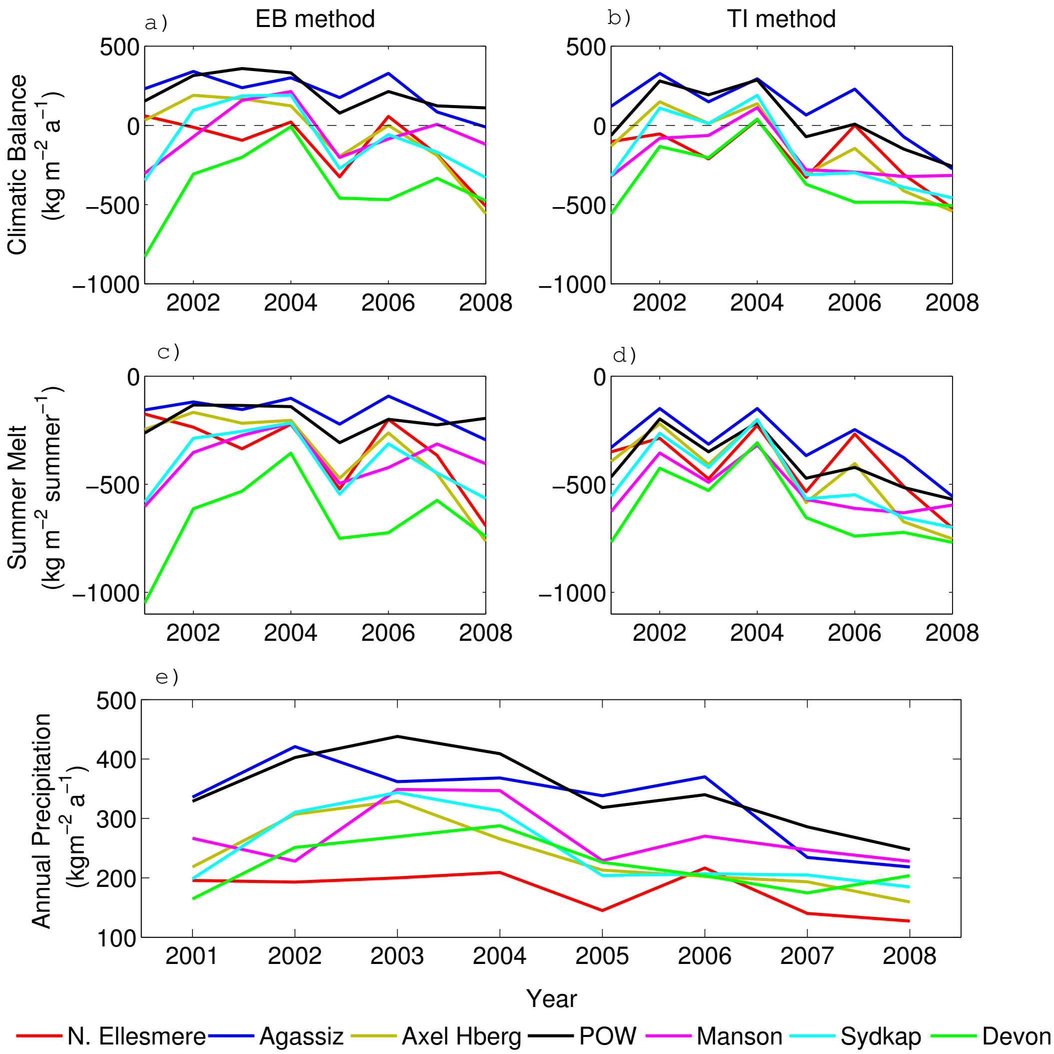

Figure 4.14: Comparison between ice caps for mean annual climatic balance for the EB method (a) and TI method (b), mean summer melt for the EB method (c) and TI method (d), and mean annual precipitation (e), which us the same in the EB and TI methods. Annual precipitation is made up of winter precipitation derived from Gardner et al. (2011), and summer precipitation taken from Polar WRF output. All horizontal axes are in years.

ances and summer melt am mounts for the EB and TI methods, and annual precipitation (same in both methods). In both methods, Devon Ice Cap had the highest melt rates and most negative climatic balance, although there was significantly more melt on Devon ice cap in the EB method than in the TI method. The inclusion of the south west arm of Devon Ice Cap, which is dynamically inactive and low in elevation (Koerner (1970), Burgess and Sharp (2004)), is the primary cause of the high melt rates and corresponding negative climatic balance, predicted by the model for Devon Ice Cap. In both methods, Agassiz Ice Cap and POW Icefield had the lowest melt rates in most years, the highest annual precipitation and the highest climatic balances. According to the EB method, POW Icefield exhibited positive balance throughout the study period, and Agassiz Ice Cap had a positive climatic balance in every year except 2008, when the climatic balance was slightly negative. However, in the TI method, POW Icefield had a negative climatic balance in 2001, 2005, 2007 and 2008, while Agassiz Ice Cap had a negative climatic balance in only 2007 and 2008. In general, the annual melt timeseries are more similar in the TI method than the EB method. With the exception of Devon Ice Cap and Manson Icefield in 2005-2006, all of the timeseries produced by the TI method display similar inflection points to one another. This is markedly different to the EB method, in which there is greater variation in the annual melt timeseries between the different ice caps, in both the shape of the curve, as well as the magnitude of melt.

Annual precipitation rates increased over every ice cap except N. Ellesmere and Agassiz between 2001 and 2004, From 2004 to 2008, annual precipitation fell substantially on all the ice caps except N. Ellesmere. The range of values of annual precipitation across the ice caps decreased from 200 kg m^{-2} yr^{-1} in 2004 to 110 kg m^{-2} yr^{-1} in 2008.

a)

Summer Melt Correlations 2001–2008

	Devon	Sydkap	Manson	POW	Axel	Agassiz	N.Ellesmere
Devon		.92	.90	.84	.73	.74	.67
Sydkap	.89		.90	.92	.86	.83	.75
Manson	.89	.87		.92	.75	.81	.70
POW	.79	.85	.85		.86	.93	.80
Axel	.80	.83	.76	.83		.89	.90
Agassiz	.77	.80	.77	.89	.85		.91
N.Ellesmere	.81	.75	.78	.79	.88	.86	

b)

Summer Precipitation Correlations 2001–2008

	Devon	Sydkap	Manson	POW	Axel	Agassiz	N.Ellesmere
Devon							
Sydkap	.59						
Manson	.66	.65					
POW	.36	.65	.69				
Axel	.34	.45	.30	.37			
Agassiz	.29	.38	.27	.61	.53		
N.Ellesmere	.29	.30	NaN	.26	.52	.63	

Table 4.7: a) Mean of the summer total correlation of daily melt totals on the 7 QEI icecaps, for the EB method (lower triangle), and TI method (upper triangle). b) Mean of the summer total correlation of daily precipitation totals on the 7 QEI icecaps. Only correlations with confidence greater than 95% are included in each mean. In a), all correlations used in the mean were significant with 95% confidence. In b), there were no correlations with greater than 95% confidence for comparison between Northern Ellesmere and Manson in any of the study years. "NaN" indicates comparisons that were not significant with 95% confidence. Ice caps are ordered by increasing latitude.

Mean Correlations for Melt and Precipitation

For each of the study years, daily timeseries of melt generated by the EB and TI methods, and precipitation, were constructed from the 3 hourly Polar WRF output. Using these daily data, correlations were computed for melt rate and precipitation timeseries for each of the icecaps (Table. B.1 and B.2 (Appendix)) for each summer. Table. 4.7 shows the 8 year mean of the summer correlations for (a) melt and (b) precipitation. Melt exhibited higher correlations between neighbouring icecaps in the TI method than in the EB method. (Neighbouring ice caps are located close to the main diagonal of the correlation table). However, the ice caps located at greater distances from each other (located in the bottom left and top right corners of the correlation table, for the EB and TI methods respectively) showed less correlation in the TI method than in the EB method. Precipitation exhibited much weaker correlations between ice caps than melt. Many of the non-neighbouring ice caps had one or more years in which the correlation was not significant at the 95% level (P-value < 0.05, where P-value is the probability of no correlation). Precipitation over Manson icefield was not significantly correlated with precipitation over N. Ellesmere for any of the study years.

Regional Correlation Indices

In order to understand the overall correlation of melt and precipitation over the seven ice caps in the QEI, we constructed a regional correlation index (RCI) for melt and precipitation. For each year, we averaged the correlations between each possible combination of pairs of ice caps in the study region.

The precipitation correlation index includes the non-significant correlations in the annual means, to prevent a systematic bias that could be introduced by excluding differing numbers of non-significant correlations from year to year. The P-value obtained for each correlation is dependent upon the correlation, and upon the number of data points. Since we ran the model for the same time period in each summer (June-Sept, 122 days), differences in the P-value between years are dependent only upon the correlation magnitudes. Thus if we did not include correlations with P-values less than 0.05 in the RCI, we would introduce a positive bias to the result. Figure. 4.15 compares trends in

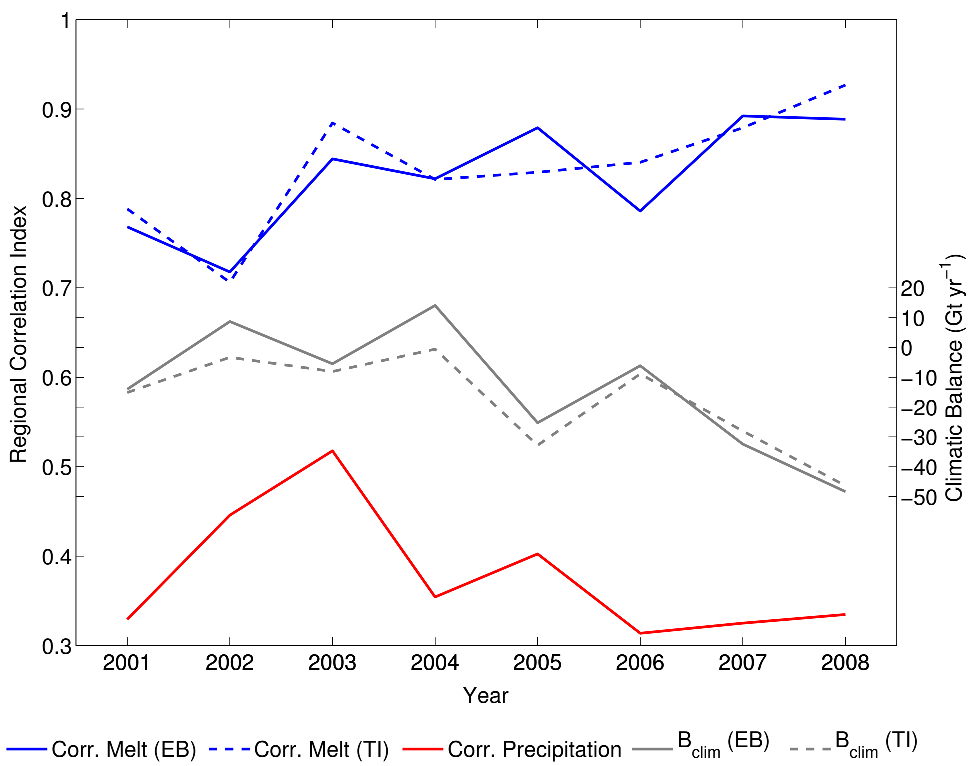

Figure 4.15: Regional Correlation Indices for melt (blue: EB method is solid, and TI method is dashed), and precipitation (red). Annual Climatic Balance in Gt yr^{-1} (grey: EB method is solid, and TI method is dashed). Note that climatic balance is plotted here for comparison, but was presented in Figure. 4.12.

the RCI for melt (using the EB and TI methods) and precipitation with that in the climatic balance.

The RCI for melt for both the EB and TI methods increased over the study period, while the climatic balance decreased. This indicates that as melt increased over the 8 year study period, the correlation length-scale for melt increased. On an annual timescale, inflections in the melt RCI timeseries coincide with inflections in the climatic balance over the period 2001-2004 for the TI method, and for the entire study period for the EB method. This indicates that there was greater melt in the years with a high melt RCI. This suggests that synoptic-scale systems affecting the entire QEI are responsible for the intense melt conditions observed in the latter part of the study period.

The precipitation RCI was much lower than the melt RCI, highlighting the comparatively short correlation length scale of precipitation. Precipitation RCI increased between 2001 and 2003, decreased from 2003 to 2008, when its value was similar to that in 2001. From 2003 to 2008, the decrease in precipitation RCI coincided with a decrease in climatic balance. This indicates that as climatic balance (and precipitation) decreased, the correlation length-scale of precipitation decreased. However, annual variations of the precipitation RCI do not follow the same pattern. From 2003 onwards, the inflections in precipitation RCI timeseries follow those of the melt RCI and mirror those of the climatic balance. Thus, in years of relatively high climatic balance (e.g. 2004 and 2006), the precipitation exhibited relatively low RCI. This suggests that, in contrast to the overall 2003 - 2008 trend explained earlier, precipitation exhibited low RCI, and therefore short correlation length-scales, in years with high climatic balance.

In summary, the RCI of melt and precipitation exhibited different trends over the study time period. However, between 2003 and 2008, the inflections in the EB method melt RCI and precipitation RCI follow one another closely. It is likely that this is caused by similar processes in both cases. In high climatic balance years, the RCIs for both melt and precipitation are relatively low, indicating spatially small disturbances moving through the domain delivering localised precipitation, and "breaking" the correlation of melt conditions between the icecaps. On the other hand, for low climatic balance years, the RCIs for melt and precipitation are relatively high, indicating that precipitation may be uniformly low across the region in the summers of those years. Thus, melt is interrupted less frequently in low climatic balance years, and melt correlation between ice caps remains high.

4.4 Conclusions

This study has used the regional climate model, Polar WRF, to simulate meteorological variables over the QEI for the summers of 2001-2008. The model output was used as input for both TI and EB climatic balance models. This high resolution study (6km) generates a new quasi-independent 8 year mass balance record for the QEI, which overlaps the work of Gardner et al. (2011), allowing 5 years of comparison. It represents the first high resolution RCM study in the QEI, and has provided the first full suite of high resolution atmospheric data for this region, although validation was only performed for the 2 meter temperature, and the LW and SW radiation fluxes.

Overall mass balance estimates of -246 ± 73Gt, and -178Gt for the period 2001-2008 were derived using the TI and EB methods respectively. It was necessary to perform a bias correction to Polar WRF air temperatures in order for the TI method to produce realistic melt estimates. However, the EB method was able to perform well with no such correction. Both methods agreed, within the bounds of uncertainty, with the two geophysical methods (GRACE and ICESat) of Gardner et al. (2011).

The study produced the first high resolution estimates of blowing snow sublimation and redistribution, and surface water vapor flux for the CAA. All of these terms are relatively small, with mean contributions of -0.1Gt yr^{-1}, -0.006 Gt yr^{-1} and -0.2 Gt yr^{-1} respectively. However, for the first time in the QEI, the regional patterns of these variables have been suggested, and there are strong spatial patterns. In the case of Q_D, the total contribution to the mass balance is negligible, but there is significant snow transport in the windiest areas of the domain, (the west side of Prince of Wales Icefield ,and west and south sides of Manson Icefield) in summer.

Internal accumulation was found to be a major term in the mass balance. Despite highly different spatial patterns for melt input, and potential retention factor in the EB and TI methods, their mean annual internal accumulations were 5.9 Gt yr^{-1} and 6.9 Gt yr^{-1} respectively; 16% and 15% of the respective regional mean annual melt.

Model output suggests that there was no significant melt acceleration according to the EB method, while, melt from the TI method accelerated by 4.4 Gt yr^{-2} for the period 2001-2008, and increased to 10 Gt yr^{-2} for the period

2004-2008. Over the same periods, annual precipitation decelerated at a rate of 1.4 Gt yr^{-1}, increasing to 2.8 Gt yr^{-2}. As internal accumulation and iceberg calving remained near constant through the period, the combined result was a decrease in climatic balance rate of between 4.9 Gt yr^{-1} (EB method) and 5.8 Gt yr^{-1} (TI method) between 2001-2008, and between 9.9 Gt yr^{-2} (EB method) and 13.2 Gt yr^{-2} (TI method) between 2004-2008. This is consistent with the findings of Sharp et al. (2011), who found extreme melting in the QEI after 2005.

Devon Ice Cap was modelled as the having the highest melt rates in the QEI. Prince of Wales Icefield and Agassiz Ice Cap had the lowest melt rates in the QEI, but at the same time, the highest average precipitation rates (per unit area). As a result, they exhibited the most positive climatic balances.

Modelled summer daily melt was more highly correlated between ice caps than precipitation. A regional correlation index was derived by averaging the correlation of each ice cap to every other icecap, for each year. From 2001 to 2008, the RCI for melt increased over time, while that for precipitation decreased after 2003. This was coincident with decreasing climatic balance. The increased RCI for melt implies that large scale synoptic systems are responsible for the decrease in climatic balance over the period. The decrease in precipitation RCI implies that smaller disturbances are delivering the smaller precipitation amounts in the low climatic balance summers, which do not have a large enough regional impact to break the high melt RCI, which we speculate is being caused by regional scale high pressure systems. These conclusions are consistent with Wang et al. (2005) who showed that annual mean melt duration on ice caps in the QEI is positively correlated with local 500hPa geopotential height on an annual timescale They are also consistent with Gardner and Sharp (2007) who demonstrated that changes in the strength and center position of the July 500 hPa circumpolar vortex, have resulted in increased occurrences of high pressure ridging in the QEI, and in the acceleration of glacier ablation in the area since 1986/87.

This study offers the first high resolution insight into the spatial and temporal variations of mass balance components in the QEI. It would be useful for future studies to derive independent estimates of blowing snow sublimation and redistribution, and surface water vapor flux, so that model skill may be more thoroughly assessed. Despite its shortcomings, the model was able to reproduce the findings of Gardner et al. (2011); Sharp et al. (2011), and thus we consider it to be a powerful, physically based tool, for mass balance studies.

4.5 Acknowledgements

The Polar WRF boundary conditions used in this study are from the Research Data Archive (RDA) which is maintained by the Computational and Information Systems Laboratory (CISL) at the National Center for Atmospheric Research (NCAR). NCAR is sponsored by the National Science Foundation (NSF). The original data are available from the RDA (http://dss.ucar.edu) in dataset number ds083.2.

Bibliography

Abdalati, W., W. Krabill, E. Frederick, S. Manizade, C. Martin, J. Sonntag, R. Swift, R. Thomas, J. Yungel, and R. Koerner. "Elevation changes of ice caps in the Canadian Arctic Archipelago." *Journal of Geophysical Research* 109 (2004).

Bindoff, N., J. Willebrand L., V. Artale, A. Cazenave, J. Gregory, S. Gulev, K. Hanawa, C. Le Quéré, S. Levitus, Y. Nojiri, C. K. Shum, L. D. Talley, and A. Unnikrishnan. 2007 : 384–432.

Bintanja, R. "Snowdrift sublimation in a katabatic wind region of the Antarctic ice sheet." *Journal of Applied Meteorology* 40 (2001): 1952–1966.

Box, J. E., D. H. Bromwich, and L.S. Bai. "Greenland ice sheet surface mass balance 1991–2000: Application of Polar MM5 mesoscale model and in situ data." *Journal of Geophysical Research* 109 (2004).

Box, J. E., D. H. Bromwich, B. A. Veenhuis, L. S. Bai, J. C. Stroeve, J. C. Rogers, K. Steffen, T. Haran, and S. H. Wang. "Greenland ice sheet surface mass balance variability (1988-2004) from calibrated polar MM5 output." *Journal of Climate* 19 (Jun 2006): 2783–2800.

Box, J. E. and K. Steffen. "Sublimation on the Greenland ice sheet from automated weather station observations." *Journal of Geophysical Research* 106 (12 2001): 33965–33981.

Budd, W. F, W. R. J. Dingle, and U. Radok. "The Byrd Snow Drift Project: Outline and basic results." *Studies in Antarctic Meteorology, Antarctic Research Service* 9 (1966): 71–134.

Burgess, D and M Sharp. "Recent changes in areal extent of the Devon Island Ice Cap, Nunavut, Canada." *Arctic, Antarctic and Alpine Research* 36 (2004): 261–271.

Burgess, D and M Sharp. "Recent changes in thickness of the Devon Island ice cap, Canada." *Journal of Geophysical Research* 113 (2008).

Chen, Fei and Jimy Dudhia. "Coupling an Advanced Land Surface–Hydrology Model with the Penn State–NCAR MM5 Modeling System. Part I: Model Implementation and Sensitivity." *Monthly Weather Review* 129 (2001).

Church, J. A. "Changes in Sea Level." *Climate Change* (2001).

Cogley, G J and W P Adams. "Mass balance of glaciers other than the ice sheets." *Journal of Glaciology* 44 (1998).

Cogley, J.G., R. Hock, L.A. Rasmussen, A.A. Arendt, A. Bauder, R.J. Braithwaite, P. Jansson, G. Kaser, M. Möller, L. Nicholson, and M. Zemp. "Glossary of Glacier Mass Balance and Related Terms." *IHP-VII Technical Documents in Hydrology.* 2011.

Colbeck, S C. "An analysis of water flow in dry snow." *Water Resources Research* 12 (1976): 523–527.

Colgan, W., J. Davis, and M. Sharp. "Is the high-elevation region of Devon Ice Cap thickening?." *Journal of Glaciology* 54 (2008): 428–436(9).

Davis, J. *PhD Thesis*. PhD thesis, University of Alberta, In Prep, 2012.

Déry, S. J. and M. K. Yau. "A Bulk Blowing Snow Model.." *Boundary-Layer Meteorology* 93 (1999): 237 – 251.

Déry, S. J. and M. K. Yau. "Simulation Of Blowing Snow In The Canadian Arctic Using A Double-Moment Model.." *Boundary-Layer Meteorology* 99 (2001): 297 – 316.

Déry, S. J. and M. K. Yau. "Large-scale mass balance effects of blowing snow and surface sublimation,." *Journal of Geophysical Research* 107(D23) (12 2002).

Déry, S.J. and M.K. Yau. "Simulation of an Arctic Ground Blizzard Using a Coupled Blowing Snow Atmosphere Model." *Journal of Hydrometeorology* 2 (2001): 579.

Duncan, A. Spatial and Temporal Variations of the Surface Energy Balance and Ablation on the Belcher Glacier, Devon Island, Nunavut, Canada. Master's thesis, University of Alberta, 2011.

Dyurgerov, M., M. Meier, and R. Armstrong. "Glacier Mass Balance and Regime: Data of Measurements and Analysis." *University of Colorado Institute of Arctic and Alpine Research Occasional Paper 55* (2002).

Dyurgerov, M., M. Meier, and R. Armstrong. "Mass Balance of Mountain and Sub-Polar Glaciers Outside the Greenland and Antarctic ice sheets.." *Supplement to the M. Dyurgerov Occasional Paper 55, 2002.* (2005).

Ettema, J, M R. van den Broeke, E van Meijgaard, W Jan van de Berg, J L. Bamber, J E. Box, and R C. Bales. "Higher surface mass balance of the Greenland ice sheet revealed by high-resolution climate modeling." *Geophys. Res. Lett.* 36 (06 2009).

Fettweis, X, H Gallée, L Lefebre, and J.P van Ypersele. "Greenland surface mass balance simulated by a regional climate model and comparison with satellite derived data in 1990-1991." *Climate Dynamics* (2005): 623–640.

Gardner, A. S., G. Moholdt, B. Wouters, G. J. Wolken, D. O. Burgess, M. J. Sharp, G. Cogley, C. Braun, and C. Labine. "Sharply increased mass loss from glaciers and ice caps in the Canadian Arctic Archipelago." *Nature* 473 (April 2011): 357–360.

Gardner, A. S. and M. J. Sharp. "Influence of the Arctic Circumpolar Vortex on the Mass Balance of Canadian High Arctic Glaciers." *Journal of Climate* 20 (2007).

Gardner, A. S., M. J. Sharp, R. M. Koerner, C. Labine, S. Boon, S. J. Marshall, D. O. Burgess, and D. Lewis. "Near-Surface Temperature Lapse Rates over Arctic Glaciers and Their Implications for Temperature Downscaling." *Journal of Climate* 22 (2011/11/04 2009): 4281–4298.

Grell, G. A. and D. Dévényi. "A generalized approach to parameterizing convection combining ensemble and data assimilation techniques." *Geophysical Research Letters* 29 (2002).

Hines, K M. and D H. Bromwich. "Development and Testing of Polar Weather

Research and Forecasting (WRF) Model. Part I: Greenland Ice Sheet Meteorology..” *Monthly Weather Review* 136 (2008): 1971–1989.

Hines, K. M., D. H. Bromwich, L. S. Bai, M. Barlage, and A. G. Slater. “Development and Testing of Polar WRF. Part III: Arctic Land*.” *Journal of Climate* 24 (2011): 26–48.

Hock, R. “Glacier melt: a review of processes and their modelling.” *Progress in Physical Geography* 29 (2005): 362–391.

Iacono, M. J., J. S. Delamere, E. J. Mlawer, M. W. Shephard, S. A. Clough, and W. D. Collin. “Radiative forcing by long-lived greenhouse gases: Calculations with the AER radiative transfer models.” *Journal of Geophysical Research* 113 (2008).

Jacob, T., J. Wahr, T. Pfeffer, and S. Swenson. “Recent Contributions of Glaciers and Ice Caps to Sea Level Rise.” *Nature* 10847 (2012).

Kalnay, E., M. Kanamitsu, R. Kistler, W. Collins, D. Deaven, L. Gandin, M. Iredell, S. Saha, G. White, J. Woollen, Y. Zhu, A. Leetmaa, R. Reynolds, M. Chelliah, W. Ebisuzaki, W.Higgins, J. Janowiak, K. C. Mo, C. Ropelewski, J. Wang, Roy Jenne, and Dennis Joseph. “The NCEP/NCAR 40-Year Reanalysis Project.” *Bulletin of the American Meteorological Society* (1996).

Koerner, R M. “The Mass Balance of Devon Island Ice Cap, Northwest Territories, Canada 1961-66.” *Journal of Glaciology* 9 (1970): 325–336.

Koerner, R. M. “Mass balance of glaciers in the Queen Elizabeth Islands, Nunavut, Canada.” *Annals of Glaciology* 42 (2005).

Long, D. G. and B.R. Hicks. QuikSCAT and Seawinds Land/Ice Image Products. Technical report, Brigham Young University, 2010.

Mair, D., D. Burgess, and M. Sharp. "Thirty-seven year mass balance of Devon Ice Cap, Nunavut, Canada, determined by shallow ice coring and melt modelling." *Journal of geophysical research* 110 (2005).

Male, D. H. and R. J. Granger. "Snow surface and energy exchange.." *Water Resources Research* 17 (1981): 609–627.

Manabe, S. and R.T. Wetherald. "The effects of doubling the CO2 concentration on the climate of a general circulation model." *Journal of Atmospheric Sciences* 32 (1975): 3–15.

Meier, M. F., M. B. Dyurgerov, R. K. Ursula, S. O'Neel, W. T. Pfeffer, R. S. Anderson, S. P. Anderson, and A. F. Glazovsky. "Glaciers Dominate Eustatic Sea-Level Rise in the 21st Century." *Science* (2007): 1143906.

Mlawer, E. J., S. J. Taubman, P. D. Brown, M. J. Iacono, and S. A. Cloug. "Radiative transfer for inhomogeneous atmospheres: RRTM, a validated correlated-k model for the longwave." *Journal of Geophysical Research* 102 (1997).

Morrison, H., G. Thompson, and V. Tatarskii. "Impact of Cloud Microphysics on the Development of Trailing Stratiform Precipitation in a Simulated Squall Line: Comparison of One- and Two-Moment Schemes." *American Meteorological Society* (2009).

Nakanishi, M. and H. Niino. "An Improved Mellor–Yamada Level-3 Model: Its

Numerical Stability and Application to a Regional Prediction of Advection Fog." *Boundary-Layer Meteorology* 119 (2006): 397–407.

Pfeffer, W.T, M.F Meier, and T.H. Illangasekare. "Retention of Greenland runoff by refreezing: Implications for projected future sea-level change.." *Journal of Geophysical Research* 96(C-12) (1991): 117–22,124.

Pomeroy, J. W and R. Essery. "Turbulent fluxes during blowing-snow: Field tests of model sublimation predictions." *Hydrological Processes* 13 (1999): 2963–2975.

Sharp, M., D. O. Burgess, J. G. Cogley, M. Ecclestone, C. Labine, and G. J. Wolken. "Extreme melt on Canada's Arctic ice caps in the 21st century." *Geophysical Research Letters* 38 (2011).

Shepherd, A., D U Zhijun, T. J Benham, J. A Dowdeswell, and E. M. Morris. "Mass balance of Devon Ice Cap, Canadian Arctic." *Annals of Glaciology* 46 (2007): 249–254(6).

Tabler, R. D. "Snow transport as a function of wind speed and height." *Cold Regions Engineering: Proceedings, Cold Regions Sixth International Specialty Conference* (1991).

Turner, J, T. A. Lachlan-Cope, G. J. Marshall, E. M. Morris, R. Mulvaney, and W. Winter. "Spatial variability of Antarctic Peninsula net surface mass balance.." *Journal of Geophysical Research* 107 (2002): 4173.

Wang, L., M. J. Sharp, B. Rivard, S. Marshall, and D. Burgess. "Melt season duration on Canadian Arctic ice caps, 2000–2004." *Geophysical Research Letters* 32 (2005).

CHAPTER 5

Conclusions

Mass balance is the fundamental quantity that measures whether a glacier is in balance with its climatic environment. It also quantifies the mass input of a glacier to the non-steric component of global mean sea level change, that has been shown to be increasing (Willis et al. (2010)). Glaciers and Ice Caps (GICs) have been shown to be a large contributor to global mean sea level rise, despite their relatively small area compared to that of the large ice sheets (Church (2001); Jacob et al. (2012)). The GICs in the Canadian Arctic Islands (CAI) represent the largest concentration of glacier ice outside the large ice sheets in Greenland and Antarctica. Thus, quantifying the mass balance of glaciers in this region is a critical scientific challenge that must be overcome in order to determine the sea level contribution from the CAI. This thesis presents the first comprehensive study of mass balance in the CAI using a Regional Climate Model (RCM). The thesis is broken into three independent studies that (i) assess the feasibility, and test the quality of output from running a RCM at high resolution over an area in the CAI, (ii) improve the performance of the RCM by introducing a new parameterization for a major surface property (glacier surface albedo) and (iii) use the model, with the improvements developed in (ii), to estimate regional mass balance over the Queen Elizabeth Islands (the islands north of Parry Channel in the CAI).

At the time that the work first began, regional climate models had been tested over Greenland and Antarctica (Bromwich et al. (2001); Cassano et al. (2001); Guo et al. (2003); Hines et al. (1997); Van Lipzig et al. (1999); Manning and Davis (1997); Van De Berg et al. (2006)), and the output from running such models over the Greenland ice sheet, had been used to estimate climatic balance (one of the major components of the overall mass balance) for the entire ice sheet (Box and Rinke (2003); Box et al. (2004, 2006); Fettweis et al. (2005)). These studies provided 24km resolution climatic balance estimates for the entire Greenland ice sheet from 1988-2004. The method was very effective on the largely flat interior of the Greenland ice sheet, but RCMs were observed to perform poorly in the areas of steep terrain around the Greenland margin, where most of the melt occurs (Cassano et al. (2001)).

In the second chapter of this thesis, the RCM Polar MM5 was applied on a high resolution (3km) grid over Devon Ice Cap for the summer of 2008. The model was run in "forecast mode", where it is reinitiated every 48 hours to prevent model drift. Output from the model was compared to data from five weather stations located at altitudes ranging from 525m to 1802m on the ice cap. The model under-predicted near surface air temperatures at all elevations, supporting the hypothesis that the albedo (assigned as a constant 0.8) was causing too much of the shortwave radiation to be reflected from the surface during the melt season, when in reality the albedo decreases due to snow metamorphism. To investigate this further, the incoming and outgoing shortwave and longwave components of the surface radiation budget were examined in detail. It was found that variability in the net radiation budget residuals (daily differences between modelled and measured values) was driven by variability in the net longwave residuals at high elevations, and by the net shortwave residuals at low elevations. This was interpreted as being suggestive that at high elevations, errors in cloud prediction drive errors in the net radiation budget, whereas at low elevations errors in albedo drive errors in the net radiation budget.

With this in mind, the second chapter concluded by developing a relationship (sigmoidal function) between mean daily near surface air temperature and albedo. The relationship was suggested as a simple parameterization that could be applied inline within Polar MM5. The advantage of developing such a parameterization was that it would be unaffected by the model being restarted every 48 hours. This was viewed as a fundamental limitation for an albedo parameterization, since the model effectively has no memory beyond each 48 hour restart, and thus an albedo parameterization cannot allow for metamorphism over periods greater than 48 hours.

The results of chapter two set the objectives for chapter three, which were to develop and test an inline albedo parameterization in Polar WRF. Polar WRF, the successor to Polar MM5, was developed and had been tested by the time work began on chapter two in early 2009 (Bromwich et al. (2009); Hines and Bromwich (2008); Hines et al. (2011)). At this time, it was decided to use Polar WRF for the remainder of the project, so that the new albedo parameterization could be a useful contribution to the Polar WRF community. In chapter three, the Greenland Ice Sheet was used as the study area since collaborators at the Byrd Polar Research Center, Ohio State University, had developed an accurate cloudmask for the region (personal communication with David Decker), which would allow the use of the MODIS MOD10A1 daily albedo dataset for calibration and validation of the model.

Given the improved model framework in Polar WRF compared to Polar MM5, we were able to implement a more ambitious albedo parameterization within the model than the sigmoidal relationship presented in chapter two. The parameterization was based closely upon the work of Bougamont et al. (2005) and Oerlemans and Knap (1998) and accounted for snow aging, increases in albedo after fresh snowfall, and shortwave radiation penetration into the snowpack. The snowpack and albedo were allowed to evolve over the course of an entire season by feeding the surface variables from the output of one 48 hour model run into the next 48 hour run as an input.

Due to computational constraints, the calibration was performed “offline”, and the optimal offline calibration was then run inline within Polar WRF. Calibration was performed for 2005, and the model was then run for 2001 (cold year), 2005 (calibration year), and 2007 (warm year). Two calibrations were presented (Cal A and Cal B), and run inline to produce the outputs WCA and WCB. Both WCA and WCB were accurate in 2005 and 2007. In 2001, WCB performed well again, but WCA performed very poorly. Feedbacks between various components of the energy and mass balance and the model albedo were investigated by comparing the poor performance of WCA with the satisfactory performance of WCB in 2001. It was discovered that all components of the energy budget were affected by the differences in the calibration of the albedo parameterization in WCA and WCB. The longwave, turbulent, and ground energy fluxes were all shown to respond to differences in albedo in a direction opposite to the net shortwave flux. Although the net shortwave flux resulted in a positive feedback on albedo, all of the remaining energy balance terms had a negative feedback on albedo. The additional shortwave energy absorbed at the surface, as a result of reducing the albedo, was significantly offset, (by up to two thirds), by the combined energy losses from the surface associated with the negative feedbacks arising from the longwave, turbulent and ground energy fluxes.

Overall, the albedo paramerization running inline within Polar WRF was able to capture the elevation profile of albedo on the western margin of the Greenland Ice Sheet. The results of chapter three showed that (i) the inline albedo parameterization had significant feedback on all components of the surface energy budget and (ii) it is necessary to have the albedo parameterization running inline in an RCM for these feedbacks to take effect. In some previous studies (e.g. Box et al. (2004)), albedo was set as a constant (0.8) during RCM runs, and a post-run correction was applied to the net-shortwave flux after the run was completed, to allow for the impact of reductions in albedo during melt. The results of chapter three suggest that the increase to the net energy balance that results from applying such a correction, would be an over-estimate, as the correction would not account for the negative feedbacks associated with the longwave, turbulent, and ground energy fluxes.

Finally, the goal of chapter four of the thesis was to apply Polar WRF to the Queen Elizabeth Islands (QEI), for the period 2001-2008, and use the output to (i) estimate regional climatic balance and its constituent components for the QEI ice caps, (ii) combine the climatic balance with ice-berg calving flux estimates to obtain estimated of total regional mass balance and (iii) investigate spatial and temporal variations of the climatic balance components on the seven major ice caps of the QEI. The model was run on a 6km grid over the entire QEI. Given that the methods used in chapter four are based closely on those employed by Box et al. (2004), the inclusion of the optimal inline albedo parameterization developed in chapter three represents a tangible step forward for the use of Polar WRF as a method for modelling climatic balance. If the albedo parameterization had not been included inline within Polar WRF, then a post-run correction to the shortwave radiation flux would have been needed to account for albedo inaccuracies. However, as described in chapter three, such a correction would be inaccurate due to the negative feedbacks of albedo change on the longwave, turbulent and ground energy fluxes.

Using the Polar WRF output, two separate methods (a temperature index (TI) model, and an energy balance (EB) model) were used to calculate climatic balance of all ice caps in the QEI. The near surface temperature data used to drive the TI model were corrected for a negative bias, whereas no correction was applied to any of the energy balance components used in the EB method. Both methods were able to reproduce, within the bounds of uncertainty, the findings from the three independent methods (repeat satellite gravimetry (GRACE), repeat satellite laser altimetry (ICESat), and a TI mass budget model) employed by Gardner et al. (2011) to estimate annual regional mass balance between 2004-2008. Although both methods reproduced the findings of Gardner et al. (2011), they showed considerable differences when compared to one another. Melt volumes from the TI method accelerated by 4.4 Gt yr^{-2} over the period 2001-2008, and by 10 Gt yr^{-2} over the period 2004-2008. Conversely, there was no significant acceleration of melt according to the EB method. Precipitation (common to both methods) decelerated at a rate of 1.4 Gt yr^{-2} between 2001-2008. The rate increased to 2.8 Gt yr^{-2} in the period 2004-2008. The combined effect of melt and precipitation trends was that the climatic balance rate decreased by between 4.9 Gt yr^{-2} (EB method) and 5.8 Gt yr^{-2} (TI method) between 2001-2008, and between 9.9 Gt yr^{-2} (EB method) and 13.2 Gt yr^{-2} (TI method) between 2004-2008. This is consistent with the findings of Sharp et al. (2011), who found that 30-48% of mass loss from four monitored glaciers since 1963, has occurred since 2005.

The work reported in chapter four produced the first regional scale, high resolution estimates of blowing snow sublimation and redistribution, surface water vapor flux and internal accumulation for the QEI ice caps. Blowing snow sublimation and redistribution and surface water vapor flux were relatively small terms in the overall mass budget, but could be an important process on smaller scales (e.g. individual basins). Internal accumulation proved to be a large term in the climatic balance, accounting for the refreezing of approximately 15% of regional scale melt.

The 6km resolution grid was sampled over each of the seven major ice caps of the QEI, and the balance components on each were compared. Devon Ice Cap was modelled as having the highest melt rate in the QEI, and the lowest overall climatic balance. Prince of Wales Icefield and Agassiz Ice Cap had the lowest melt rates in the QEI and the highest average precipitation rates (per unit area). As a result, they exhibited the most positive climatic balances amongst the QEI ice caps.

In order to evaluate the inter-dependence of climatic balance components between each of the icecaps, the "Regional Correlation Index" (RCI) was devised for melt and precipitation. By correlating melt and precipitation daily time-series between each pair of ice caps, and computing the mean of all of these correlations, it was possible to quantify the regional inter-dependence for melt and precipitation on ice caps in the QEI. A high RCI indicates a high degree of inter-dependence, whereas a low RCI indicates more independent variations.

From 2001 to 2008, the RCI for melt increased, whereas the RCI for precipitation decreased after 2003. During the same time period, climatic balance decreased significantly. The increased RCI for melt implies that large synoptic systems are responsible for the dramatic decrease in climatic balance over the study period. The decrease in precipitation RCI implies that smaller disturbances are delivering the smaller precipitation amounts in the low climatic balance summers, and that they do not have a large enough regional impact to disrupt the high level of correlation in climatic balance across the QEI ice caps.

Overall, the work in this thesis has demonstrated that the RCM Polar MM5/WRF can be successfully applied to the complex topography of the CAI. This was by no means a certainty at the beginning of the thesis, as it required running the model at a much higher resolution than in previous studies. The second chapter was a feasibility study, and gave insight into a key weakness of the model: the over-simplified treatment of albedo. The third chapter addressed the issue of glacier surface albedo variation, by developing and programming a glacier albedo parameterization inline in Polar WRF. The parameterization represents a tangible contribution to the Polar WRF community, and will be included in a future release of the model. We were able to show the importance of running an albedo parameterization inline within an RCM, by studying the feedback on each of the energy balance terms, when the calibration of the parameterization was adjusted. The logical conclusion of this thesis was to use the parameterization developed in the second chapter in a regional scale, 6km resolution simulation over the QEI. Regional scale mass balance estimates generated using these data to drive two different climatic balance models agreed within the bounds of uncertainty with those generated by three different methods (Gardner et al. (2011)). The modelled trends in the climatic balance components agreed with observed increases in melt, and decreases of climatic balance in the CAI (Sharp et al. (2011)). Furthermore, the high resolution output allowed calculation of mass balance variations and trends over the seven major ice caps of the QEI.

Given the success of Polar WRF in simulating the climatic balance of ice caps in the QEI between 2001-2008, it is hoped that future studies will apply the model to the Southern CAI, and to longer time periods. The energy balance calculations of climatic balance were not bias corrected or tuned to the QEI, yet successfully modelled climatic balance in the region. This gives credibility to the energy balance method as a physically based approach for estimating climatic balance. With such a physically based approach, it is likely that the method could perform with high skill under a variety of climatic forcings. Future forecasts of climatic balance could be achieved by running Polar WRF, initiated and forced at the boundaries by output from a General Circulation Model. The use of the energy balance approach would likely produce climatic balance estimates that are consistent with the climatic forcing from the GCM.

In chapter four of this work, climatic balance was calculated offline, rather than inline in Polar WRF (as has been done in RACMO2 (Ettema et al. (2009))). However, it is only the internal accumulation, and blowing snow sublimation and redistribution terms in the climatic balance that are not calculated fully inline. It would be relatively straightforward to integrate an internal accumulation scheme into the model, if a scheme optimized for use on a short timestep (i.e. equal to that of Polar WRF $\sim$ 3 mins) was used. It would be much more challenging to fully integrate the blowing snow sublimation and redistribution terms into Polar WRF, and even if it were done, this course of action might significantly slow down the model. However, it was shown in the fourth chapter that blowing snow sublimation and redistribution are relatively small terms in the overall mass budget. Thus, ignoring them, but fully integrating an internal accumulation scheme into Polar WRF, would allow inline estimates of climatic balance with high accuracy.

Bibliography

Bougamont, M, J Bamber, and W Greuell. "A surface mass balance model for the Greenland Ice Sheet." *Journal of Geophysical Research* 110 (2005).

Box, J. E., D. H. Bromwich, and L.S. Bai. "Greenland ice sheet surface mass balance 1991–2000: Application of Polar MM5 mesoscale model and in situ data." *Journal of Geophysical Research* 109 (2004).

Box, J. E., D. H. Bromwich, B. A. Veenhuis, L. S. Bai, J. C. Stroeve, J. C. Rogers, K. Steffen, T. Haran, and S. H. Wang. "Greenland ice sheet surface mass balance variability (1988-2004) from calibrated polar MM5 output." *Journal of Climate* 19 (Jun 2006): 2783–2800.

Box, J. E. and A. Rinke. "Evaluation of Greenland Ice Sheet Surface Climate in the HIRHAM Regional Climate Model Using Automatic Weather Station Data." *Journal of Climate* 16 (2003).

Bromwich, D. H., J. J. Cassano, T. Klein, G. Heinemann, K. M. Hines, K. Steffen, and J. E. Box. "Mesoscale modeling of katabatic winds over Greenland with the Polar MM5." *Monthly Weather Review* 129 (2001): 2290–2309.

Bromwich, D.H., K. M. Hines, and L. S. Bai. "Development and testing of

Polar Weather Research and Forecasting model: 2. Arctic Ocean." *Journal of Geophysical Research* 114 (2009).

Cassano, J. J., J. E. Box, D. H. Bromwich, L. Li, and K. Steffen. "Evaluation of polar MM5 simulations of Greenland's atmospheric circulation." *Journal of Geophysical Research* 106 (Dec 2001): 33867–33889.

Church, J. A. "Changes in Sea Level." *Climate Change* (2001).

Ettema, J, M R. van den Broeke, E van Meijgaard, W Jan van de Berg, J L. Bamber, J E. Box, and R C. Bales. "Higher surface mass balance of the Greenland ice sheet revealed by high-resolution climate modeling." *Geophys. Res. Lett.* 36 (06 2009).

Fettweis, X, H Gallée, L Lefebre, and J.P van Ypersele. "Greenland surface mass balance simulated by a regional climate model and comparison with satellite derived data in 1990-1991." *Climate Dynamics* (2005): 623–640.

Gardner, A. S., G. Moholdt, B. Wouters, G. J. Wolken, D. O. Burgess, M. J. Sharp, G. Cogley, C. Braun, and C. Labine. "Sharply increased mass loss from glaciers and ice caps in the Canadian Arctic Archipelago." *Nature* 473 (April 2011): 357–360.

Guo, Z. C., D. H. Bromwich, and J. J. Cassano. "Evaluation of Polar MM5 simulations of Antarctic atmospheric circulation." *Monthly Weather Review* 131 (Feb 2003): 384–411.

Hines, K M. and D H. Bromwich. "Development and Testing of Polar Weather Research and Forecasting (WRF) Model. Part I: Greenland Ice Sheet Meteorology.." *Monthly Weather Review* 136 (2008): 1971–1989.

Hines, K. M., D. H. Bromwich, L. S. Bai, M. Barlage, and A. G. Slater. "Development and Testing of Polar WRF. Part III: Arctic Land*." *Journal of Climate* 24 (2011): 26–48.

Hines, K. M., D. H. Bromwich, and Z. Liu. "Combined global climate model and mesoscale model simulations of Antarctic climate." *Journal of Geophysical Research* 102 (Jun 1997): 13747–13760.

Jacob, T., J. Wahr, T. Pfeffer, and S. Swenson. "Recent Contributions of Glaciers and Ice Caps to Sea Level Rise." *Nature* 10847 (2012).

Manning, K.W. and C. A.A. Davis. "Verification and Sensitivity Experiments for the WISP94 MM5 Forecasts." *Weather and Forecasting* 12 (December 1997): 719–735.

Oerlemans, J. and W.H. Knap. "A 1 year record of global radiation and albedo from the ablation zone of the Morteratschgletscher, Switzerland." *Journal of Glaciology* (1998).

Sharp, M., D. O. Burgess, J. G. Cogley, M. Ecclestone, C. Labine, and G. J. Wolken. "Extreme melt on Canada's Arctic ice caps in the 21st century." *Geophysical Research Letters* 38 (2011).

Van De Berg, W. J., M. R. van den Broeke, C. H. Reijmer, and E. van Meijgaard. "Reassessment of the Antarctic surface mass balance using calibrated output of a regional atmospheric climate model." *Journal of Geophysical Research* 111 (2006).

Van Lipzig, N.P.M, E. Van Meijgaard, and Oerlemans. J. "Evaluation of a Regional Atmospheric Model Using Measurements of Surface Heat Exchange

Processes from a Site in Antarctica." *Monthly Weather Review* 127 (1999): 1994–2011.

Willis, J.K., D.P. Chambers, C.-Y. Kuo, and C.K. Shum. "Global sea level rise: Recent progress and challenges for the decade to come.." *Oceanography* 23 (2010): 26–35.

APPENDIX A

chapter 2 appendix

Here are the latitude/month separated figures and a summary table.

Table A.1: Summary of Polar WRF vs. MOD10A1 elevation transect RMSEs for different latitude bands and months.

	A (2001)	B (2001)	A (2005)	B (2005)	A (2007)	B (2007)
lat 63.5 - 55.6	0.27	0.056	0.077	0.078	0.07	0.052
lat 66.5 - 69.7	0.18	0.068	0.089	0.08	0.079	0.065
lat 69.7 - 72.8	0.25	0.058	0.084	0.078	0.074	0.078
lat 72.8 - 76.0	0.22	0.096	0.12	0.078	0.11	0.1
June	0.13	0.071	0.051	0.088	0.039	0.041
July	0.26	0.1	0.044	0.045	0.046	0.044
August	0.28	0.05	0.048	0.07	0.053	0.052
September	0.24	0.09	0.039	0.096	-	0.1

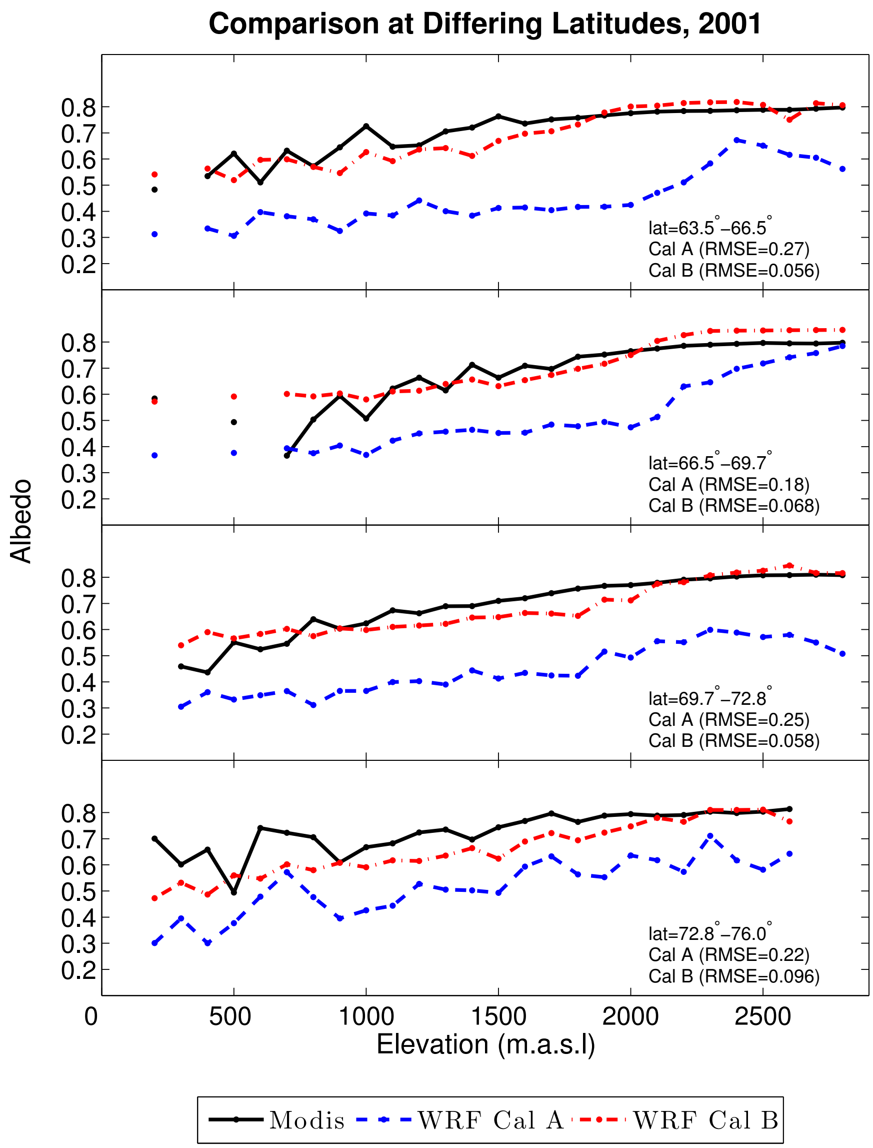

Figure A.1: Elevation profiles for 3 parameterizations alongside MOD10A1, split into 4 equal size latitude bands.

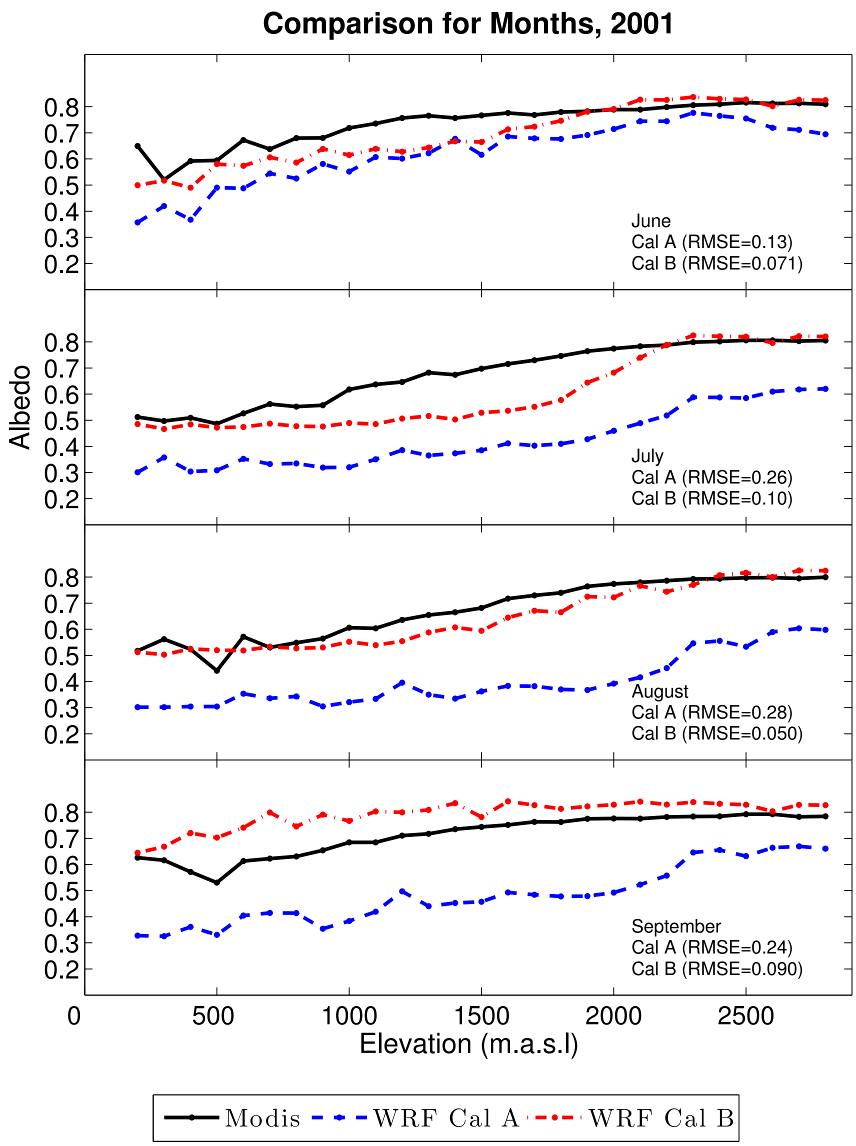

Figure A.2: Elevation profiles for 3 parameterizations alongside MOD10A1, for the entire domain, but split into separate months.

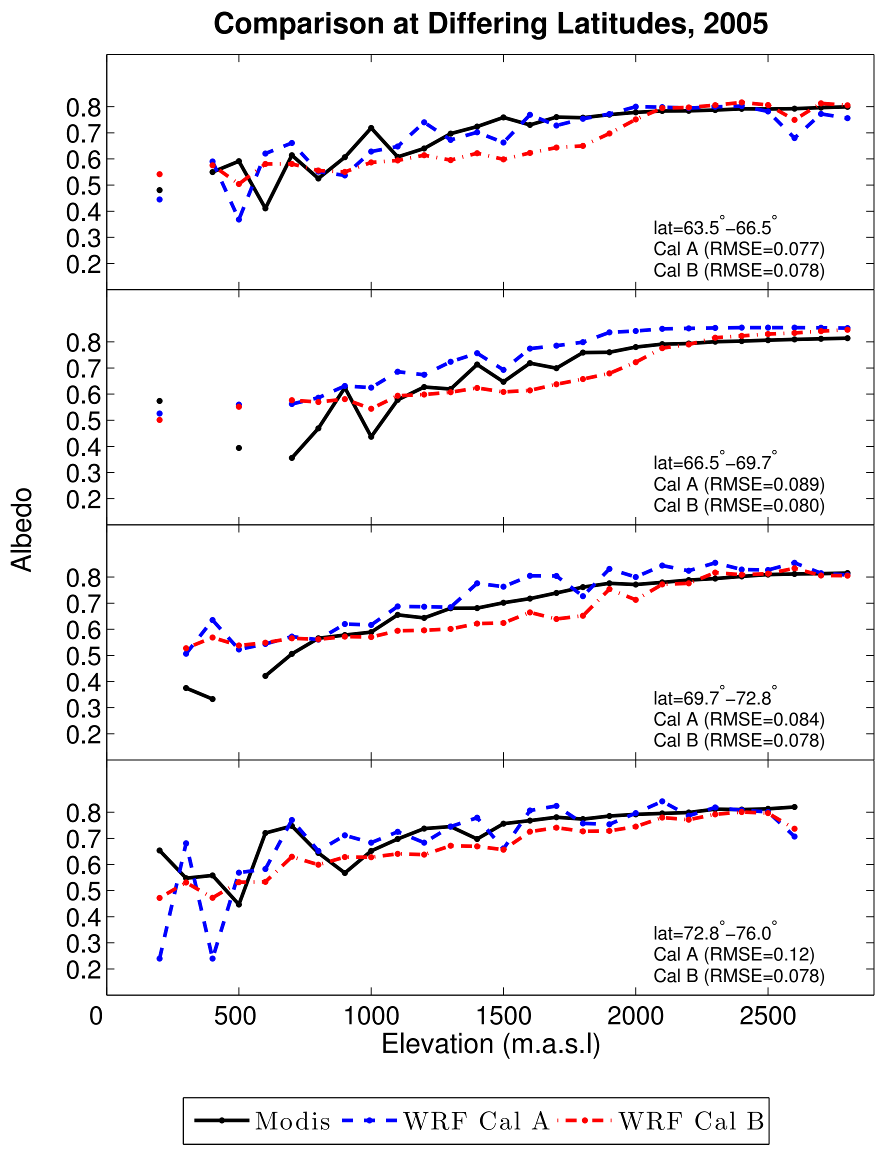

Figure A.3: Elevation profiles for 3 parameterizations alongside MOD10A1, split into 4 equal size latitude bands.

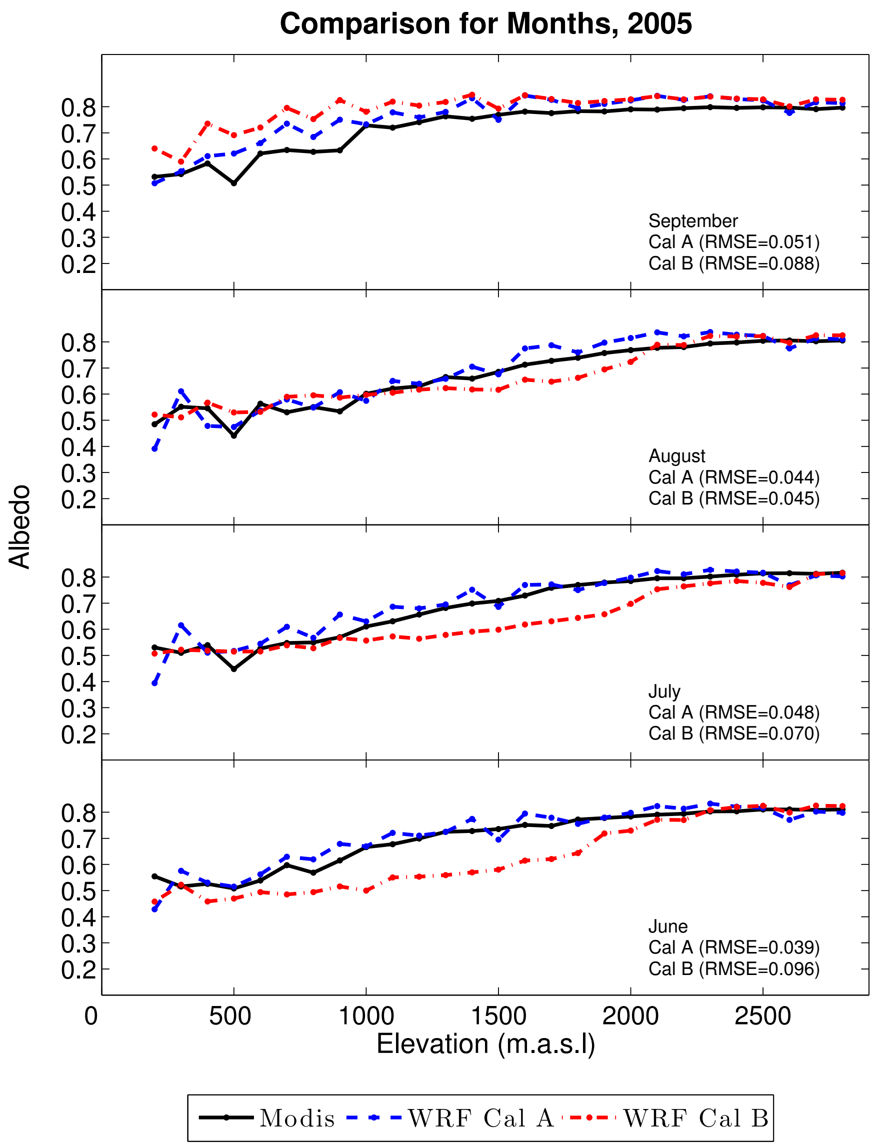

Figure A.4: Elevation profiles for 3 parameterizations alongside MOD10A1, for the entire domain, but split into separate months.

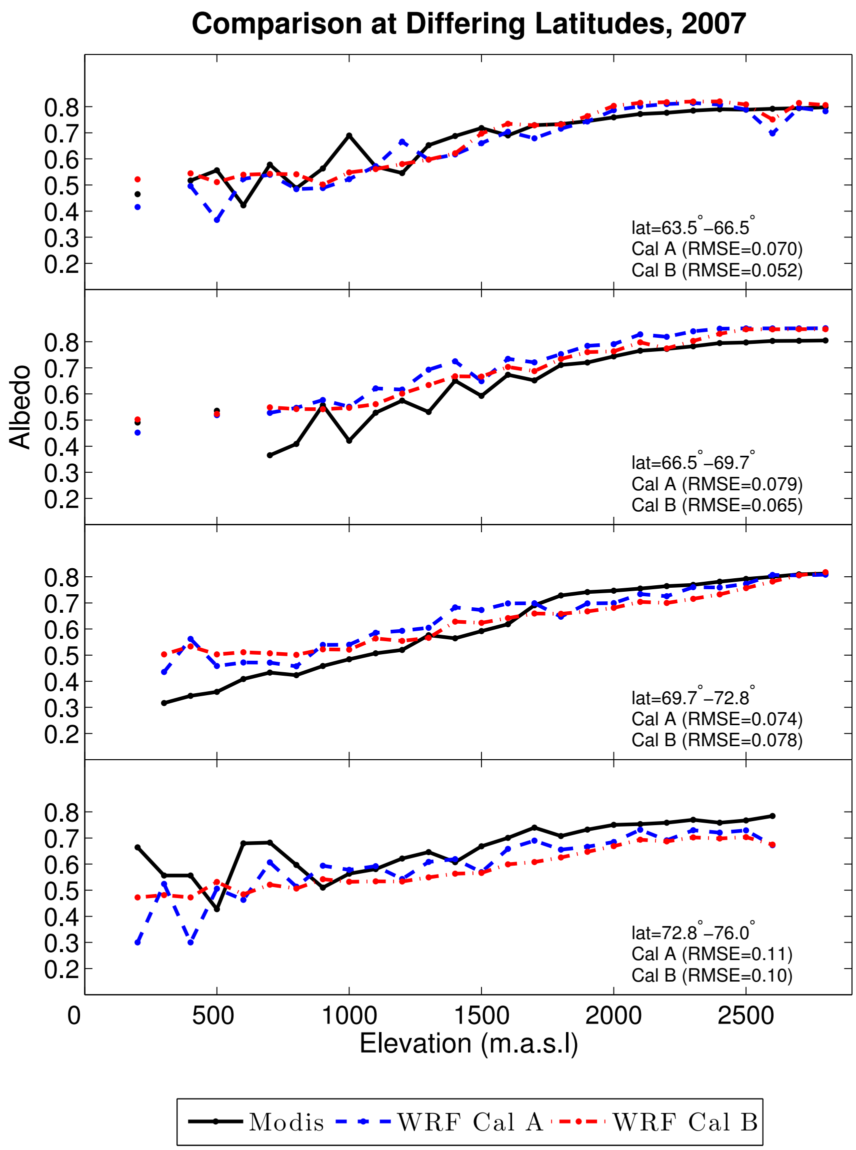

Figure A.5: Elevation profiles for 3 parameterizations alongside MOD10A1, split into 4 equal size latitude bands.

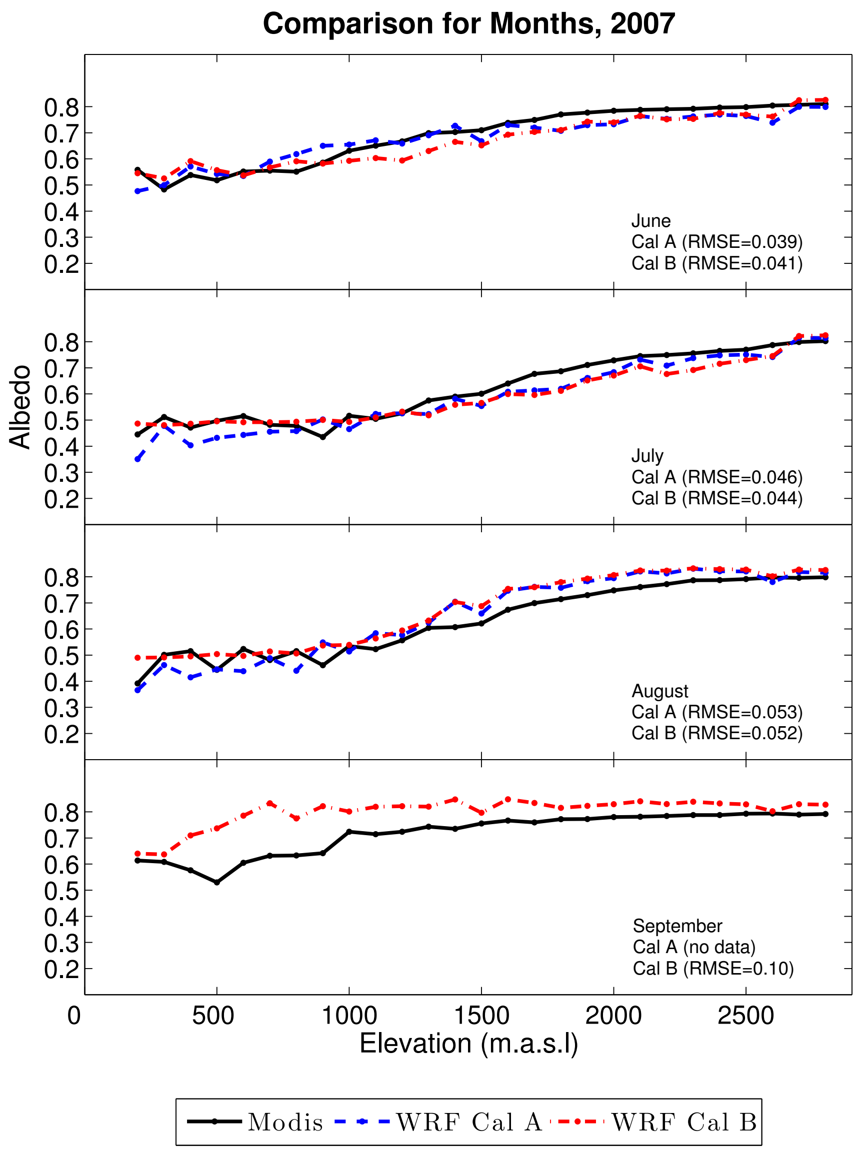

Figure A.6: Elevation profiles for 3 parameterizations alongside MOD10A1, for the entire domain, but split into separate months.

APPENDIX B

chapter 3 appendix

Melt Correlations 2001

	Devon	Sydkap	Manson	POW	Axel	Agassiz	N.Ellesmere
Devon		.90	.91	.80	.58	.59	.50
Sydkap	.91		.92	.92	.78	.75	.66
Manson	.91	.96		.91	.70	.73	.62
POW	.82	.87	.89		.84	.88	.78
Axel	.58	.60	.57	.76		.92	.92
Agassiz	.71	.71	.71	.89	.88		.95
N.Ellesmere	.62	.60	.59	.76	.89	.91	

Melt Correlations 2002

	Devon	Sydkap	Manson	POW	Axel	Agassiz	N.Ellesmere
Devon		.94	.81	.81	.61	.74	.53
Sydkap	.84		.78	.84	.74	.78	.57
Manson	.86	.77		.86	.43	.70	.43
POW	.65	.79	.67		.62	.91	.55
Axel	.75	.85	.70	.68		.67	.75
Agassiz	.51	.70	.53	.80	.64		.76
N.Ellesmere	.82	.71	.82	.65	.72	.60	

Melt Correlations 2003

	Devon	Sydkap	Manson	POW	Axel	Agassiz	N.Ellesmere
Devon		.90	.92	.82	.79	.76	.77
Sydkap	.85		.92	.94	.93	.89	.86
Manson	.85	.81		.93	.86	.86	.83
POW	.76	.86	.83		.94	.95	.88
Axel	.75	.91	.76	.85		.95	.94
Agassiz	.79	.86	.77	.89	.92		.95
N.Ellesmere	.82	.86	.82	.87	.93	.97	

Melt Correlations 2004

	Devon	Sydkap	Manson	POW	Axel	Agassiz	N.Ellesmere
Devon		.86	.81	.73	.65	.63	.61
Sydkap	.84		.86	.89	.89	.83	.80
Manson	.81	.82		.92	.78	.83	.78
POW	.75	.81	.91		.86	.93	.86
Axel	.85	.91	.74	.79		.89	.91
Agassiz	.84	.79	.85	.91	.86		.95
N.Ellesmere	.87	.71	.74	.75	.83	.88	

Melt Correlations 2005

	Devon	Sydkap	Manson	POW	Axel	Agassiz	N.Ellesmere
Devon		.93	.91	.84	.68	.71	.67
Sydkap	.93		.91	.91	.81	.81	.78
Manson	.92	.88		.91	.69	.78	.72
POW	.85	.84	.90		.86	.92	.83
Axel	.86	.83	.88	.90		.90	.92
Agassiz	.83	.80	.86	.94	.87		.92
N.Ellesmere	.88	.81	.90	.91	.96	.90	

Melt Correlations 2006

	Devon	Sydkap	Manson	POW	Axel	Agassiz	N.Ellesmere
Devon		.96	.93	.87	.77	.75	.64
Sydkap	.89		.95	.94	.85	.82	.68
Manson	.91	.84		.93	.81	.78	.64
POW	.82	.85	.87		.93	.93	.79
Axel	.82	.77	.79	.88		.93	.88
Agassiz	.72	.75	.71	.84	.80		.89
N.Ellesmere	.70	.59	.70	.70	.82	.74	

Melt Correlations 2007

	Devon	Sydkap	Manson	POW	Axel	Agassiz	N.Ellesmere
Devon		.96	.96	.90	.84	.84	.73
Sydkap	.95		.95	.94	.90	.88	.76
Manson	.91	.93		.95	.84	.87	.73
POW	.85	.87	.90		.90	.95	.81
Axel	.86	.86	.85	.91		.92	.92
Agassiz	.87	.88	.89	.93	.93		.91
N.Ellesmere	.84	.85	.85	.88	.96	.95	

Melt Correlations 2008

	Devon	Sydkap	Manson	POW	Axel	Agassiz	N.Ellesmere
Devon		.95	.92	.93	.91	.91	.88
Sydkap	.93		.95	.96	.95	.93	.88
Manson	.94	.91		.96	.91	.90	.85
POW	.86	.92	.86		.94	.97	.90
Axel	.90	.90	.83	.86		.95	.95
Agassiz	.90	.91	.86	.91	.93		.95
N.Ellesmere	.90	.82	.84	.81	.94	.93	

Table B.1: Melt Correlation tables for the years 2001 for the EB method (lower triangle), and TI method (upper triangle). Correlations are for summer daily melt.

Precipitation Correlations 2001

	Devon	Sydkap	Manson	POW	Axel	Agassiz	N.Ellesmere
Devon							
Sydkap	.55						
Manson	.60	.71					
POW	.27	.57	.69				
Axel	NaN	NaN	NaN	.26			
Agassiz	NaN	.22	NaN	.60	.65		
N.Ellesmere	NaN	NaN	NaN	NaN	.64	.61	

Precipitation Correlations 2002

	Devon	Sydkap	Manson	POW	Axel	Agassiz	N.Ellesmere
Devon							
Sydkap	.85						
Manson	.76	.71					
POW	.50	.58	.68				
Axel	.24	.39	.30	.53			
Agassiz	NaN	.21	.25	.59	.72		
N.Ellesmere	NaN	NaN	NaN	.25	.73	.78	

Precipitation Correlations 2003

	Devon	Sydkap	Manson	POW	Axel	Agassiz	N.Ellesmere
Devon							
Sydkap	.62						
Manson	.58	.70					
POW	.47	.76	.75				
Axel	.44	.59	.29	.53			
Agassiz	.37	.59	.47	.71	.67		
N.Ellesmere	.29	.34	NaN	.30	.57	.67	

Precipitation Correlations 2004

	Devon	Sydkap	Manson	POW	Axel	Agassiz	N.Ellesmere
Devon							
Sydkap	.52						
Manson	.66	.55					
POW	.31	.68	.74				
Axel	NaN	.53	NaN	.33			
Agassiz	NaN	.39	.23	.60	.35		
N.Ellesmere	NaN	.21	NaN	.24	.37	.70	

Precipitation Correlations 2005

	Devon	Sydkap	Manson	POW	Axel	Agassiz	N.Ellesmere
Devon							
Sydkap	.38						
Manson	.62	.73					
POW	.28	.83	.80				
Axel	NaN	.31	NaN	.29			
Agassiz	NaN	.60	.25	.62	.63		
N.Ellesmere	NaN	.34	NaN	.30	.70	.74	

Precipitation Correlations 2006

	Devon	Sydkap	Manson	POW	Axel	Agassiz	N.Ellesmere
Devon							
Sydkap	.59						
Manson	.61	.59					
POW	.40	.63	.68				
Axel	NaN	.39	NaN	.34			
Agassiz	.20	.38	.18	.65	.23		
N.Ellesmere	NaN	NaN	NaN	NaN	.19	.50	

Precipitation Correlations 2007

	Devon	Sydkap	Manson	POW	Axel	Agassiz	N.Ellesmere
Devon							
Sydkap	.68						
Manson	.68	.63					
POW	.37	.56	.79				
Axel	NaN	.46	NaN	.29			
Agassiz	NaN	.32	.22	.42	.50		
N.Ellesmere	NaN	NaN	NaN	NaN	.43	.51	

Precipitation Correlations 2008

	Devon	Sydkap	Manson	POW	Axel	Agassiz	N.Ellesmere
Devon							
Sydkap	.57						
Manson	.77	.55					
POW	.26	.57	.42				
Axel	NaN	.49	NaN	.36			
Agassiz	NaN	.35	NaN	.67	.54		
N.Ellesmere	NaN	NaN	NaN	.20	.51	.57	

Table B.2: Precipitation Correlation tables for the years 2001. Correlations are for summer daily precipitation. “Nan” values indicate that correlation was not significant with 95% confidence.

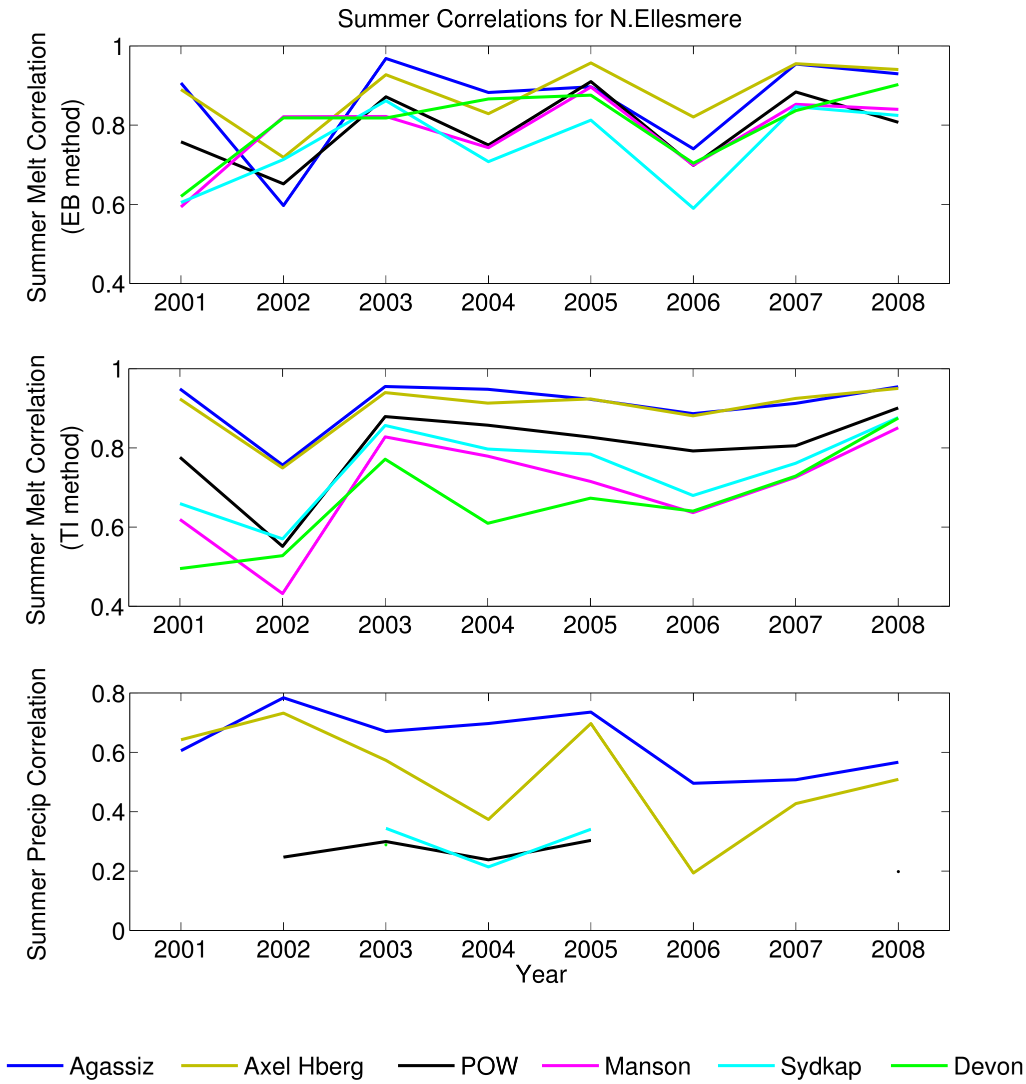

Figure B.1: Comparison of correlations for melt (EB and TI) and precipitation, with each of the QEI icecaps for N.Ellesmere.

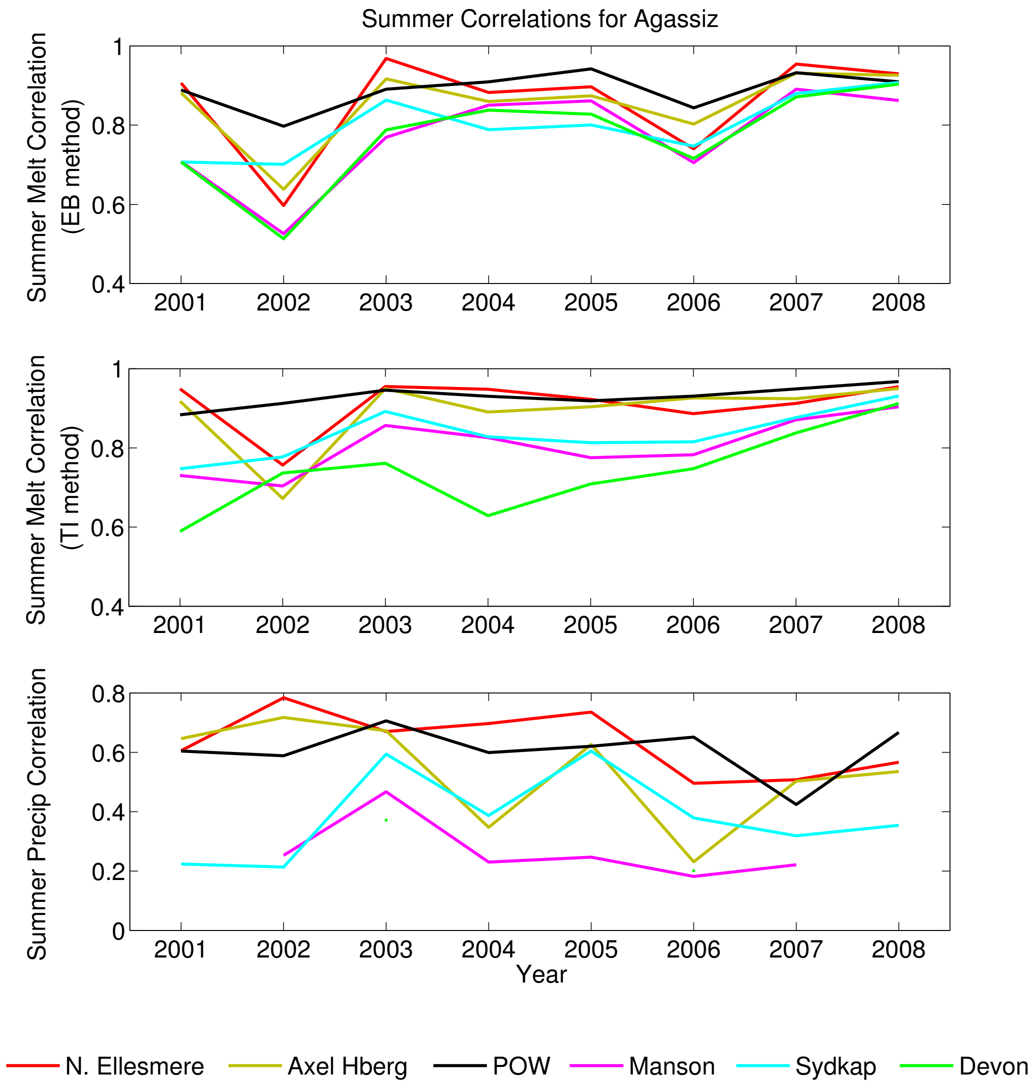

Figure B.2: Comparison of correlations for melt (EB and TI) and precipitation, with each of the QEI icecaps for Agassiz.

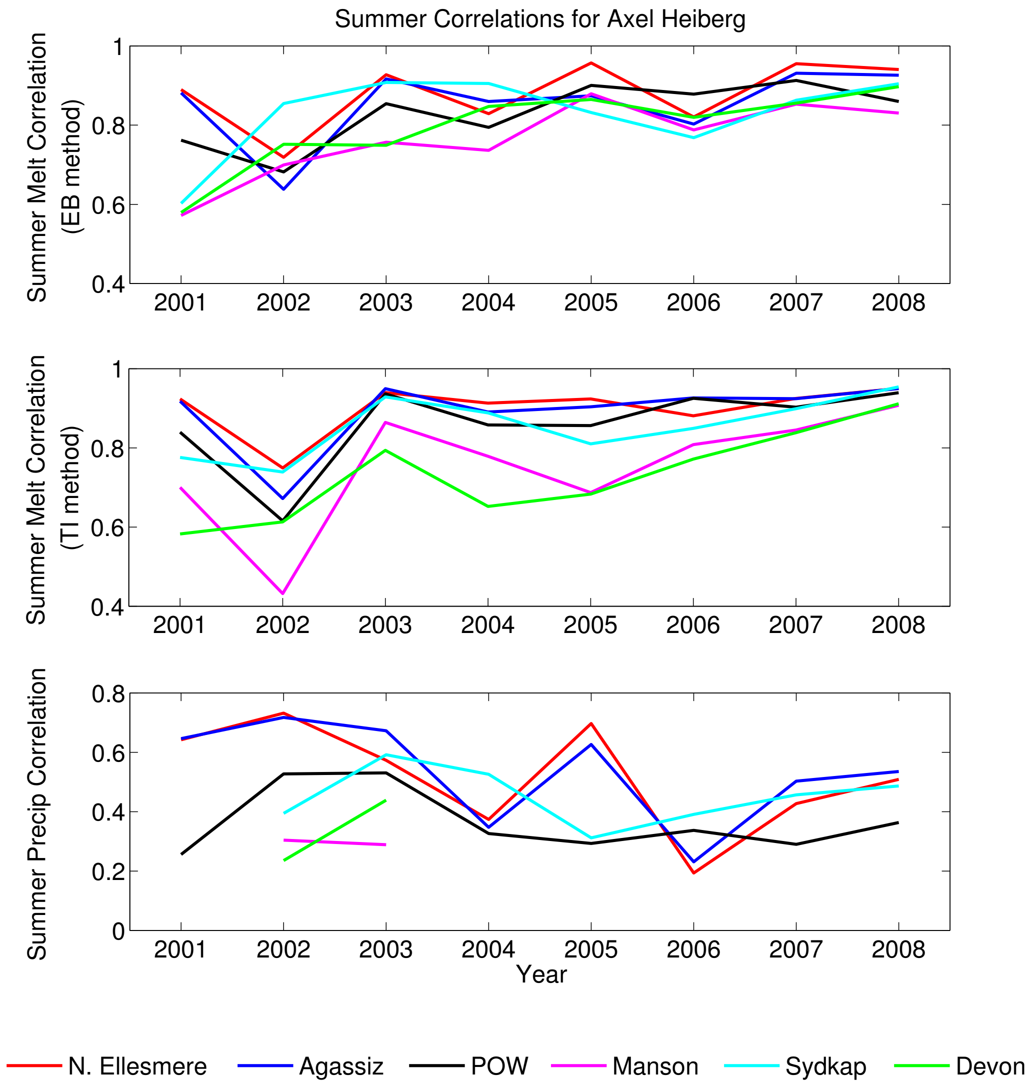

Figure B.3: Comparison of correlations for melt (EB and TI) and precipitation, with each of the QEI icecaps for Axel Heiberg.

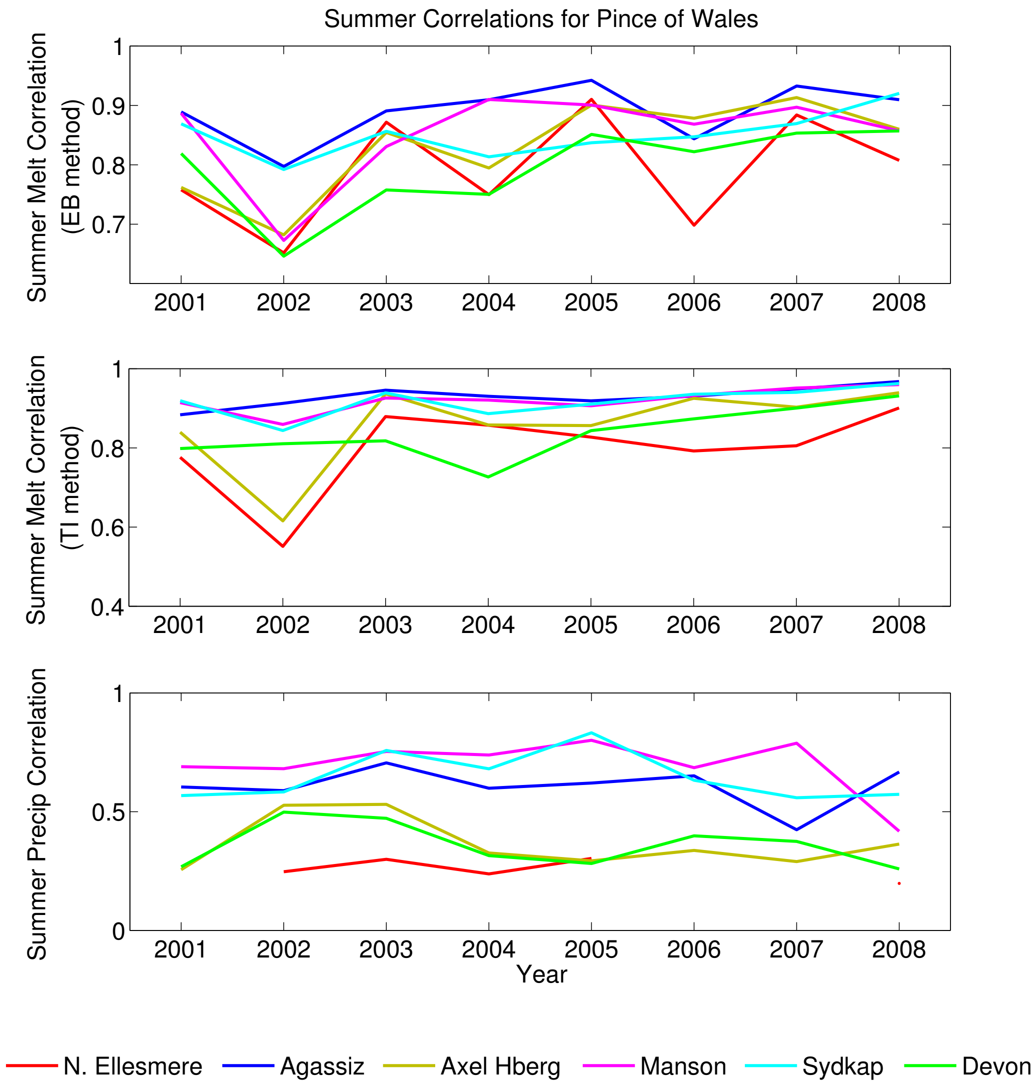

Figure B.4: Comparison of correlations for melt (EB and TI) and precipitation, with each of the QEI icecaps for Prince of Wales.

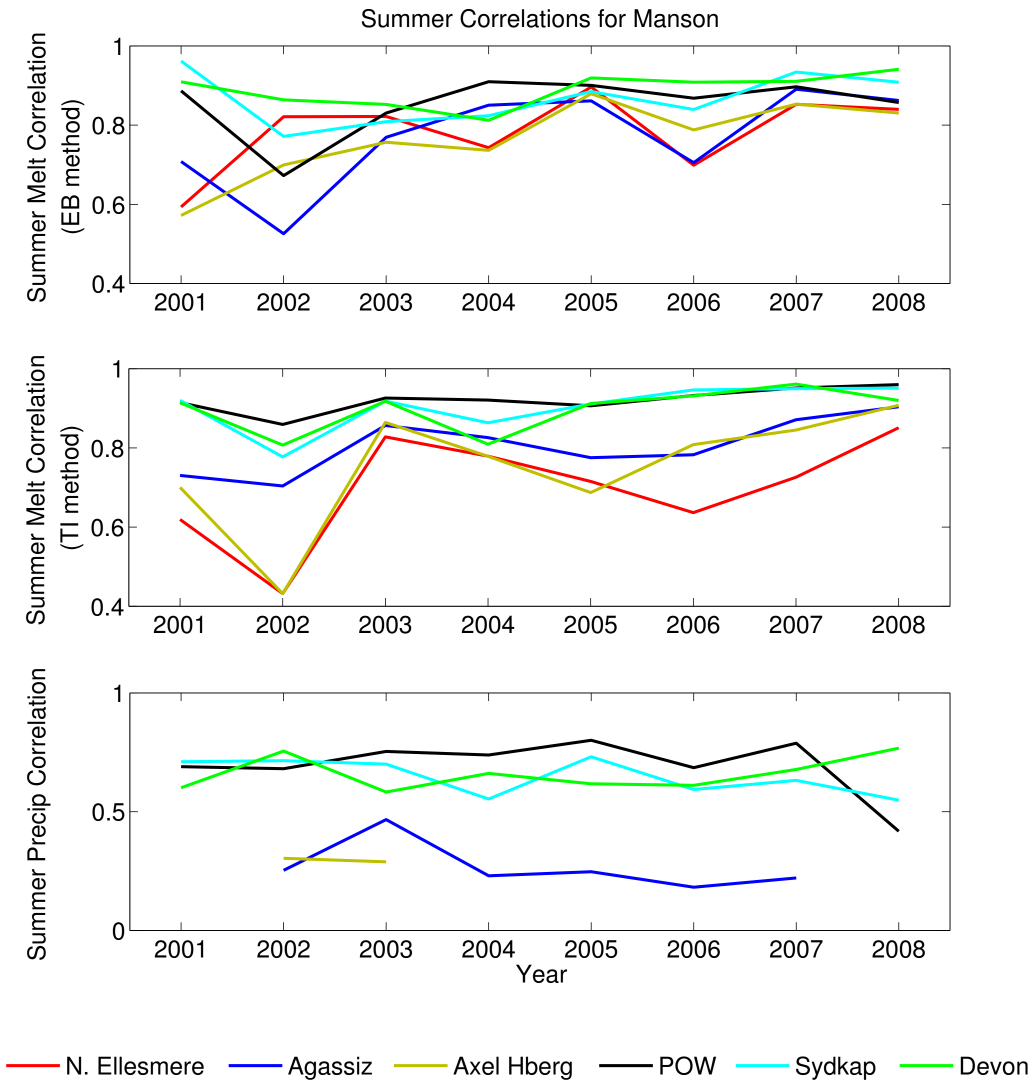

Figure B.5: Comparison of correlations for melt (EB and TI) and precipitation, with each of the QEI icecaps for Manson.

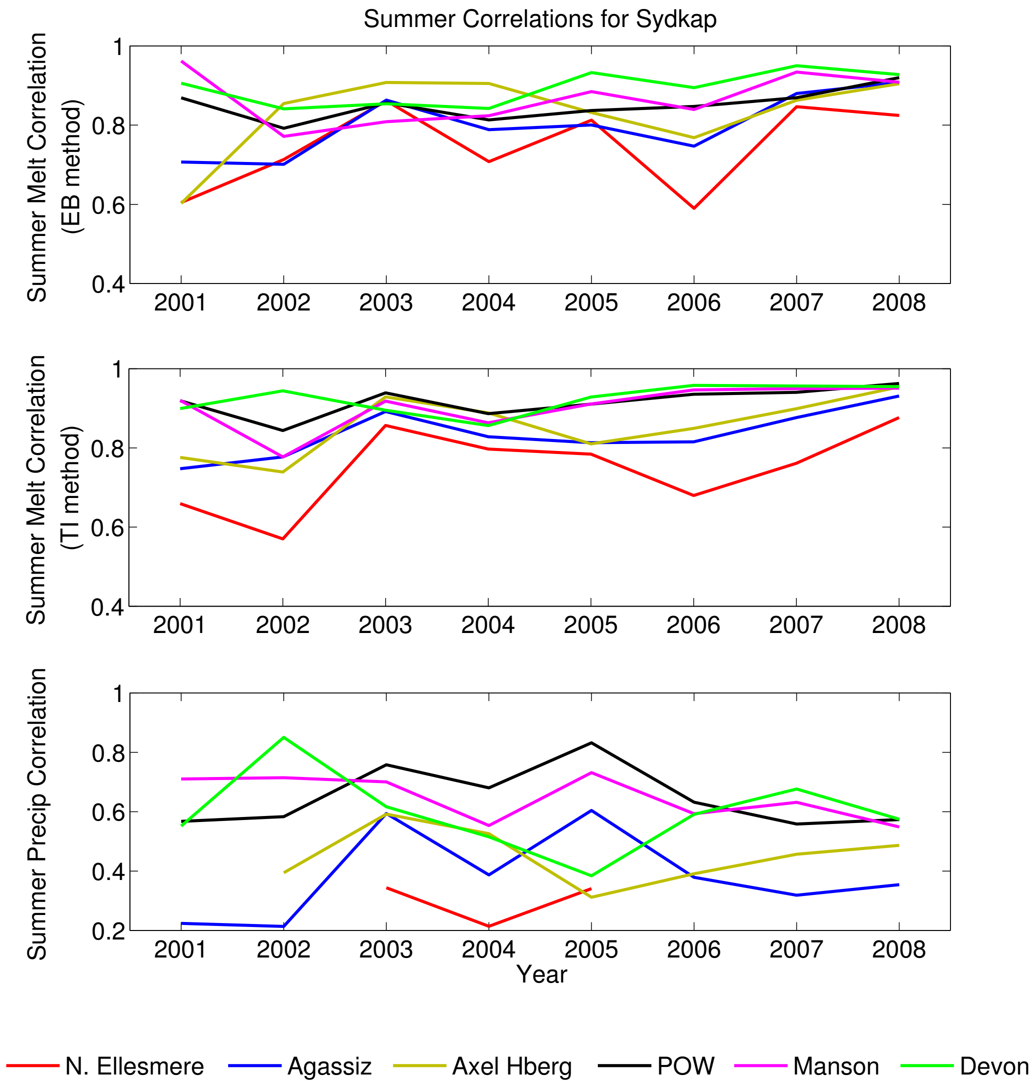

Figure B.6: Comparison of correlations for melt (EB and TI) and precipitation, with each of the QEI icecaps for Sydkap.

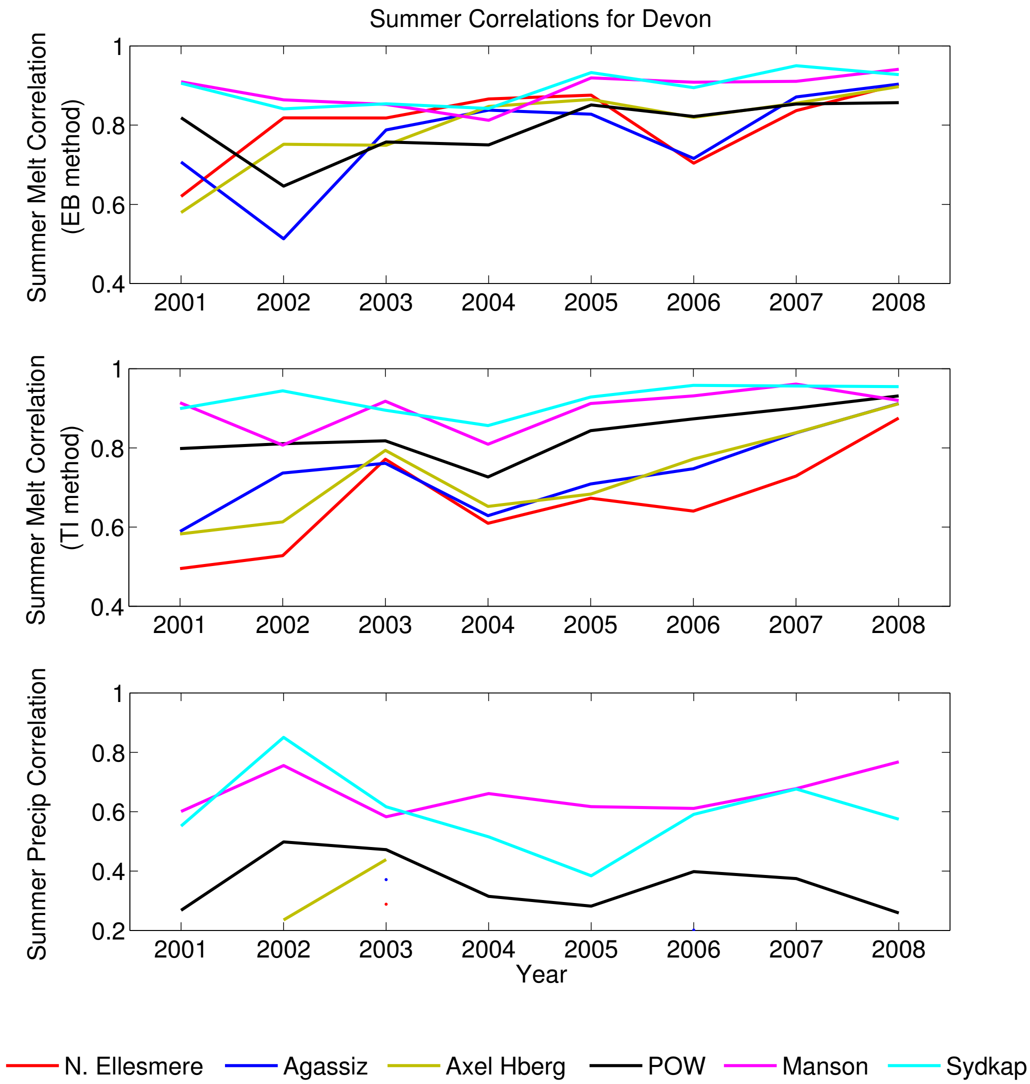

Figure B.7: Comparison of correlations for melt (EB and TI) and precipitation, with each of the QEI icecaps for Devon.